REPORT NO. FRA/ORD-77/34.1

PB

NONDESTRUCTIVE MEASUREMENT OF LONGITUDINAL RAIL STRESSES

Application of the Acoustoelastic Effect to Rail Stress Measurement

January 1978

Final Report

This document is available to the public through
The National Technical Information Service,
Springfield, Virginia 22161

Prepared for

U.S. DEPARTMENT OF TRANSPORTATION
FEDERAL RAILROAD ADMINISTRATION
Office of Research and Development
Washington, D.C. 20590

NOTICE

This document is disseminated under the sponsorship of the Department of Transportation in the interest of information exchange. The United States Government assumes no liability for the contents or use thereof.

Technical Report Documentation Page

1. Report No.	2. Government Accession No.	3. Recipient's Catalog No.
FRA/ORD-77/34.1 I		

4. Title and Subtitle	5. Report Date
Nondestructive Measurement of Longitudinal Rail Stresses: Application of The Acoustoelastic Effect To Rail Stress Measurement.	January 1978
	6. Performing Organization Code
	8. Performing Organization Report No.
7. Author(s) D. M. Egle and D. E. Bray	
9. Performing Organization Name and Address University of Oklahoma School of Aerospace, Mechanical & Nuclear Eng'g 865 Asp Avenue, Room 200 Norman, Oklahoma 73069	10. Work Unit No. (TRAIS)
	11. Contract or Grant No. DOT-OS-40091
12. Sponsoring Agency Name and Address Department of Transportation Federal Railroad Administration Washington, D.C. 20590	13. Type of Report and Period Covered Final Report 6/1/75 to 1/31/77
	14. Sponsoring Agency Code

15. Supplementary Notes

16. Abstract

An ultrasonic probe has been designed, evaluated and shown capable of measuring longitudinal stress changes in railroad rails. The probe utilizes the effect of applied stress on wave velocity (acoustoelastic effect) to determine the stress change. Both laboratory and field evaluation has shown that the probe is capable of measuring stress changes with an accuracy of $\pm$ 6.9 MN/m^2 ($\pm$ 1 ksi).

17. Key Words	18. Distribution Statement
Rail Stress Measurement, Nondestructive Stress Measurement, Ultrasonic Stress Measurement, Acoustoelasticity, Guided Waves, Rail Material Properties.	Document is available to the public through the National Technical Information Service, Springfield, VA 22151

19. Security Classif. (of this report)	20. Security Classif. (of this page)	21. No. of Pages	22. Price
UNCLASSIFIED	UNCLASSIFIED		

Form DOT F 1700.7 (8-72)

* U. S. GOVERNMENT PRINTING OFFICE : 1973 725-504/328

DEPARTMENT OF TRANSPORTATION
FEDERAL RAILROAD ADMINISTRATION
WASHINGTON, D.C. 20590

1-30-78

TO: Report Distribution List;

Erratum Notice

Report Title: NONDESTRUCTIVE MEASUREMENT OF LONGITUDINAL RAIL STRESS.

Report Date: January 1978.

Authors: D. M. Egle and D. E. Bray

Correction: The Report Number shown on the Standard Title Page is incorrect. The number as printed, is; FRA/ORD-77/09.1. The correct number is; FRA/ORD-77/34.I which agrees with the number on the report cover.

ACKNOWLEDGMENTS

The authors would like to acknowledge the contribution of many individuals who, through discussion, material assistance or otherwise, have contributed to the progress of this research. Mr. W. B. O'Sullivan, Technical Monitor in the Federal Railroad Administration, offered frequent and useful comments on operational and technical matters. Dr. W. J. Harris, Jr., Vice-President, Research and Test Department, Association of American Railroads, also provided valuable technical comments as well as a financial contribution. The Atchison, Topeka and Santa Fe Railway Company showed a continued interest in the work through the contribution of several rail samples and the personal interest of Mr. W. S. Autrey, Chief Engineer-System, Mr. L. D. Vallet of Mr. Autrey's staff and Mr. C. W. Groh, Assistant Division Engineer, Oklahoma City. Others whose contributions have also been of assistance in various ways include Mr. W. H. Chidley, Chairman, Technical Committee on Railway Materials, American Iron and Steel Institute, Mr. Charles O. Frederick, Project Manager (Track), The Railway Technical Centre, British Rail, Dr. Roger Steel, Transportation Systems Center, and Mr. Dan Stone, Research Metallurgist, Research Center, Association of American Railroads. The able assistance of Mr. Philip Mayes and Mr. Rustom Irani, students at the University of Oklahoma, contributed substantially to the execution of this project.

TABLE OF CONTENTS

	Page
INTRODUCTION	1
Purpose	1
Background	1
Thermally Induced Stress Variations Along the Rail Length.	4
Changes in Rail Stresses with Service	6
Present State of Knowledge	9
ACOUSTOELASTIC AND THIRD ORDER ELASTIC CONSTANTS FOR RAIL STEEL	11
Theoretical Background	11
Measurement Technique	15
Experimental Results	19
DESIGN OF AN ULTRASONIC PROBE FOR LONGITUDINAL STRESS MEASUREMENT	27
Instrumentation for Travel-Time Measurements	28
Probe I	30
Evaluation of Probe I.	34
Temperature Effects	38
Probe II	47
Temperature Effects on Probe II	52
Repeatability of Wave Travel-Time Measurements	52
Probe III	59
Probe IV	64
Changes in Wave Travel-Times Associated with Varying Elastic Properties	67
Summary	70
FIELD EVALUATION OF THE ULTRASONIC PROBE	71
Field Tests	71
Field Tests at Pueblo	72
Field Test Results	78
Results of Norman Field Test	78
Results of the Pueblo Field Test	81
Stress Relieving Tests at Station 32	90
CONCLUSION	95

Page

APPENDIX A-Rail Stress Measurement in the Union of Soviet Socialist Republics (USSR) and the United Kingdom (UK). . 97

Introduction. 97
Transducer 98
Operation. 98
Application and Results 98
Evaluation and Comparison to Proposed Ultrasonic Measurement Technique 100
Other Discussion Topics at British Rail . . 100

APPENDIX B-Residual Stress Measurement in Used Rail . . . 101

Method 101
Data Analysis 102
Summary 110

REFERENCES 111

LIST OF FIGURES

Figure		Page
1-1	Stress Variations Along a 285 m (986 ft) Length of Continuously Welded Rail (reference 9).	8
2-1	Instrumentation for the Acoustoelastic Measurements.	18
2-2	Relative Changes in Wave Speeds for Rail Specimen 1.	21
3-1	Electronic Instumentation for Travel-Time Measurements	29
3-2	Schematic Diagram of Frequency Divider.	31
3-3	Typical Oscilloscope Traces for Travel-Time Measurements.	32
3-4	Probe I Rail Stess Measurement Assembly.	34
3-5	Total Travel-Time Measurements with Ultrasonic Probe Assembly.	36
3-6	Illustration of the Effect of Initial Curvature on the Surface Stresses.	37
3-7	Inverse Travel-Time Measurements on Reference Bar.	39
3-8	The Effect of Temperatue on Inverse Travel-Time Measurements Made with Probe I.	40
3-9	Temperature Dependence of the Speed of Longitudinal Waves Propagating Parallel to the Longitudinal Axis of the Rail.	42
3-10	Temperature Dependence of the Speed of Longitudinal Waves Propagating Perpendicular to the Longitudinal Axis of the Rail.	43
3-11	Temperature Dependence of Transverse Wave Speed in Rail Steel.	44

Figure		Page
3-12	Longitudinal Wave Speed As A Function of Temperature for Plexiglas.	46
3-13a	Differential Technique for Measuring Travel-Times. . .	49
3-13b	Metal Comb for Detection of Waves.	49
3-14	Two View Drawing of Probe II.	51
3-15	Temperature Induced Changes in Travel-Time Measurements for Probe II.	53
3-16	Repeated Travel-Time Measurements on Rail Specimen 4 Using Probe II.	54
3-17	Repeated Travel-Time Measurements on the Web of Rail 9 Using Probe II.	56
3-18	Travel-Time Measurements for Eight Rail Web Surfaces Using Probe II.	58
3-19	Two View Drawing of Probe III.	60
3-20	Travel-Time Measurements on Rail Web Surfaces with Probe III.	62
3-21	Travel-Time Measurements on Two Full Length Rails with Probe III.	63
3-22	Travel-Time Measurements on Two New Full Length Rails with Probe IV.	65
3-23	Longitudinal Wave Travel-Time Along the Length of A New 119 lb,11.9 m (39 ft) Rail.	66
3-24	Travel-Time Measurement Before and After Annealing A 4140 Cold Rolled Steel Bar.	69
4-1	Schematic Diagram of the Test Zone At Pueblo. . .	73

Figure		Page
4-2	LIM Access Spur Looking West.	74
4-3	Typical Strain Gage Installation.	76
4-4	Ultrasonic Probe Clamped to Rail Web.	77
4-5	Travel-Time Measurements on Reference Rail-Field Test at Norman.	79
4-6	Travel-Time Measurements at Mile Post 400-Norman Field Test.	80
4-7	Strain Histories at Stations 26 and 29-Pueblo Field Test.	82
4-8	Strain Histories at Stations 32 and 35-Pueblo Field Test.	83
4-9	Stress Changes Measured with Strain Gages During The Pueblo Field Test.	85
4-10	Travel-Time Measurements on Reference Rail During Pueblo Field Test.	87
4-11	Longitudinal Wave Travel-Time Measurements on Four Rail Stations at Pueblo.	88
4-12	Shear Wave Travel-Time Measurements on Four Rail Stations at Pueblo.	89
4-13	Strain Measurements During Stress Relief Test at Station 32.	92
4-14	True Rail Stress at Station 32.	94
A-1	Annulus for Rail Force Measuring Transducer. (British Rail).	99

Figure		Page
B-1	Strain Gage Locations for Residual Stress Measurement in Rail.	103
B-2	Nomenclature for Data Analysis.	104
B-3	Average Longitudinal Stess As A Function of Depth for 92 lb/yd Used Rail.	109

LIST OF TABLES

Table		Page
2-1a	Rail Steel Specimens	16
2-1b	Specifications for Rail Steel in Specimens 1 and 3 . .	16
2-2	Summary of Acoustoelastic Constants	22
2-3	Second and Third Order Elastic Constants for Two Samples of Rail Steel	23
2-4	Comparison of Measured Acoustoelastic Constants for Steel	24
3-1	Analysis of the Relative Effects of the Three Sources of Temperature Induced Changes in f_L and f_s . . .	48
3-2	Condition of Rail Sample Web Surfaces Used in Repeatability Study	57

INTRODUCTION

This report gives the results of the second phase of a two phase study investigating the potential usefulness of ultrasonic wave velocity changes as a method for measuring stress variations in railroad rail. Phase one results have been previously reported [1].

Purpose

The work performed under this contract had a dual objective. One was to study the effect of applied stress on the propagation of ultrasonic pulses in high carbon, railroad quality rail steel. This was accomplished by the experimental measurement of the acoustoelastic effect for bulk waves and guided waves in samples of rail steel. The major objective, however, was to initiate research utilizing ultrasonic pulses that will result in techniques adaptable to the in-situ measurement of longitudinal stresses. It is contemplated that these tests can be performed with both a small portable device similar to existing ultrasonic flaw detection instruments. Measurements via a test car moving at standard operating speeds will be more difficult since probe contact on the rail web is required. Measurement of these stresses will enable operating railroads to locate highly stressed areas in rail. These highly stressed areas often cause rail and track deformation and are a major cause of derailments.

Background

The overriding goal of the project was to develop a technique for in-situ measurement of rail stresses caused by changes in ambient temperature. The expansion and contraction of materials with temperature

change is well known phenomenon. This is particularly noticeable in railroad rails since they are exposed to the full range of outdoor temperatures, typically 47.7°C to -41.7°C (118°F to -43°F). Actual rail temperature is often much higher than the ambient because of the absorption of radiant heat from the sun [2].

The effect of the rail expansion and contraction is more noticeable in continuous welded rail than in bolted (or jointed) rail. Relative motion within the joints in bolted rail can prevent high stresses from occurring. High maintenance costs and the propensity for fatigue cracks at the joint, plus the occurrence of end batter on the rail have all led to the replacement of this type of rail with continuous welded rail (CWR). In most cases, these strings of CWR are 439 m (1440 feet) long. These rails, while clearly superior to the old jointed rail, do not have the ability to release the expansion and contraction forces through linear movement. Instead, this is accounted for by changes in the internal stresses of the rail. Typical high temperature stresses for properly installed rail have been estimated to be near 83.7 MN/m^2 (12,000 psi) [3].

Normal installation practice usually considers the annual temperature range of the location and the temperature of the rail at the time of installation. An attempt is made to adjust the installed stress level to such that the rail will not exceed acceptable compressive or tensile stresses throughout the annual temperature range. This estimate of installation stress level is, at best, guesswork based on prior experience. During periods of extreme temperatures track personnel must maintain a vigil over the rail in order to detect overstressed conditions.

The judgement of overstressed conditions is based on the ability of an individual inspector to detect such a situation.

When the temperature is high and rail expansion has created excessive longitudinal compressive stresses in the rail, it is primed for buckling. Track buckling occurs because rails react to axial loads much like any structural column. A perturbation such as an additional temperature increase or train motion can trigger the lateral buckling. Extreme cold puts tensile stresses in the rail. If the rail stresses are not properly adjusted upon installation, these low temperature tensile stresses can create forces sufficient to pull apart welded joints. A more detailed discussion of this behavior is contained in references 2, 3, 4 and 5.

A well-documented accident that was attributed to track buckling occurred at Glen Dale, Maryland on 28 June 1969, when the passenger train, the Silver Star, derailed while running at a speed between 134 and 138 km/hr (83 and 85 mph). In this instance 144 of the 541 passengers were treated at area hospitals for injuries. This derailment occurred at 38°C (100°F) temperature on Penn Central track which regularly handled the Metroliners travelling at speeds near 201 km/hr (125 mph). The National Transportation Safety Board (NTSB) investigated the accident and reported" . . . the derailment was caused by lateral movement of the track under the train. The lateral movement was caused by buckling of the track." [6] Other statements from the NTSB report which are relative to the study are as follows:

> "The railroad industry needs badly a portable stress measuring device which would give instant

> readings of the compression or tension in a rail without disturbing it." In the general conclusion, the NTSB reported, "A more significant conclusion for the long term is that the general state of the art of railroad track design and maintenance is scientifically weak, and that safety relies on judgement of individuals rather than on any firm or logical criteria." In the recommendations, the report states, "The Safety Board recommends that the American Railway Engineering Association and the Association of American Railroads undertake studies to determine more accurately the stresses developed in welded rail track in extremes of temperature and the role of these stresses in hazardous track movements."

It is clear from the above discussion that there is a need for a technique for the nondestructive measurement of longitudinal rail stresses. This report addresses that need.

The problem caused by high stress conditions in rail exists throughout the United States and the rest of the world. It is more acute in areas where daily temperatures have an extreme range. A large seasonal range also creates stress problems. Many desert or arid areas experience large daily variations in temperature while the northern states have the largest seasonal changes. Obviously, the temperate climates such as in Florida would have the least problem.

Thermally Induced Stress Variations Along the Rail Length

The research discussed in this report relates to the measurment of rail stress changes which result from temperature variations. An understanding of the strain characteristics in rail in service could

enhance the usefulness of any stress measurement technique. This section will present a brief review related to stress variations along the length of continuously-welded rail.

Rail welded into long lengths and installed in the track is constrained by the cross-ties to where, for the most part, there is negligible longitudinal strain as the rail passes through the temperature cycle. Toward the end of each welded string the cross-tie constraining forces will be insufficient to prevent rail movement. This length where rail movement occurs is determined by the type of rail, the number of ties and the type of ballast.

In early tests on a one-mile length of main-line, continuously-welded rail, McGee reported rail movement up to approximately ten (10) rail lengths from each end [7]. This corresponds to approximately 119 meters (390 feet) from each end. The test data compared rail strain at temperatures ranging from -11°C (+13°F) to +0.5°C (33°F) in the winter and 42°C (108°F) to 48°C (118°F) in the summer. Rail strain at the ends was approximately $\pm$ 275 μm/m while that at locations less than ten rail lengths from the end was generally less than 34 μm/m.

A more general discussion of rail stress variation with temperature has been given by Hay [3]. Where joint forces are neglected, the number of ties (N_T) necessary to fully constrain the rail is given by

$$N_T = \frac{F}{T}$$

where F = total rail force

and T = restraining force per tie.

The force (F) to be constrained can be calculated using the rail expansion

coefficient. This is given by

$$F = \mu(\Delta T)\, EA$$

where μ = coefficient of thermal expansion

ΔT = temperature change

E = Young's modulus

and A = rail cross-sectional area

For a typical situation with 115 lb AREA rail having a cross-sectional area of $7.26 \times 10^{-3} m^2$ ($11.26\ in^2$) and a coefficient of thermal expansion of 11.2 $\mu m/m/^{o}C$, the force change with $28^{o}C$ ($50^{o}F$) degree temperature increase is:

$$F = 0.471\ MN\ (106\ kips)$$

Considering a tie restraint of 2.22×10^{3} N/tie (500 lb/tie) the number of ties required to constrain the rail is

$$N_T = \frac{106 \times 10^{3}}{500} = 212$$

At 0.56 meter (22 inch) tie spacing, the rail length (L) required for full constraint is

$$L = 212\ (0.56) = 118.7\ \text{meters (389 feet)}.$$

Thus, any stress measurement for 115 lb rail under these track conditions must be made at least 118.7 meters (389 feet) from the rail end. This figure is in good agreement with the data given by McGee. Other rail sections would yield slightly different values for the length of rail movement.

Changes in Rail Stresses with Service

When welded rail is installed in the track, long lengths are pulled

from the rail train and layed on the ties. In this case, the train is pulled out from under each welded rail length. After the rail is partially installed, track maintenance personnel either stretch or compress the rail end in order to achieve a theoretical zero stress level at a predetermined temperature. Complete installation procedures have been given by the American Railway Engineering Association [8].

After the rail is welded, there can be considerable variation in the longitudinal stress levels along the rail length because of the installation practice. Very little information on these stress variations has appeared in the published literature. The results of one test, conducted by the Missouri Pacific Railroad [9], are shown in figure 1-1.

In this test, welded rail sections were manufactured from twenty-four 39 foot rail lengths which were welded into a continuous rail 285 meters (936 feet) long. Strain gauge data at several locations were initially taken at the rail welding plant. Additional data were taken during the installation and thereafter for several months. Figure 1-1 shows the data taken on one of the rail sections. The location along the welded section is shown in rail lengths from the right hand end.

The data were normalized such that the rail at a zero stress condition after it was removed from the train but before being installed in the track. This is shown by line 1. The rail was then stretched at each end, in accordance with standard practice, producing tension on either end of the welded string as shown by line 2. The center portion shows little stress change with the stretching.

The effect of freight train traffic is shown by the stress changes indicated by the succeeding lines. One day's service causes the end to

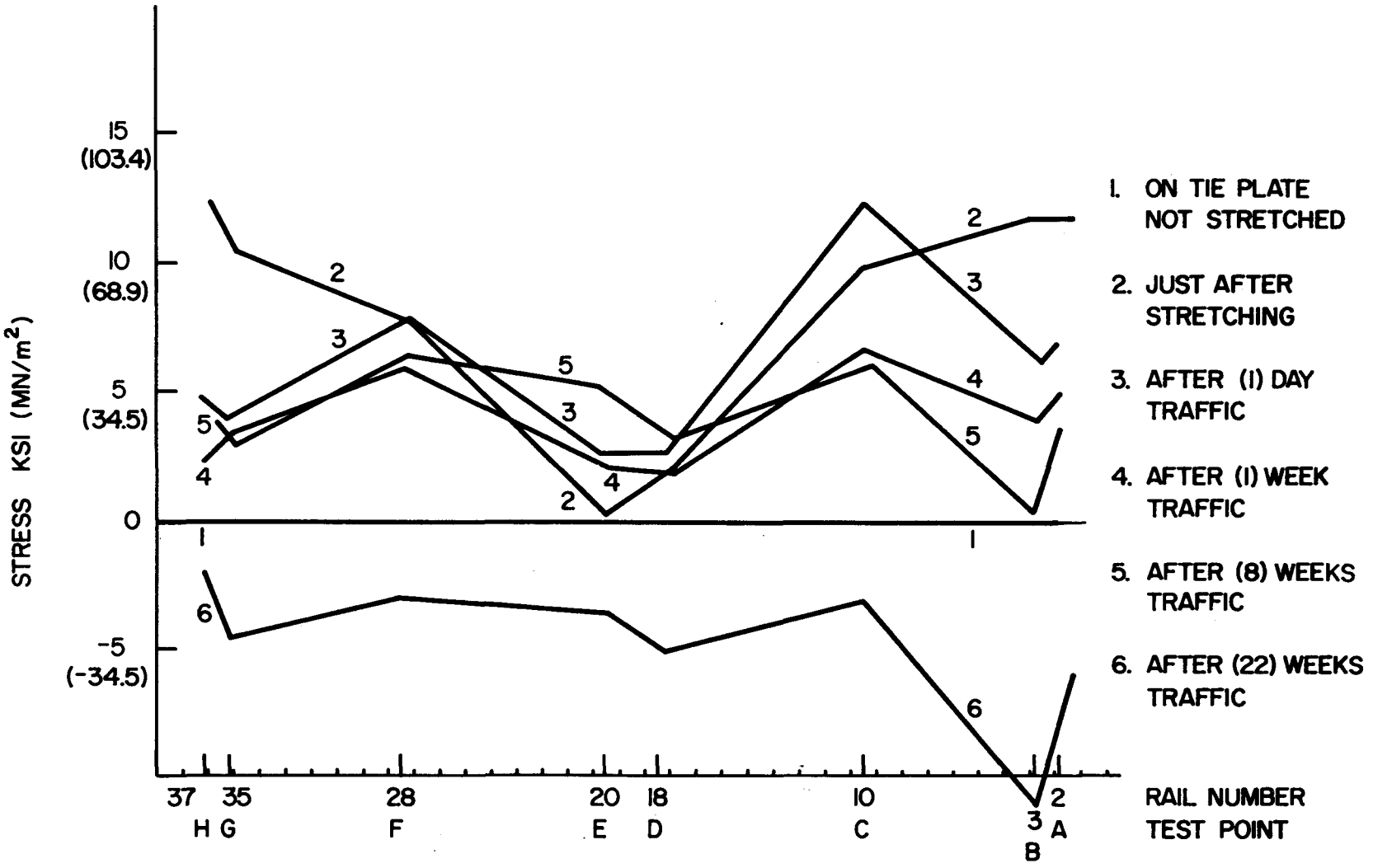

Figure 1-1 Stress Variations Along a 285 m (986 ft) length of Continuously Welded Rail (reference 9).

become less tensile while the center stresses become more tensile. This stress redistribution pattern continues until, at eight weeks, the stress is somewhat uniform along the rail length (line 5). Finally, after 22 weeks of service, the stresses have become compressive and very uniform, except for one data point near the right hand end. In this discussion, the authors note several difficulties encountered with the Berry strain gauges which could account for some of the erratic behavior. Nonetheless, the process of stress redistribution with service is well demonstrated.

The foregoing discussion indicates that stress measurement with any technique could be expected to produce erratic results until after the rail stresses have been redistributed with service.

Present State of Knowledge - Nondestructive measurement of residual stress in structural members is certainly not a new problem. Several techniques have been developed that have been sucessfully applied by other industries. X-ray diffraction is perhaps the most well known today. Other methods which are emerging from the laboratory to field usage are Barkhausen Noise Analysis and shear wave acoustic birefringence. X-ray diffraction and Barkhausen Noise Analysis [10,11] are both surface effect techniques, that is, they are techniques used to measure surface stresses. A fundamental difficulty arises in applying either of these methods to the measurement of rail stresses in that the high loads generated by the contact of wheel and rail severely deform the rail head. The top of the rail head has a surface layer of plastically deformed metal that has properties different from body of the rail. Estimates of the depths of this zone are from 6.4 to 9.6 mm (1/4 in to 3/8 in) below the surface [12].

Moreover, the sides of the rail heads are distorted by this plastic working giving a generally nonuniform rail geometry. Hence, the method chosen for the rail stress measurement must be independent of this plastic working on the head. The reliability of surface effect measurement of body stresses through plastically deformed surfaces has not been established. On the other hand, the acoustic birefringence technique is capable of measuring body stresses and thus, of the three methods, is the one warranting further study.

A summary of early work on the acoustoelastic effect has been given in the interim report for this study and will not be repeated here [1].

ACOUSTOELASTIC AND THIRD ORDER ELASTIC CONSTANTS FOR RAIL STEEL

The basis of the longitudinal stress measurement technique is the stress induced anisotropic behavior of solids. It is caused by non-linearities in the strain-displacement and constitutive relations of the material. The acoustoelastic effect refers to the changes in the speed of elastic waves propagating in a body which is simultaneously undergoing static elastic deformation. In this section, which is based on reference [13], techniques and results of the measurement of the acoustoelastic and third order elastic constants (which define the constitutive relationship for an initially isotropic material, up to the second order) for steel typical of that found in railroad rail are presented.

Previous work on the use of the acoustoelastic effect for stress measurement [14-19] has concentrated on using the difference in speed of shear waves polarized parallel and perpendicular to the uniaxial stress and traveling perpendicular to the stress axis. Our approach has been to use shear and longitudinal waves propagating parallel to the stress axis. It is shown that for rail steel the relative change in wave speed per unit change in axial strain is largest for longitudinal waves propagating parallel to the stress axis.

Theoretical Background

Hughes and Kelly [20] derived expressions for the speeds of elastic waves in a stressed solid using Murnaghan's theory of finite deformations [21] and third order terms in the strain energy expression. They showed that the speeds of plane waves propagating in the 1 direction

and having particle displacements in the 1, 2 or 3 directions in an initially isotropic body subjected to a homogeneous triaxial strain field are given by

$$\rho_o V_{11}^2 = \lambda + 2\mu + (2\ell + \lambda)\theta + (4m + 4\lambda + 10\mu)\alpha_1$$

$$\rho_o V_{12}^2 = \mu + (\lambda + m)\theta + 4\mu\alpha_1 + 2\mu\alpha_2 - \frac{1}{2} n\alpha_3 \qquad (2\text{-}1a\text{-}c)$$

$$\rho_o V_{13}^2 = \mu + (\lambda + m)\theta + 4\mu\alpha_1 + 2\mu\alpha_3 - \frac{1}{2} n\alpha_2$$

where

ρ_o - initial density

V_{11}, V_{12}, V_{13} - speeds of waves propagating in the 1 direction with particle displacements in the 1, 2, 3 direction respectively

λ, μ - Lamé or second order elastic constants

ℓ, m, n - Murnaghan's third order elastic constants

$\alpha_1, \alpha_2, \alpha_3$ - components of the homogeneous triaxial principal strains in the 1, 2, 3 direction

$\theta = \alpha_1 + \alpha_2 + \alpha_3$

For a state of uniaxial stress, there are five unique wave speeds which may be determined from equations (2-1a-c). First consider the stress acting in the 1 direction. The strains are then

$$\alpha_1 = \epsilon \quad , \quad \alpha_2 = \alpha_3 = -\nu\epsilon$$

where ν is Poisson's ratio.

Equations (2-1) reduce to

$$\rho_o V_{11}^2 = \lambda + 2\mu + [4(\lambda + 2\mu) + 2(\mu + 2m) + \nu\mu\,(1 + 2\ell/\lambda)]\epsilon$$

(2-2a-b)

$$\rho_o V_{12}^2 = \rho_o V_{13}^2 = \mu + [4\mu + \nu(n/2) + m(1 - 2\nu)]\epsilon$$

The speeds of plane waves traveling perpendicular to the uniaxial stress may also be determined from equations (2-1) and are

$$\rho_o V_{22}^2 = \lambda + 2\mu + [2\ell(1 - 2\nu) - 4\nu(m + \lambda + 2\mu)]\epsilon$$

$$\rho_o V_{21}^2 = \rho_o V_{31}^2 = \mu + [(\lambda + 2\mu + m)(1 - 2\nu) + \tfrac{1}{2} n\nu]\epsilon \qquad (2\text{-}3a\text{-}c)$$

$$\rho_o V_{23}^2 = \rho_o V_{32}^2 = \mu + [(\lambda + m)(1 - 2\nu) - 6\nu\mu - \tfrac{1}{2} n]\epsilon$$

The relative changes in wave speed with axial strain may be calculated from equations (2-2 and 2-3) and are, if it is assumed that the relative changes are small,

$$\frac{dV_{11}/V_{11}^o}{d\epsilon} = 2 + [\mu + 2m + \nu\mu\,(1 + 2\ell/\lambda)] / (\lambda + 2\mu)$$

$$\frac{dV_{12}/V_{12}^o}{d\epsilon} = 2 + \nu n/4\mu + m/[2(\lambda + \mu)]$$

$$\frac{dV_{22}/V_{22}^o}{d\epsilon} = -2\nu[1 + (m - \mu\,\ell/\lambda)/(\lambda + 2\mu)] \qquad (2\text{-}4a\text{-}e)$$

$$\frac{dV_{21}/V_{21}^o}{d\epsilon} = (\lambda + 2\mu + m)/[2(\lambda + \mu)] + \nu n/4\mu$$

$$\frac{dV_{23}/V_{23}^o}{d\epsilon} = (m - 2\lambda)/2(\lambda + \mu) - n/4\mu$$

In equations (2-4), the superscript o indicates the wave speed at zero axial strain.

The third order constants, ℓ, m, n, may be evaluated in terms of the relative changes in wave speeds by inverting the set of three equations consisting of either equation (2-4a) or (2-4c) and two of equations (2-4b, d, e). Using the last three of equations (2-4), one may express the constants as

$$\ell = \frac{\lambda}{1 - 2\nu}\left[\frac{1 - \nu}{\nu}\frac{dV_{22}/V_{22}^{o}}{d\epsilon} + \frac{2}{1 + \nu}\left(\frac{dV_{21}/V_{21}^{o}}{d\epsilon} + \nu\frac{dV_{23}/V_{23}^{o}}{d\epsilon}\right) + 2\nu\right]$$

$$m = 2(\lambda + \mu)\left[\frac{\nu}{1 + \nu}\frac{dV_{23}/V_{23}^{o}}{d\epsilon} + \frac{1}{1 + \nu}\frac{dV_{21}/V_{21}^{o}}{d\epsilon} + 2\nu - 1\right] \qquad (2\text{-}5a\text{-}c)$$

$$n = \frac{4\mu}{1 + \nu}\left[\frac{dV_{21}/V_{21}^{o}}{d\epsilon} - \frac{dV_{23}/V_{23}^{o}}{d\epsilon} - 1 - \nu\right]$$

Combining equations (2-4b & d) and equations (2-4a, c, d, e) results in the following relations among relative changes

$$\frac{dV_{12}/V_{12}^{o}}{d\epsilon} = 1 + \nu + \frac{dV_{21}/V_{21}^{o}}{d\epsilon} \qquad (2\text{-}6a,b)$$

$$\frac{dV_{11}/V_{11}^{o}}{d\epsilon} = \frac{dV_{22}/V_{22}^{o}}{d\epsilon} + \frac{2}{1 - \nu}\left[\frac{dV_{21}/V_{21}^{o}}{d\epsilon} + \nu\frac{dV_{23}/V_{23}^{o}}{d\epsilon}\right] + \frac{(1 + \nu)(1 + 2\nu)}{2(1 - \nu)}$$

Equations (2-6a,b) may be used as a redundant check on the accuracy of the measurement of the five relative changes and the applicability of Hughes and Kelly's Theory.

Measurement Technique

The stress induced changes in wave speed were measured in three test specimens machined from lengths of railroad rail. Specimen geometry and origin are given in Table 2-1. The specimens were loaded uniaxially in tension and compression with a conventional testing machine having a maximum capacity of 2.67×10^5 N.

The changes in speed for waves propagating perpendicular to the load axis were measured with commercially available wide band ultrasonic transducers having center frequencies of 2.5 or 5 MHz and coupled directly to the specimen in one of two ways. For a few of the tests, the transducers were bonded to the specimens with a cellulose nitrate cement. However, for most of tests, the transducers were coupled with a viscous resin and held in place with vinyl tape or spring-loaded holders. The method of coupling the transducers to specimen had no apparent effect on the measured wave speed changes provided sufficient time was allowed for the viscous resin layer to achieve equilibrium.

The waves propagating parallel to the load axis were generated and detected with longitudinal transducers mounted on Plexiglas wedges (28° for longitudinal and 55° for shear waves in the specimen) which in turn were clamped to the specimen. The source transducer was a 25.4 mm square PZT-5 plate 1.27 mm thick giving a nominal resonant frequency of 1.61 MHz. A 5 MHz wide band longitudinal transducer was used as a receiver.

Initially several techniques for measuring pulse travel time were compared. The "sing-around" technique [22], although desirable

SPECIMEN No.	DIMENSIONS mm (in.)	
1	607 x 62.4 x 26.2 (23.9 x 2.46 x 1.03)	Head of 115 lb new, control cooled rail, manufactured 1969
3	425 x 67.2 x 14.8 (16.7 x 2.64 x 0.58)	Web of 115 lb new, control cooled rail, manufactured 1969
4	609 x 56.8 x 21.6 (24.0 x 2.24 x 0.85)	Head-70 lb used, non control cooled rail, manufactured 1907

TABLE 2-1a RAIL STEEL SPECIMENS

Nominal Yield Strength	504 MN/m^2 (73 KSI)
Carbon (Percent)	0.67-0.80
Manganese (Percent)	0.70-1.00
Phosphorous, Max (Percent)	0.04
Sulfur, Max (Percent)	0.05
Silicon (Percent)	0.10-0.25

TABLE 2-1b SPECIFICATIONS FOR RAIL STEEL IN SPECIMENS 1 AND 3

because it allowed an automatic and continuous measurement of travel-time as a function of applied load, yielded inconsistent and often unrepeatable travel-time measurement at low stresses because of slight changes in received wave form probably due to change in material damping with stress. Due to the nature of the "sing-around" technique, the wave form changes are manifested as apparent changes in travel-time which could not be separated from the actual changes. A resonant frequency technique utilizing the phase difference between a generated and received CW signal for detecting resonance, which proved to be very sensitive, also yielded inconsistent results at low stress levels probably also due to the damping changes.

The most consistent results were yielded by a pulse overlay technique, a modification of the pulse-echo-overlap method used by Hsu [18] and similar to the pulse superposition described in reference [22]. A schematic of the instrumentation used for this technique is shown in Figure 2-1.

The upper diagram shows the instrumentation used in the earlier wave speed change measurement involving waves propagating perpendicular to the applied load. The variable frequency oscillator (VFO) triggered a gated wave generator which produced ten cycles of a 3 MHz simple harmonic signal. This signal and the amplified received signal were superimposed on the oscilloscope display by adjusting the oscillator period to coincide with time required for the wave to travel across the specimen. Inaccuracies in the travel-time measurement arise largely from errors in superimposing the two oscilloscope traces. The superposition error is a function of the rise times of the signals, the

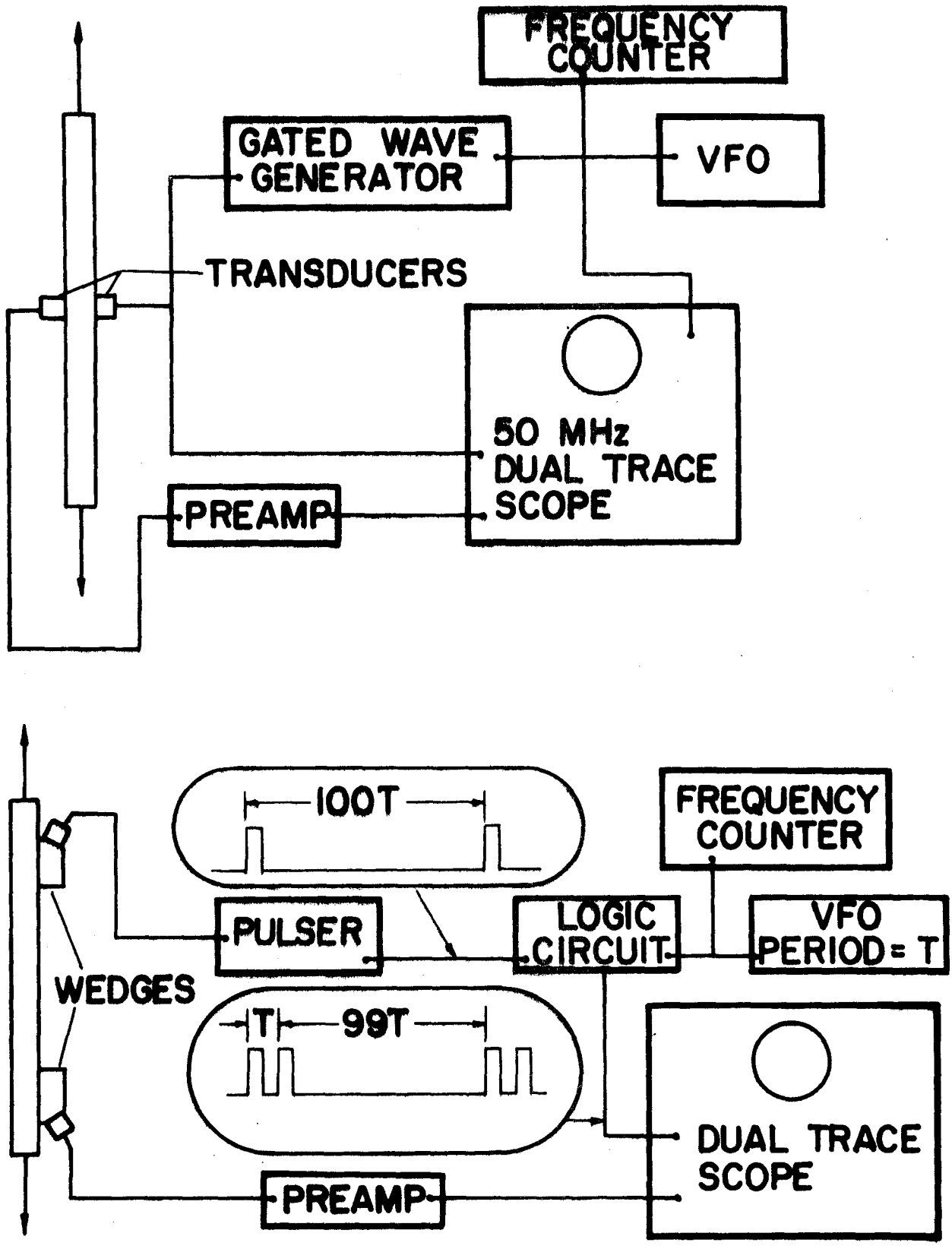

Figure 2-1 Instrumentation for The Acoustoelastic Measurements.

maximum sweep rate of the scope and the scope dc drift which affects the trace position. An estimate of the overall accuracy, which was confirmed by repeating measurements yields a maximum error of 4 parts in 10^5.

The lower diagram in Figure 2-1 shows the instrumentation used for waves propagating parallel to the applied load. The frequency divider and logic network produce two signals as shown. One of these drives the ultrasonic pulser and the second is superimposed on the received pulse for the travel-time measurement.

In order to determine the relative changes in wave speed, the changes in path length due to the specimen strain must be accounted for in the data reduction. For any given wave path, the change in wave speed V (with applied strain) is related to the changes in path length L and travel-time T according to

$$dV/V^o = dL/L^o - dT/T^o \qquad (2\text{-}7)$$

where the subscript zero indicates evaluation at zero load. The term dL/L^o is the nominal strain in the direction of wave propagation. The time T_o is the travel-time of the wave in the specimen which, for waves propagating parallel to the applied load, is the difference between the total travel-time and the wave travel-time in the wedges only. The latter was determined by measuring the wave-travel time with the two wedges placed face to face.

Experimental Results

A plot of the relative changes in wave speed as a function of axial strain for the five types of waves mentioned previously is shown

in Figure 2-2. As predicted by the theory the wave speed changes are linear functions of the strain. The largest relative change in wave speed is associated with longitudinal waves propagating parallel to the applied load. The smallest relative changes are associated with V_{23}, shear waves propagating perpendicular to the load and polarized perpendicular to the load axis.

The acoustoelastic constants defined by equations (2-4) are the slopes of the lines in Figure 2-2. These slopes along with the data from two other specimens are given in Table 2-2. The differences between the wave speed changes in tension and compression are within the range of experimental error and are not considered significant. The last row in Table 2-2 shows the estimated error in the wave speed changes. The total error is a worst case superposition of the errors in the travel-time change, strain, travel-time, material properties and transducer clamping point (for V_{11}, V_{12}) measurements. The large error estimates in the relative changes in V_{23}, V_{22}, and V_{12} are due to the travel path correction (i.e., dL/L^{o} in equation 2-7) being nearly equal to the relative time delay. The scatter in the change in V_{12} is attributed primarily to errors in determining the exact clamping point of the plastic wedges used to generate and detect the shear wave. The inaccuracy in clamping position produces an uncertainity in the path length correction term in equation 2-7 and a significant uncertainity in the relative change in V_{12}.

Table 2-3 shows the second and third order elastic constants for specimens 1 and 4. The second order constants were determined by the customary dilatational and distortional wave speed measurements.

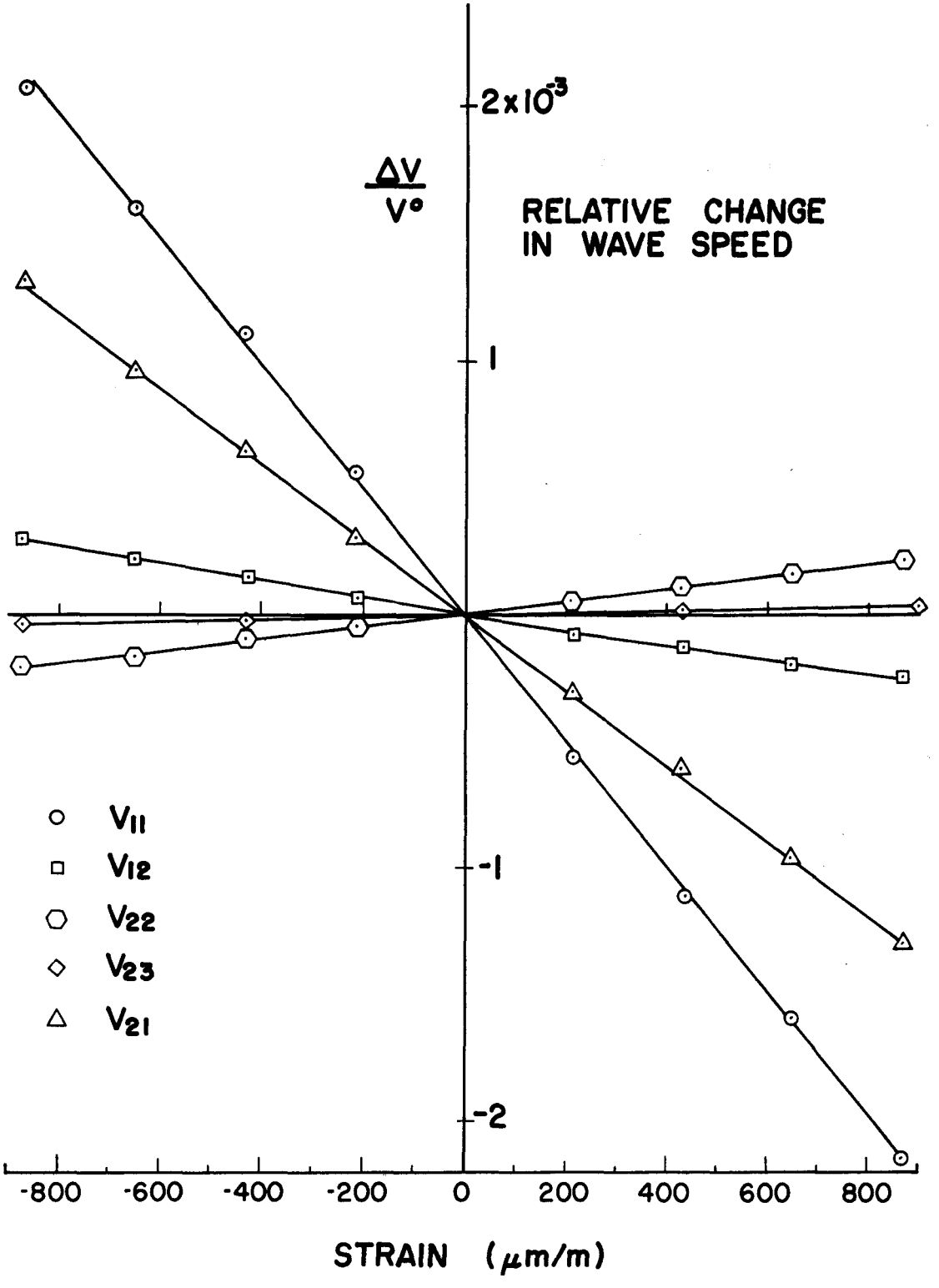

Figure 2-2 Relative Changes in Wave Speeds for Rail Specimen 1.

Specimen No.	Load	$\frac{dV_{21}/V_{21}^{o}}{d\epsilon}$	$\frac{dV_{23}/V_{23}^{o}}{d\epsilon}$	$\frac{dV_{22}/V_{22}^{o}}{d\epsilon}$	$\frac{dV_{11}/V_{11}^{o}}{d\epsilon}$	$\frac{dV_{12}/V_{12}^{o}}{d\epsilon}$
1	T	-1.50	-0.09	+0.27	-2.38	-0.15
1	C				-2.45	-0.20
3	T				-2.40	-0.35
3	C				-2.44	-0.27
4	T	-1.51	+0.06	+0.28	-2.47	-0.33
4	C	-1.53	+0.06	+0.27	-2.45	-0.32
Estimated Maximum Error		$\pm$ 2.3%	$\pm$ 62%	$\pm$ 24%	$\pm$ 7.5%	$\pm$ 29%

* (T) Tension; (C) Compression

TABLE 2-2 Summary of Acoustoelastic Constants

Specimen No.	ρ_o kg/m^3	λ N/m^2 x10^{10}	μ N/m^2 x10^{10}	ℓ N/m^2 x10^{10}	m N/m^2 x10^{10}	n N/m^2 x10^{10}	$\frac{dV_{11}/V_{11}^o}{de}$	$\frac{dV_{12}/V_{12}^o}{de}$
1	7800	11.58	7.99	-24.8	-62.3	-71.4	-2.52	-0.25
4	7799	11.07	8.24	-30.2	-61.6	-72.4	-2.55	-0.22
Estimated Error	± 0.3%	± 2.3%	± 2.3%	± 2.8%	± 4.1%	± 2.7%	± 12%	± 24%

TABLE 2-3 Second and Third Order Elastic Constants for Two Samples of Rail Steel

SOURCE	$\frac{dV_{21}/V_{21}^{o}}{d\epsilon}$	$\frac{dV_{23}/V_{23}^{o}}{d\epsilon}$
Present Study	-1.51	+0.06
Ref 1	-1.58	+0.05
Ref 5	-1.6	0
Ref 6	-1.44	+0.05

TABLE 2-4 Comparison of Measured Acoustoelastic Constants for Steel

The third order constants were calculated from equations (2-5a-c) using the relative changes in V_{21}, V_{23} and V_{22} shown in Table 2-2. The relative changes in V_{11} and V_{12} per unit strain shown in Table 2-3 were determined from the measured changes in V_{21}, V_{23}, V_{22} and equations (2-6a,b). As can be seen the values in the last columns of Table 2-3 are in reasonable agreement, considering the estimated errors, with their measured counterparts shown in the last two columns of Table 2-2.

A comparison of measured relative changes in wave speed per unit strain for steel from several sources is shown in Table 2-4. The agreement is remarkably good considering the difficulty of the measurement. It should be noted that although several specimens were evaluated in reference [19], sufficient data to calculate the relative change per unit strain was given for only one specimen and that one exhibited the lowest travel-time changes of the group.

DESIGN OF AN ULTRASONIC PROBE FOR LONGITUDINAL STRESS MEASUREMENT

The general configuration of the probe was determined in phase I [1]. Since the acoustoelastic effect is greatest for longitudinal waves propagating in the direction of the applied stress, at minimum, the probe should be capable of propagating and receiving a longitudinal wave parallel to the rail axis. The measurements of longitudinal wave speeds in several samples of new and used rail reported in reference [1] indicated that if an absolute measure of stress is needed a reference wave speed would probably be necessary. For this reason, the probe was designed to propagate and receive surface (or shear) wave parallel to the rail axis.

The same data also indicated that the variations in longitudinal, surface and shear wave speeds for several samples of new and used rail were smaller in the rail web as compared to the rail head. The smaller variations make the web the more desirable portion of the rail in which the wave speeds are measured. Further, using the rail web allows measurement on two opposite surfaces which has the advantage of cancelling the effects of surface curvature by averaging. The data presented in section 2 showed that the relative change in speed for longitudinal waves propagating along the direction of the applied stress is

$$\frac{dV_L/V_L^o}{d\epsilon} = -2.45 \qquad (3\text{-}1)$$

where V_L - speed of longitudinal waves

V_L^o - speed of longitudinal waves in the absence of stress

ϵ - longitudinal strain corresponding to stress σ.

The relative change in travel-time may be shown to be

$$\frac{d(t_L/t_L^o)}{d\epsilon} = +2.45 \qquad (3\text{-}2)$$

or, in terms of the change of applied stress $d\sigma$

$$dt_L = \frac{2.45\ t_L^o}{E}\, d\sigma \qquad (3\text{-}3)$$

where E is Young's modulus.

Proceeding in the same manner, the change in transverse wave travel-time may be shown to be

$$dt_T = \frac{0.25\ t_T^o}{E}\, d\sigma \qquad (3\text{-}4)$$

With the exception of probe I, the probes described below are designed to measure the wave travel-times over a nominal distance of 216 mm (8.5 in). Typical wave speeds in rail steel are 5900 m/sec (2.32×10^5 in/sec) and 3230 m/sec (1.27×10^5 in/sec) for longitudinal and transverse waves, respectively. Hence the expected changes in travel-times are 0.44 nsec/MN/m^2 (3 nsec/ksi) and 0.09 nsec/MN/m^2 (0.6 nsec/ksi) respectively.

The probe design evolved through a series of four steps. The electronic instrumentation for generating and detecting the ultrasonic waves and for measuring the wave travel-times was identical for all of the probes.

Instrumentation for Travel-Time Measurements

The electronic instrumentation used for the travel-time measurements is shown in figure 3-1. Although similar to the instrumentation used for the measurement of the acoustoelastic constants, figure 2-1,

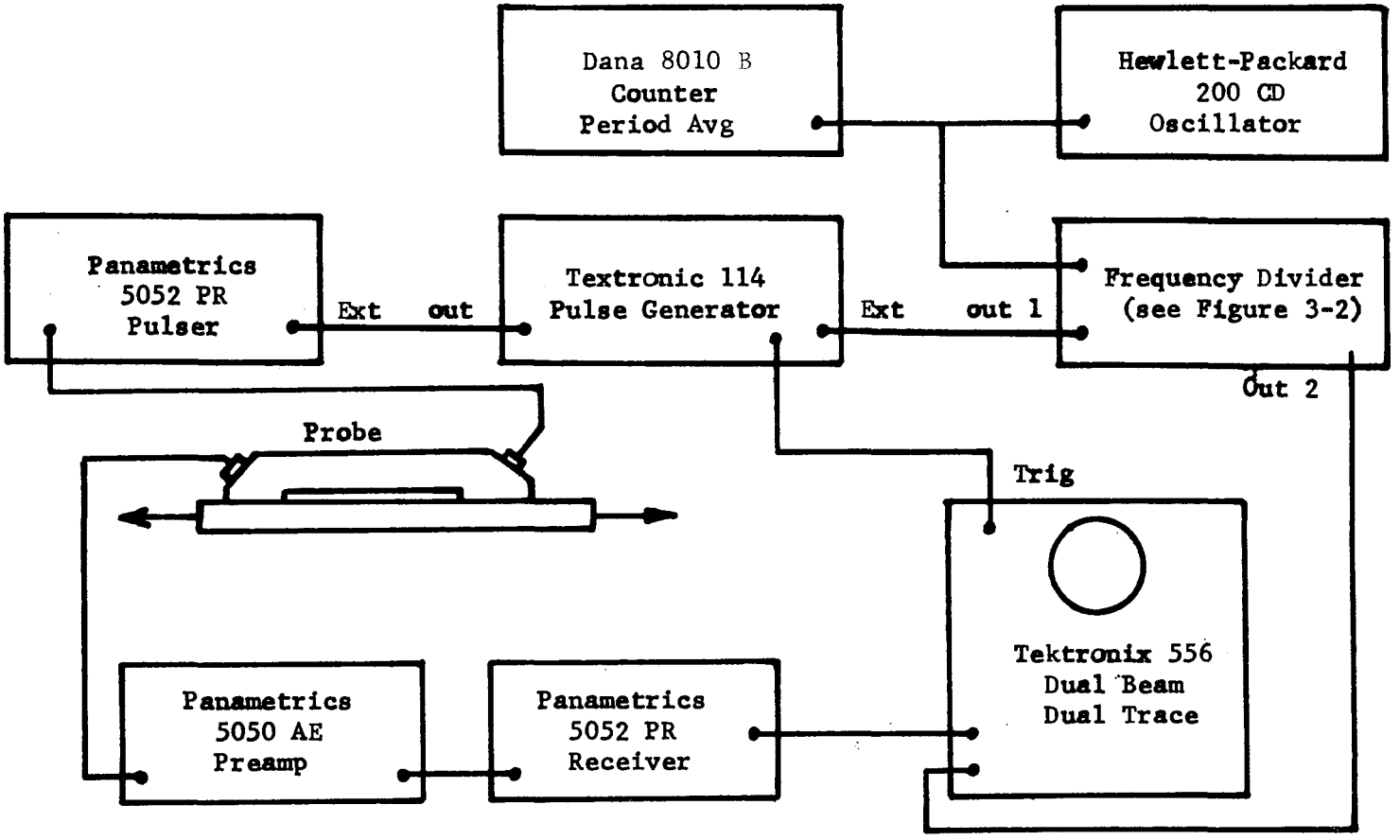

Figure 3-1 Electronic Instrumentation for Travel-Time Measurements

the changes shown resulted in better performance. The oscillator drives a frequency divider, shown in figure 3-2, which produces a single pulse (out 1) with a period of 100 times the oscillator period, T. As shown in figure 3-2, a double pulse (out 2) having a separation of period T is also generated. The leading edges of the single pulse and the first double pulse are coincident. The single pulse is used to trigger a short duration pulse from the pulse generator which in turn drives the transsucer pulser. The received signal is amplified 40 db in the preamp and further amplified from 10-30 db in the receiver. A typical received signal is shown in figure 3-3a. This signal and the double pulse are superimposed on the scope. The oscillator period is adjusted such that the leading edge of the second pulse coincides with the first positive going zero crossing of the received signal as shown in figure 3-3b. The time from pulse initiation to reception of that zero crossing then equals the oscillator period which is measured to 0.1 nanosecond by averaging over 1000 periods and then rounded to 1 nanosecond.

The accuracy of the travel-time measurements with this system is about 3 nanoseconds. The major cause of inaccuracy in the measurement is in superimposing the two traces. Nevertheless these errors were found to be less than variations introduced by other sources.

Probe I

A photograph of the first version of the probe is shown in figure 3-4. It consisted of four ultrasonic transducers bonded to a one-piece machined Plexiglas body. The body was designed such that the angle between the normal to the transducer surface and the normal to the rail surface

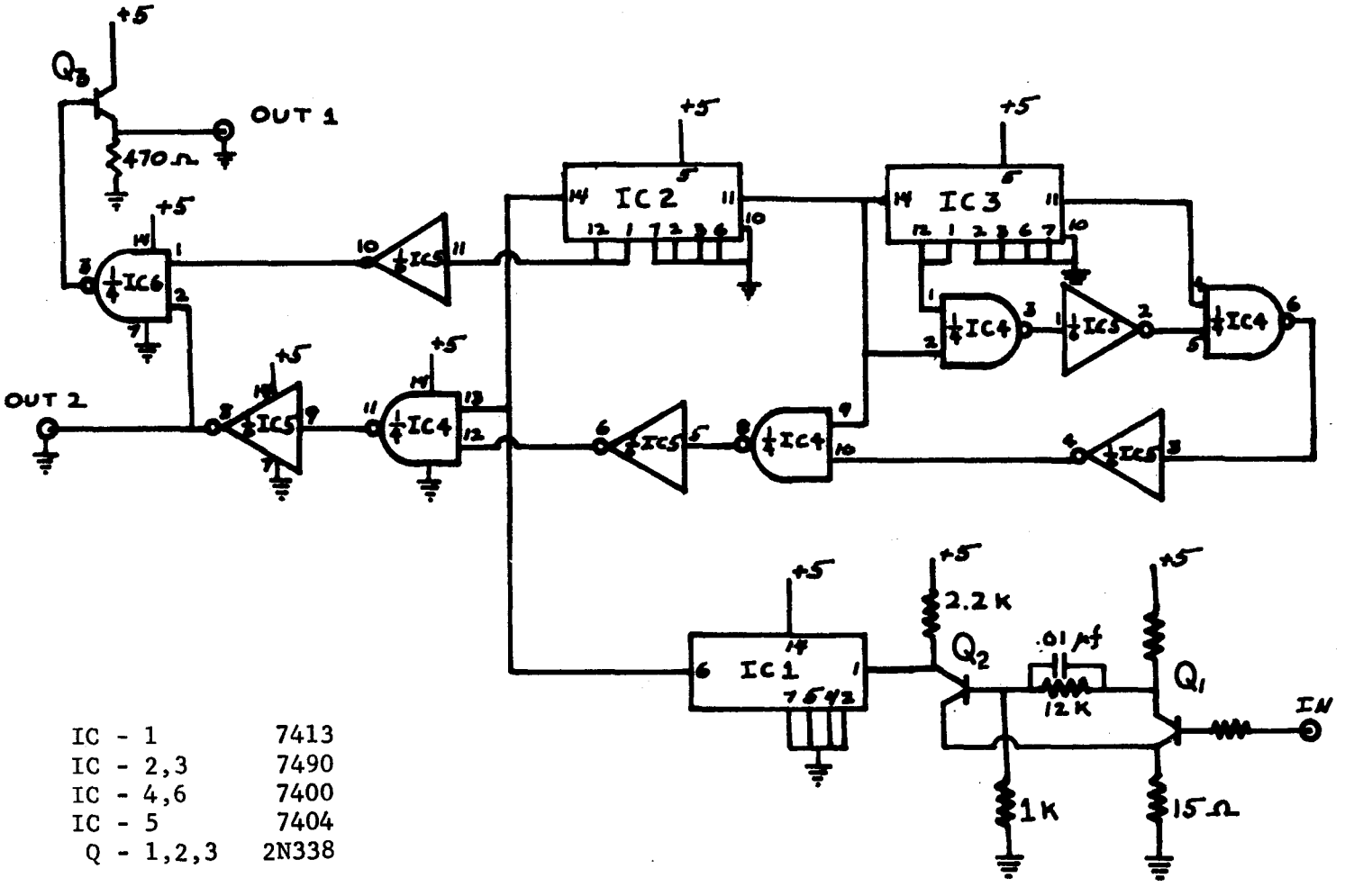

IC - 1	7413
IC - 2,3	7490
IC - 4,6	7400
IC - 5	7404
Q - 1,2,3	2N338

Figure 3-2 Schematic Diagram of Frequency Divider.

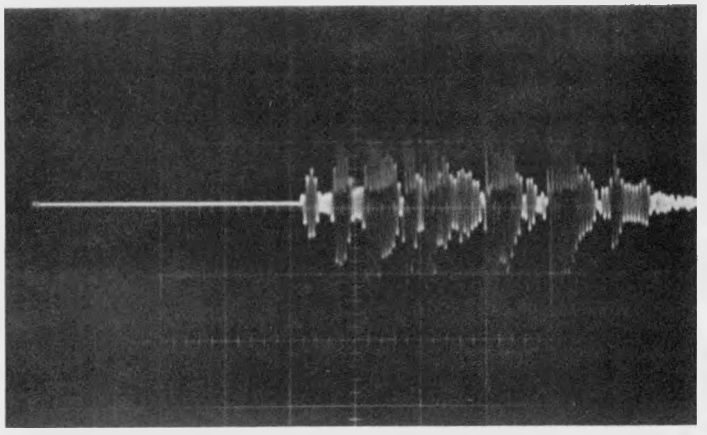

(a) Sweep speed 10 μs/cm

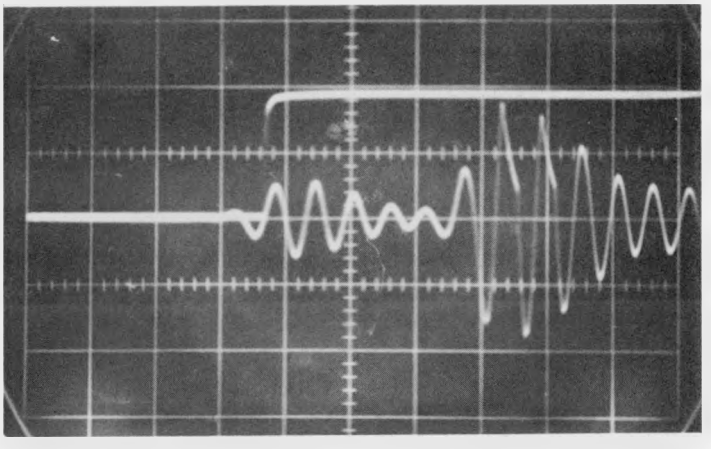

(b) Sweep delay 35 μs ; sweep speed 1 μs/cm

Figure 3-3 Typical Oscilloscope Traces for Travel-Time Measurements

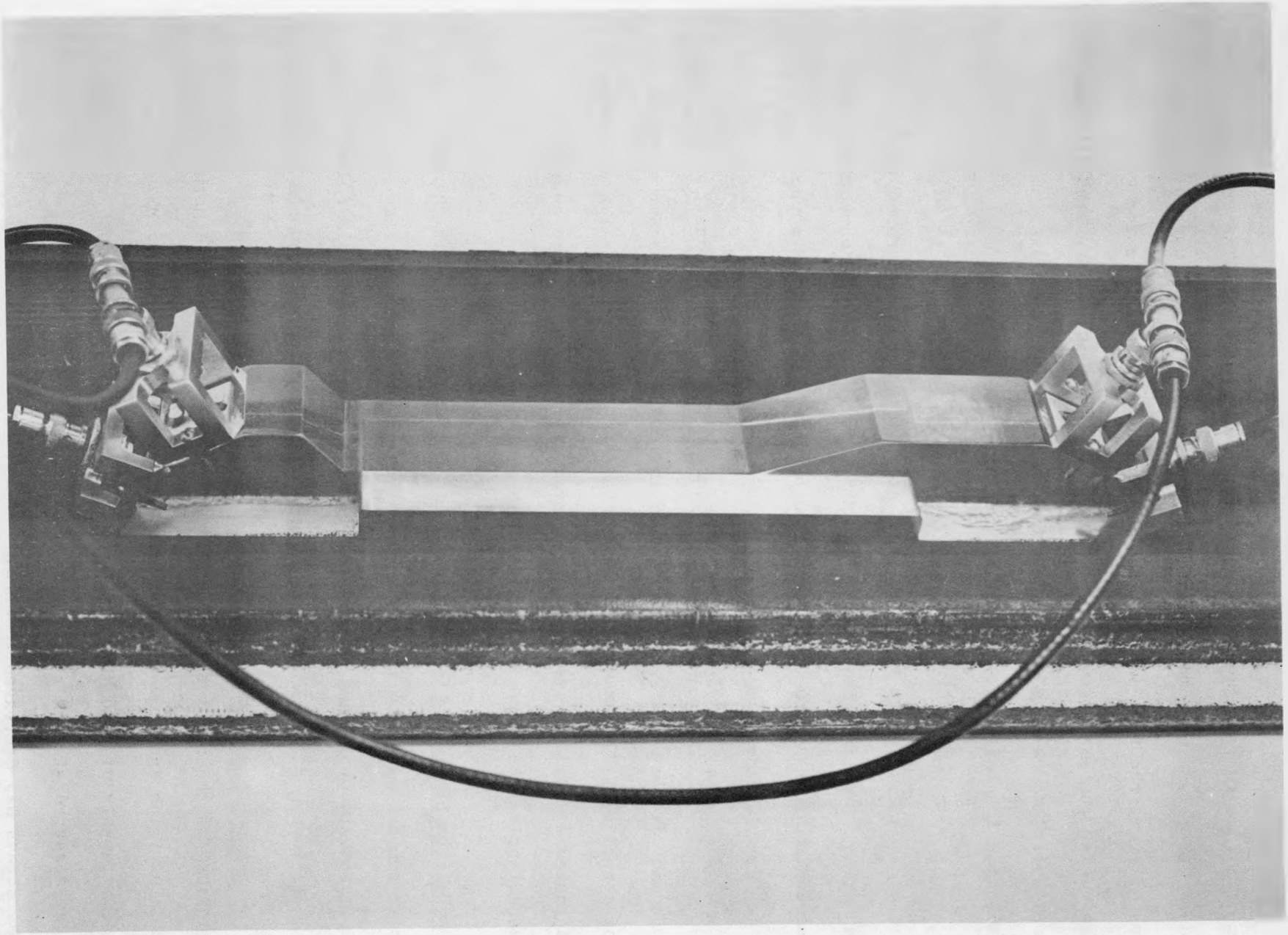

Figure 3-4 Probe I Rail Stress Measurement Assembly

was 28^{o} for two transducers and 67^{o} for the other pair. The 28^{o} transducer pair were used to generate and detect longitudinal wave propagating parallel to the rail surface; the 67^{o} transducer pair were for generating and detecting surface waves. The probe was held in contact with the rail web by large C clamps bearing on the flat parts of the Plexiglas body adjacent to the longitudinal wave transducers.

The transmitting and receiving trandsucers were 25.4 mm (1 in) square PZT-5 plate of thickness 1.27 mm (0.050 in). The transducers have a nominal resonant frequency of 1.6 MHz. The electrical connections were made through BNC connectors supported by machined aluminum supports bolted to the Plexiglas body as shown.

Two nominally identical versions of probe I were constructed. One was made for use on flat surfaces and the other for the concave surface of a rail web. The convex mating surface of the second version was constructed by milling the Plexiglas surface to the approximate shape and hand lapping the probe to the rail web surface.

Evaluation of Probe I - The accuracy of the probe for stress change measurements was evaluated by repeated longitudinal and surface wave speed measurements on a 12.7 x 76.3 x 914 mm (0.5 x 3 x 36 in) cold rolled steel bar subjected to uniaxial tensile loads. A measurement sequence consisted of the following steps. The total travel-times of both waves on both surfaces of the specimen were measured before it was placed in the testing machine. The specimen was subjected to stresses up to 166.5 MN/m^2 (24.1 ksi) in increments of 41.6 MN/m^2 (6.03 ksi). Travel-times for both wave types were measured at each stress increment up to the maximum and repeated as the stress was decreased to zero.

A plot of the typical results is shown in figure 3.5. As can be seen the travel-times and hence wave speeds show measurable differences on the two sides of the specimen. Also notable is the nonlinear behavior of the change in travel-time as a function of applied stress. Both of these effects can be explained by assuming the presence of an initial curvature in the bar.

The initial curvature in the specimen gives rise to a bending moment on the cross-section due to the eccentricity of the applied load. This is illustrated in figure 3-6. Since δ is large at low loads the stress at the lower surface increases at a faster rate than the stress at the upper surface. As P increases the bar tends to straighten, hence δ decreases. At the higher loads, the slopes of the stress vs. load diagram for the two surfaces approach each other. The behavior of the wave speeds as P changes will show the same nonlinear behavior.

In figure 3-5, the average of the data taken on the two surfaces is shown by the dashed line. The average total travel-time shows a nearly linear change with applied stress as would be predicted from the simple model of figure 3-6. The change in average total travel-time agrees quantitatively with the changes expected from the acoustoelastic data measured earlier, Table 2-2, even though the acoustoelastic data was obtained from specimen of rail steel.

A statistical analysis of the errors encountered using the probe on the specimen showed short term accuracy of 7.6 MN/m^2 (1.1 ksi) which is considered to be the best attainable with this type probe. A long term bias in the measurements was also observed and later found to be a function of temperature.

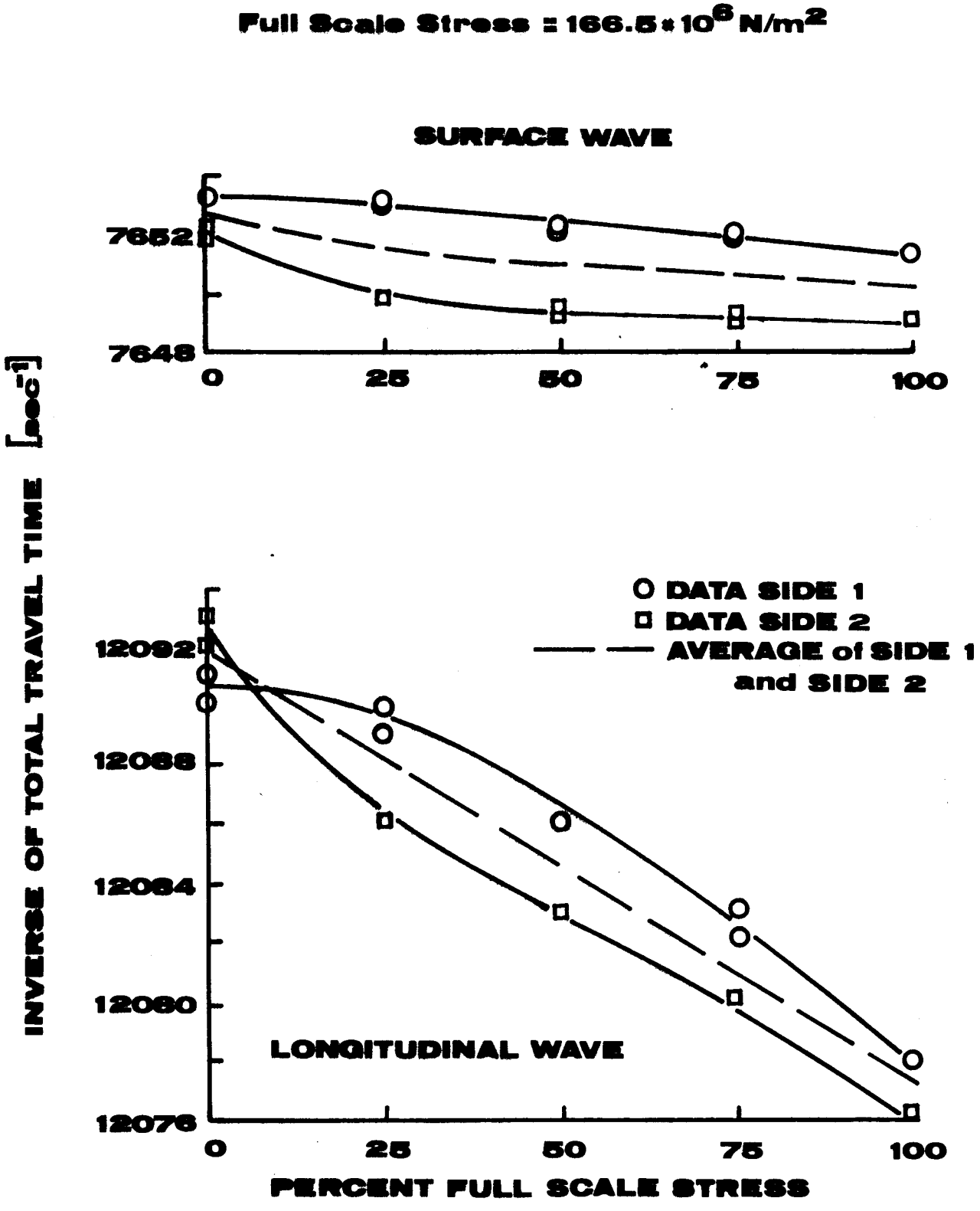

Figure 3-5 Total Travel-Time Measurements with Ultrasonic Probe Assembly.

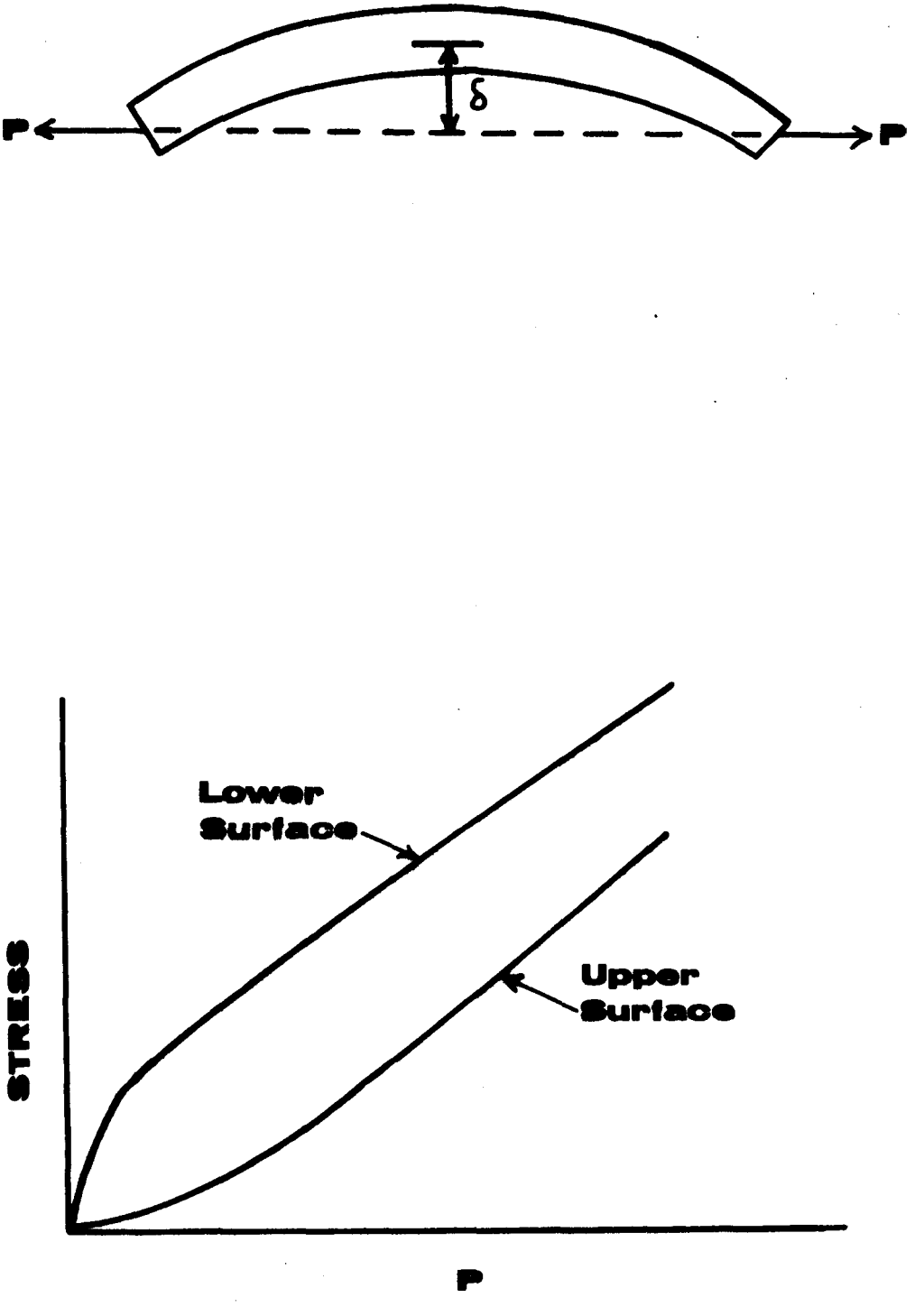

Figure 3-6 Illustration of the Effect of Initial Curvature on The Surface Stresses

Temperature Effects - The temperature dependency of the probe measurements can be seen from the data presented in figure 3-7. These data are measurements made with probe I on a stress free specimen machined from the head of a rail. The measurements were made over a period of three weeks. The straight line shows the expected variation of inverse travel times due to changes of temperature only. The agreement verifies that temperature has a significant effect on the measurements.

The effect of temperature on the inverse travel times of probe I is shown in figure 3-8. These data were collected by subjecting the probe mounted on a reference bar to a range of temperatures from $0^{o}C$ to $50^{o}C$. A small environmental chamber was used to control the temperature of probe and bar, with sufficient time being allowed for the probe and bar to reach thermal equilibrium. Note that the change in f_s per unit change in f_L is equal to the ratio of slopes in figure 3-8. That ratio is numerically equal to 0.63.

As indicated in the interim report [1], the temperature induced variations in the speed of ultrasonic waves are quantitatively comparable (for the temperature changes expected in a field environment) to the expected stress induced changes. Thus temperature is an important variable in the application of the acoustoelastic technique to rail stress measurement.

Although a comprehensive survey [23] of the influence of temperature on the elastic constants (from which the wave speeds may be determined) of a number of commercial steel alloys is available, the composition and heat treatment of the materials for which data is presented is sufficiently different to make quantitative use questionable especially for the high

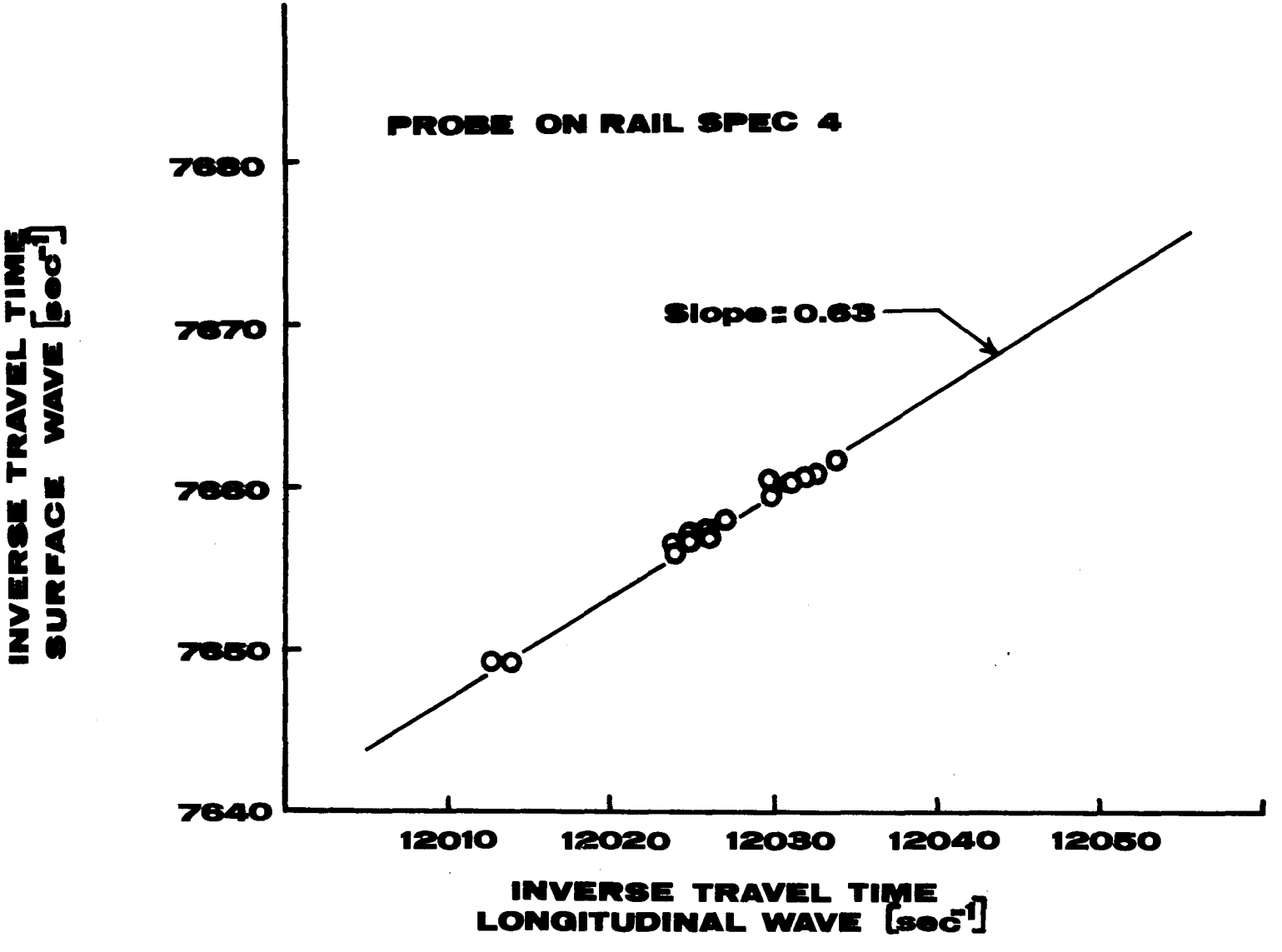

Figure 3-7 Inverse Travel-Time Measurements on Reference Bar.

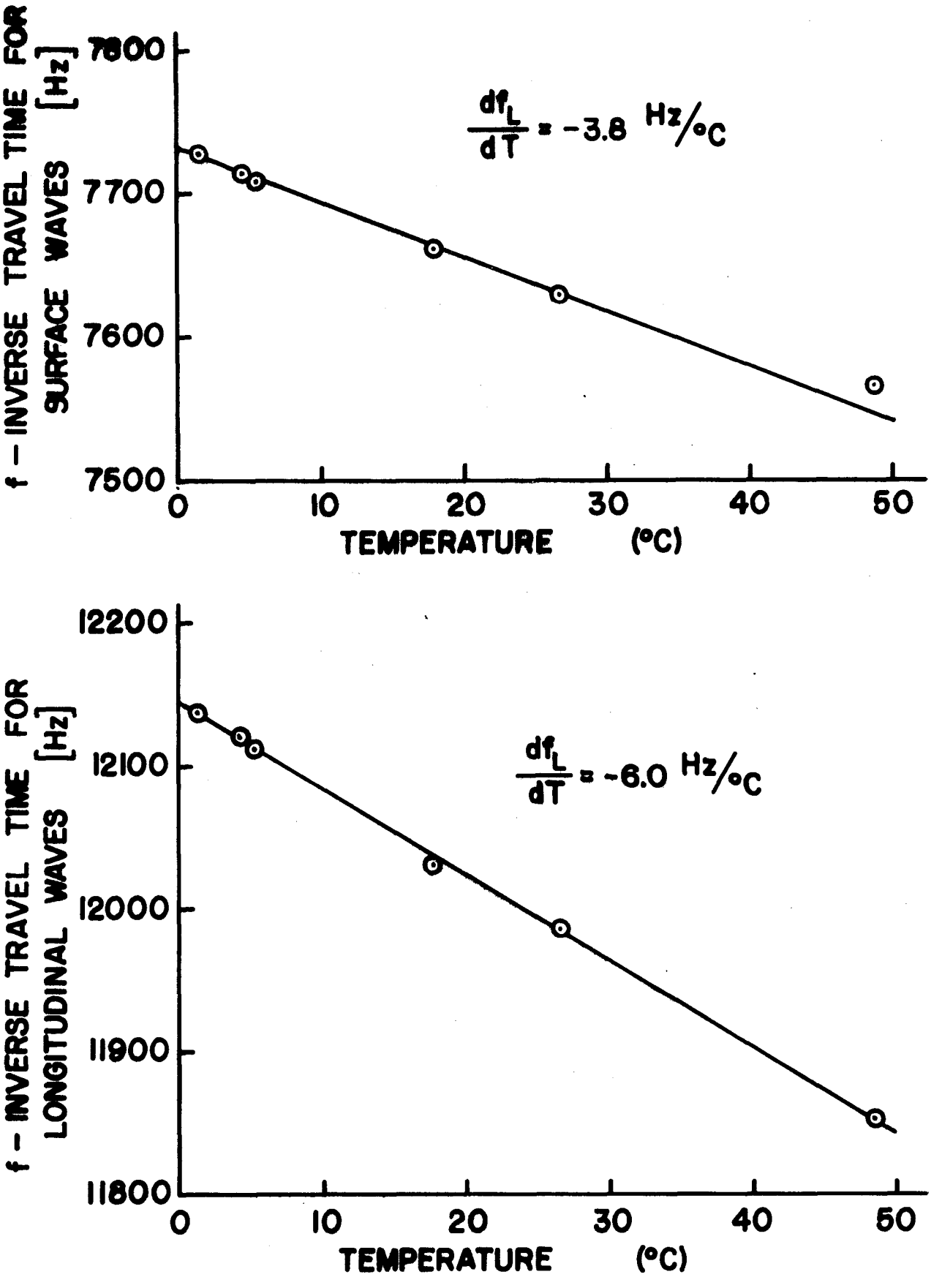

Figure 3-8 The Effect of Temperature on Inverse Travel Time Measurements Made with Probe I.

precision needed here. Hence a limited experimental study of the temperature induced changes in wave speeds was undertaken.

The effects of temperature on the wave speeds of rail steel are shown in figures 3-9, 3-10 and 3-11. The sample of dimensions 25.4 x 52.7 x 152 mm (1 x 2 x 6 in) was taken from the head of a 70 lb noncontrol cooled rail manufactured in 1907. The wave speeds were determined by a pulse echo technique using the same instrumentation devised for the acoustoelastic measurements. Commercial ultrasonic transducers (Panametrics 5 MHz wide band longitudinal and Panametrics 2.5 MHz wide band shear) were coupled to the specimen with a light oil for the longitudinal waves or a viscous resin for the shear waves. At the higher temperatures the shear wave transducer was bonded to the surface with a cellulose-nitrate based cement. The travel-time between the first and second reflection was determined by independently subtracting the measured times from pulse initiation to the first zero crossing of each reflection. This method of determining the wave travel-time eliminates temperature effects in the transducer and couplant layer. The wave speeds were calculated using the path length (105.4 mm) at 21.2^{o}C and correcting for the change in path length due to thermal expansion. The coefficient of thermal expansion used for the correction (11.2 x $10^{-6}/^{o}$C) was obtained from reference 24 and is representative of data for medium carbon steels (0.6-1.2%C) in the range 0-100^{o}C.

A small 300 x 300 x 300 mm (12 x 12 x 12 in) environmental chamber was used to control the specimen temperature. The accuracy of the wave speed measurement is estimated to be 1 part in 10^{5}. Accuracy of the temperature measurements was 0.1^{o}C. However, the largest source of error in

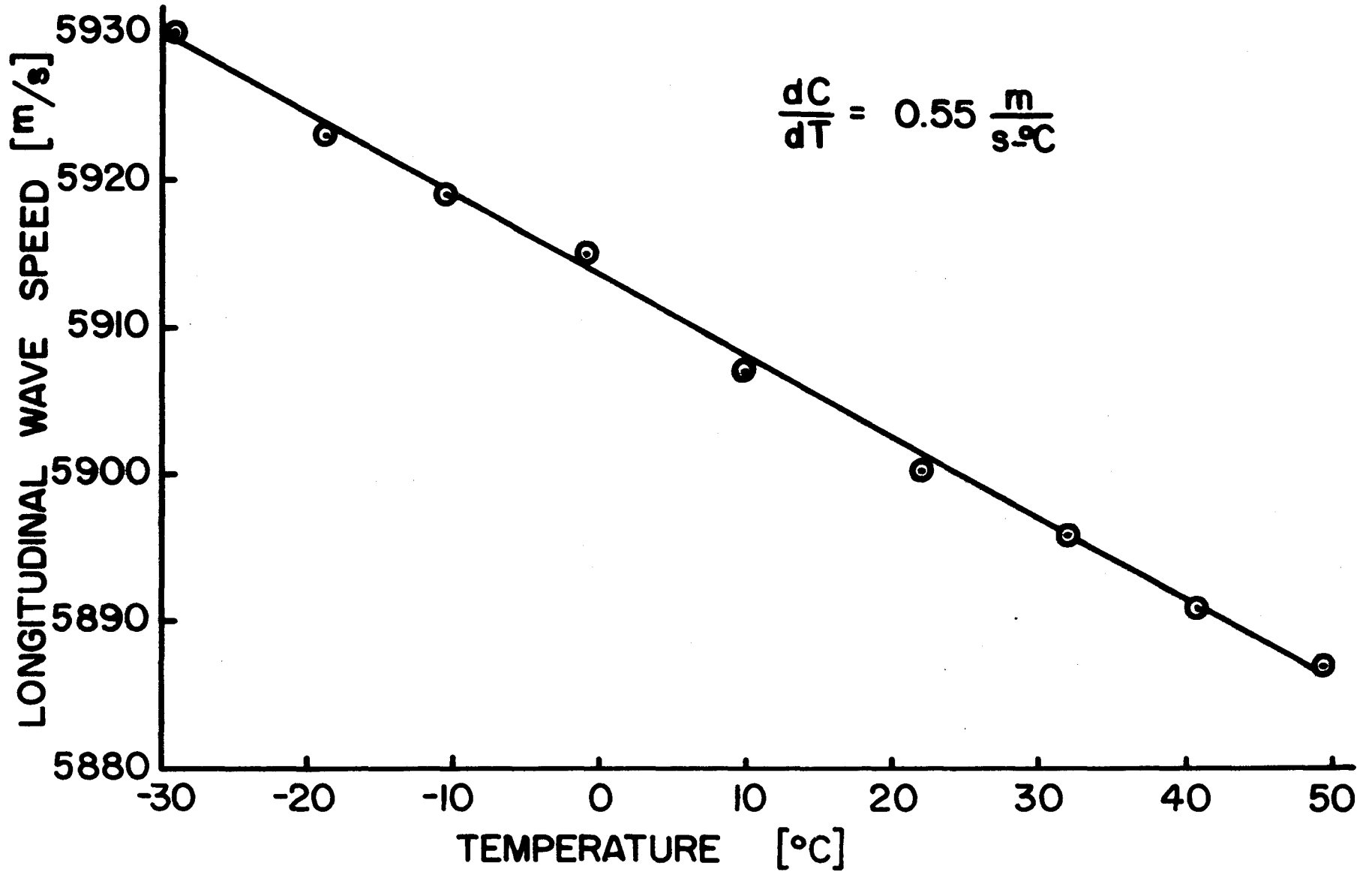

Figure 3-9 Temperature Dependence of the Speed of Longitudinal Waves Propagating Parallel to The Longitudinal Axis of The Rail.

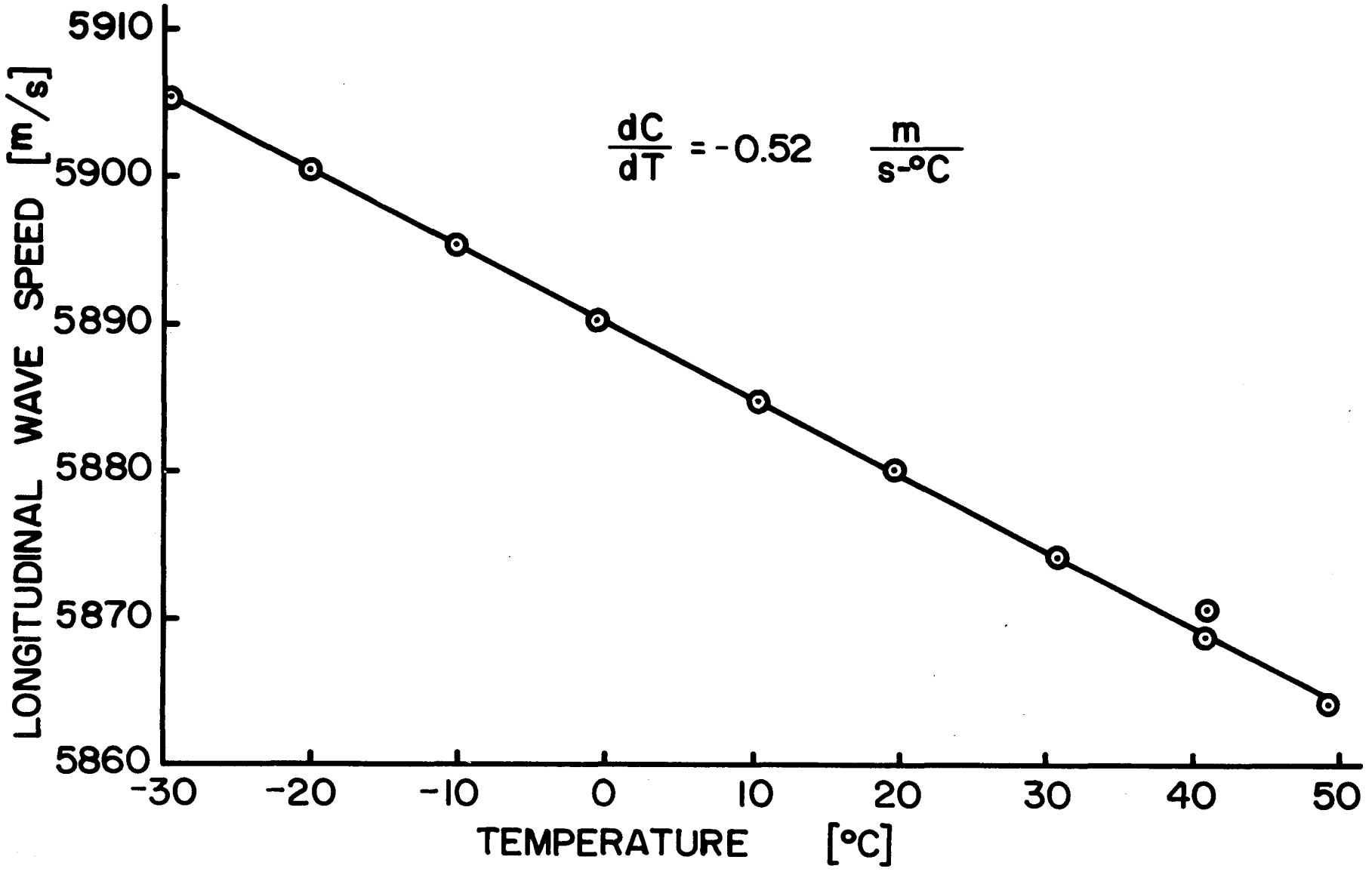

Figure 3-10 Temperature Dependence of the Speed of Longitudinal Waves Propagating Perpendicular to The Longitudinal Axis of the Rail.

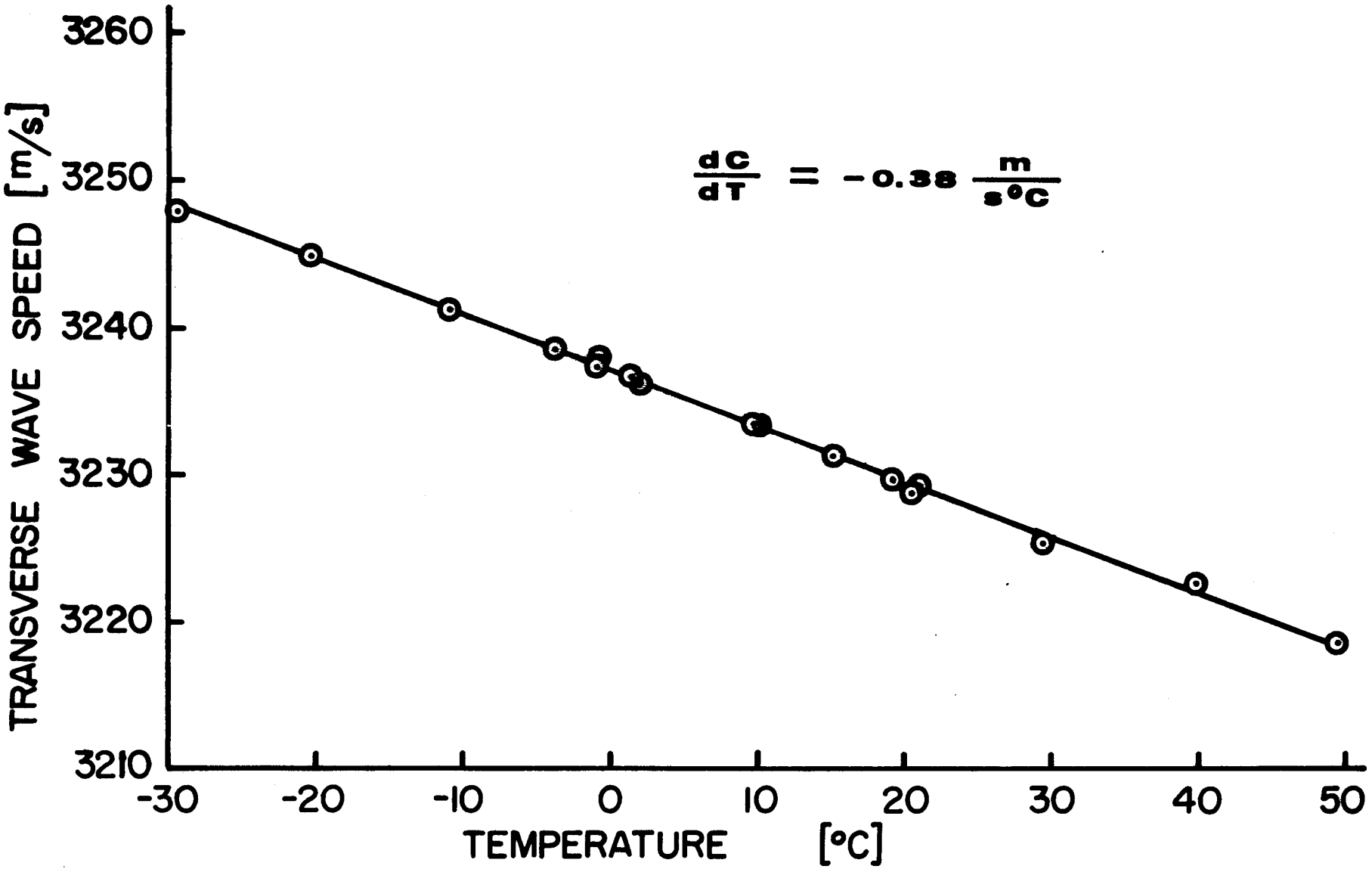

Figure 3-11 Temperature Dependence of Transverse Wave Speed in Rail Steel.

the measurement was probably due to variations in temperature in the specimen caused by the environmental chamber controller cycling. For the data points shown approximately fifteen minutes were allowed for the specimen to reach thermal equilibrium.

The slopes of the lines in figures 3-10 and 3-11 give the relative change in wavespeed per unit change in temperature and are (at $20^{o}C$)

$$\frac{dC_1/C_1^o}{dT} = -0.884 \times 10^{-4}/^{o}C \text{ for longitudinal waves}$$

$$\frac{dC_2/C_2^o}{dT} = -1.176 \times 10^{-4}/^{o}C \text{ for transverse waves}$$

A calculation of relative change in wave speed per unit temperature change using the experimentally determined changes in elastic moduli for a 1% carbon steel (drill rod) [23] yields the following values

$$\frac{dC_1/C_1^o}{dT} = -0.61 \times 10^{-4} \text{ per } ^{o}C$$

$$\frac{dC_2/C_2^o}{dT} = -1.01 \times 10^{-4} \text{ per } ^{o}C$$

These values, though not corrected for adiabatic effects, are in reasonable agreement with the data for rail steel.

The temperature dependence of the speed of longitudinal waves in plexiglas is shown in figure 3-12. The technique used for these measurements is the same as that used for rail steel above. A comparison of figure 3-12 to figures 3-9, 3-10, 3-11 shows that that the temperature induced changes in wave speed in the plexiglas are significantly greater than that in rail steel.

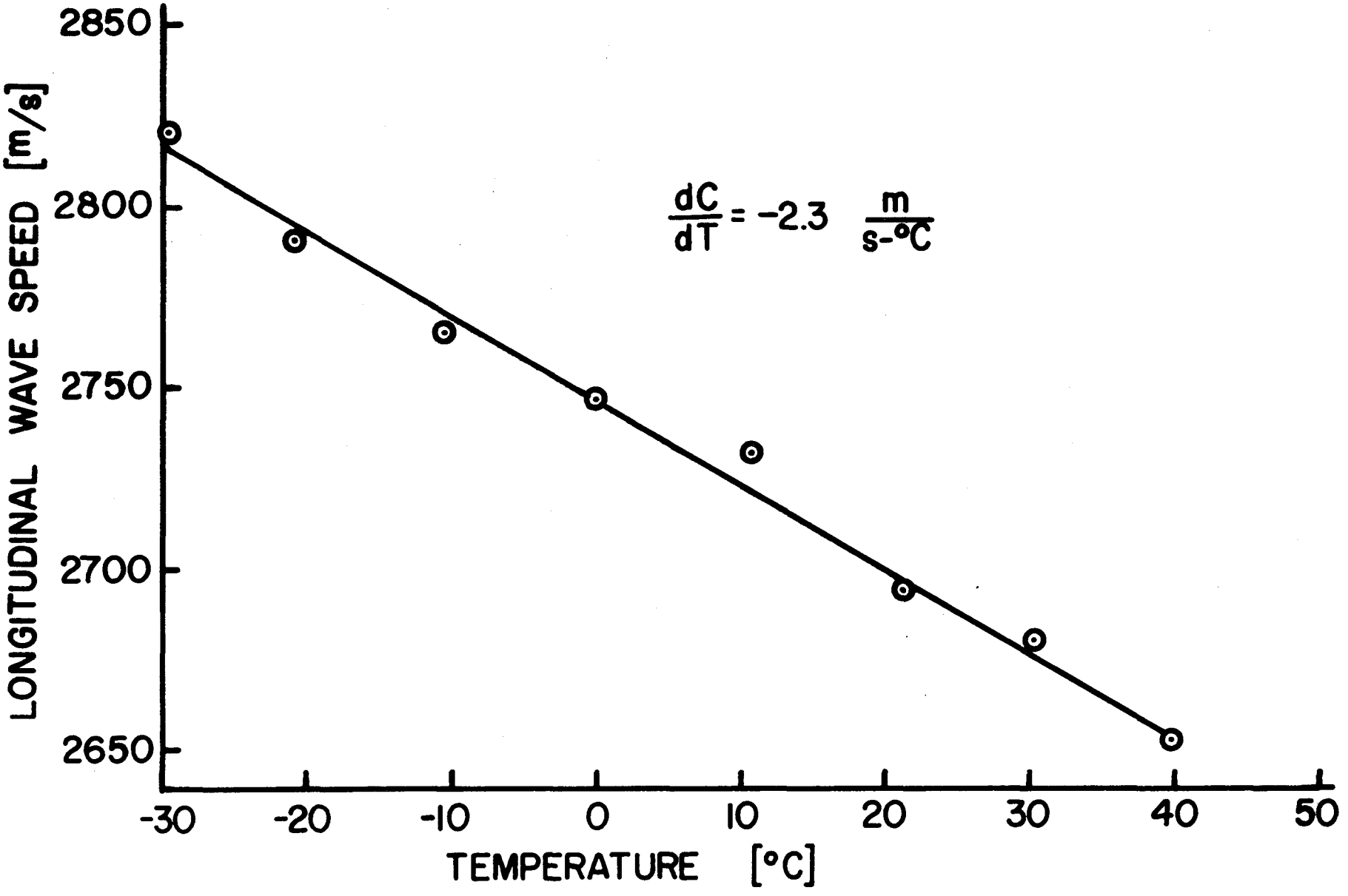

Figure 3-12 Longitudinal Wave Speed as a Function of Temperature for Plexiglas.

A calculation of the relative effects on f_L and f_S due to the three effects of (1) the change in longitudinal wave speed in the plastic wedges, (2) the change in longitudinal or shear wave speeds in the steel, and (3) the change in length of the plastic probe assembly due to the thermal expansion of the plastic yields the data shown in Table 3-1.

Obviously the combined effects of the changes in wave speed and the thermal expansion of the plastic in the probe assembly are significantly greater than the temperature induced wave speed changes in the steel.

The conclusion drawn from the analysis shown in Table 3-1 along with the results presented in the previous section is that the temperature induced change in wave speed in the plastic wedge is the main source of the irrepeatability shown in the rail measurements and that the probe design must be altered to eliminate this thermal effect.

Probe II

The second probe design differs from the original concept in two basic features. First, it is a differential device, that is, in order to determine travel-time the times for the wave to propagate two different distances are subtracted. As shown schematically in figure 3-13a the wave is generated at point A and detected at both points B and C. The travel-times from A to B, t_{AB}, and from A to C, t_{AC}, are measured and the travel-time from B to C, t_{BC}, found by subtracting t_{AB} from t_{AC}.

The advantage of using a differential technique is that the changes induced by extraneous factors are subtracted out of the final travel-time measurement provided the changes affect both of the measured

Source of Temperature-Induced Change	$\frac{df_L}{dT}$ Hz/°C	$\frac{df_S}{dT}$ Hz/°C
Longitudinal Wave Speed in Plastic	-4.7	-2.2
Wave Speed in Steel	-0.6	-0.7
Thermal Expansion in Plastic	-0.6	-0.5
Total	-5.9	-3.4

TABLE 3-1 Analysis of the Relative Effects of the Three Sources of Temperature Induced Changes in f_L and f_S

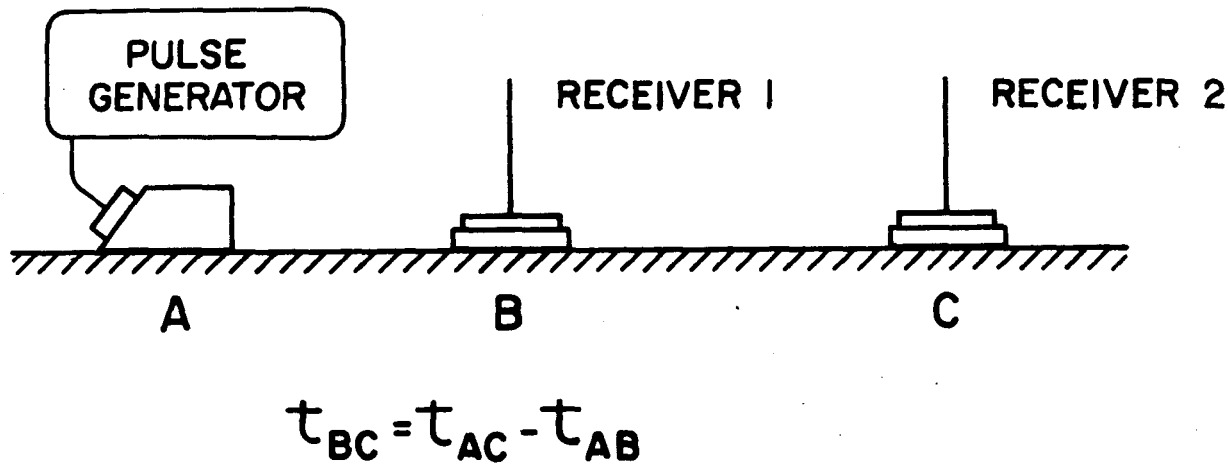

Figure 3-13a Differential Technique for Measuring Travel Times.

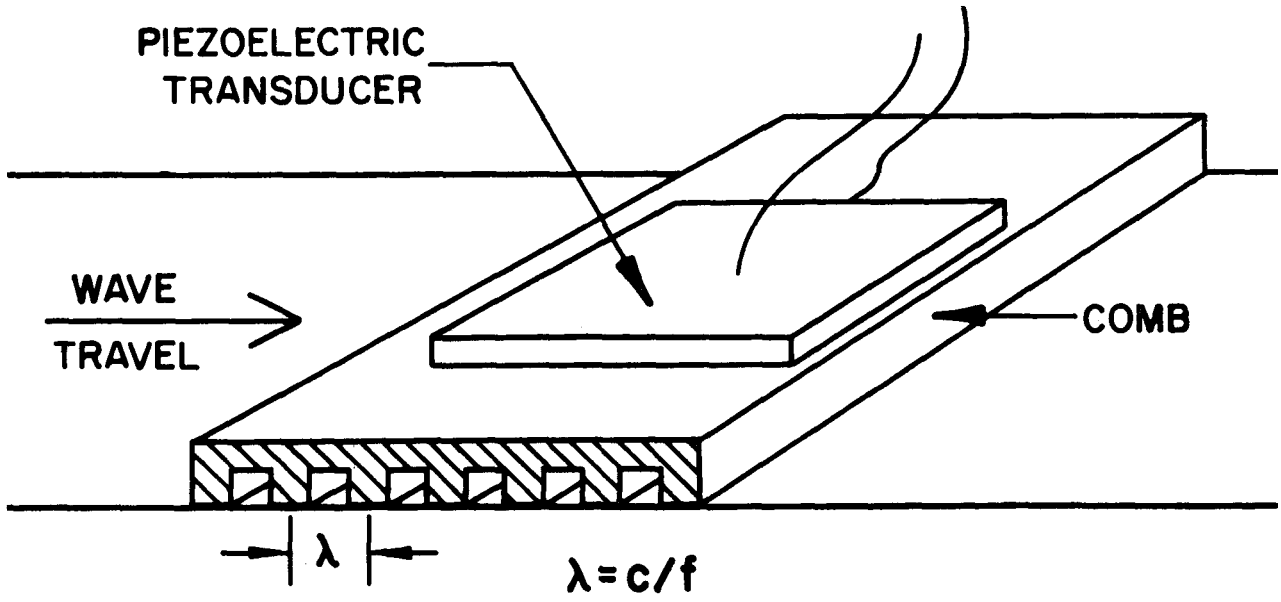

Figure 3-13b Metal Comb for Detection of Waves.

times equally. Thus, changes in the travel-time induced by irregularities in surface condition will affect both t_{AB} and t_{AC}. However, if the effects are equal, the difference t_{BC} will not be affected.

The second feature employed was the use of metal combs for the receiving transducers in place of plastic wedges as shown in figure 3-13b. The comb is a thin metal plate in which rows of equally spaced grooves are machined. The grooved surface is placed in contact with the surface of the piece in which the wave is propagating. The grooves are situated perpendicular to the direction of wave travel. A piezoelectric transducer is attached to the top surface of the comb. The grooved plate acts as a mechanical filter passing those disturbances whose wavelength equals the groove spacing. In the present case, the generating transducer produces a wave whose frequency is 1.6 MHz. Hence, the groove spacing should be 1.8 mm (0.07in) for surface waves and 3.3 mm (0.13 in) for the longitudinal waves.

A two view drawing of probe II is shown in figure 3-14. The plexiglas surface and P wave generators are clamped between two side rails. The surface and P wave combs are mounted in the steel comb holders. The combs were machined of brass which was used to improve the impedance match between the transducers and the steel rail. The rear comb holder is also attached to the side rails by machine screws. The spacing between the two comb holders is maintained by a thin steel flexure. This flexure allows the rear comb holder to be firmly clamped to the rail web while the front comb holder is in contact with the rail or raised off the rail surface. In order to avoid changes in surface wave speed, the front combs must be raised off the rail surface when measurements are being made with the rear combs.

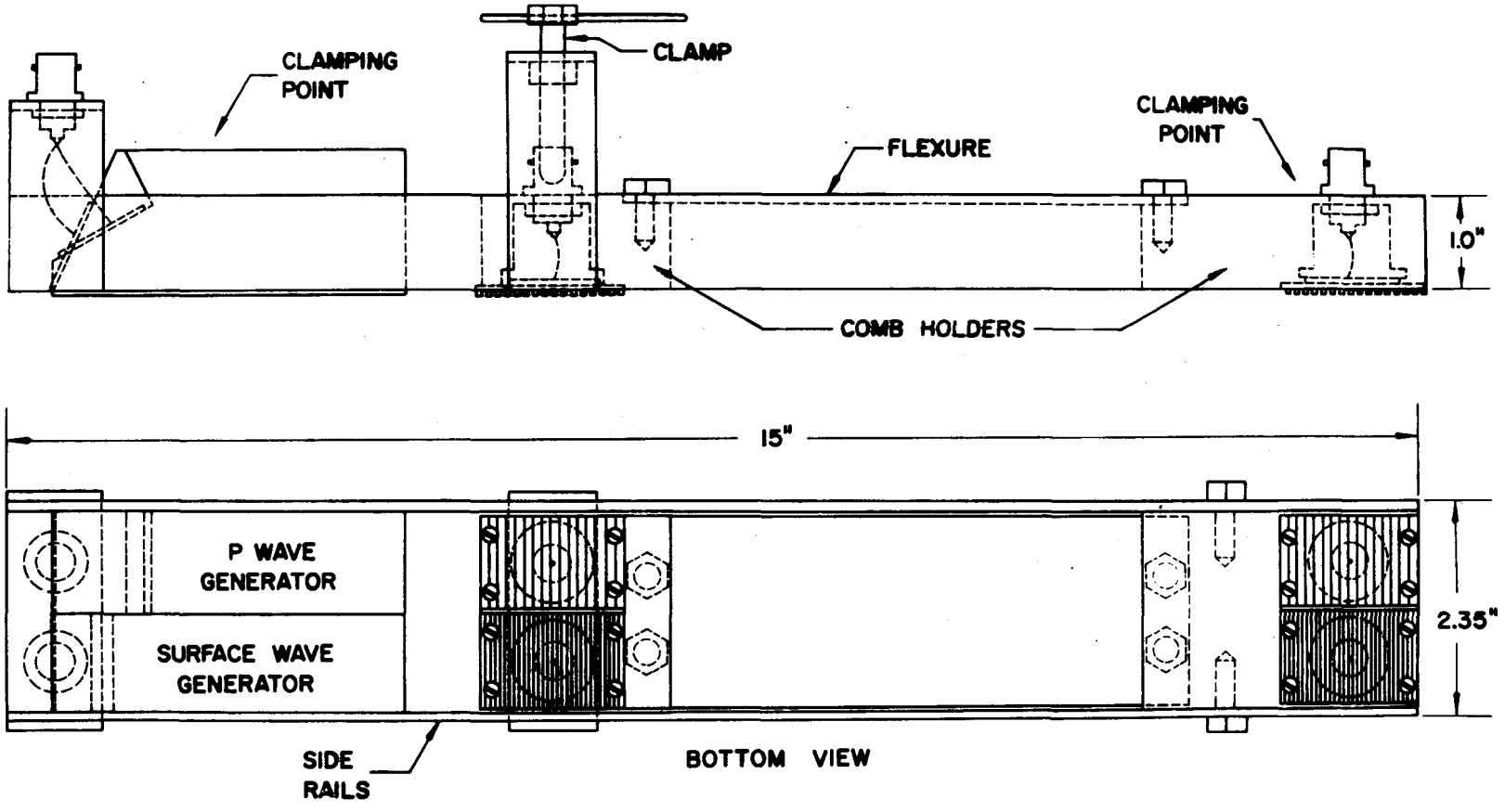

Figure 3-14 Two View Drawing of Probe II.

Temperature Effects on Probe II - The effects of temperature on probe II are shown in figure 3-15. As can be seen, the temperature induced changes in travel-time are 6.06 nsec/^{o}C and 3.84 nsec/^{o}C for the surface and longitudinal waves, respectively. These are about an order of magnitude lower than the changes measured with the original probe design. From figure 3-8 the temperature induced changes in travel-time for the probe I was 64.1 nsec/^{o}C and 41.7 nsec/^{o}C for surface and longitudinal waves, respectively. Thus, one of the major objectives, that of reducing the temperature induced changes in travel-time measurements, was achieved by the new probe design.

Repeatability of Wave Travel-Time Measurements - Evaluating the repeatability of the probe measurements measurements was conducted in three steps. First, repeated measurements were made on a laboratory specimen (No. 4) machined from the head of a new rail. These tests were conducted to assess the effect of factors other than specimen surface condition and curvature. A sequence of ten measurements of both P wave and surface wave travel-times were made as described earlier. After each measurement set (of four travel-times) the probe was removed and cleaned; the couplant reapplied and the probe clamped to a cleaned specimen. This sequence of ten measurements was repeated numerous times in order to evaluate the effects of different couplants, clamping techniques and minor modifications to the probe. Typical results are shown in figure 3-16. The rectangle drawn in that figure indicates the expected variation in the travel-time measurements based on $\pm$ one standard deviation of the measured travel-times. Thus, in this case, the expected variations are

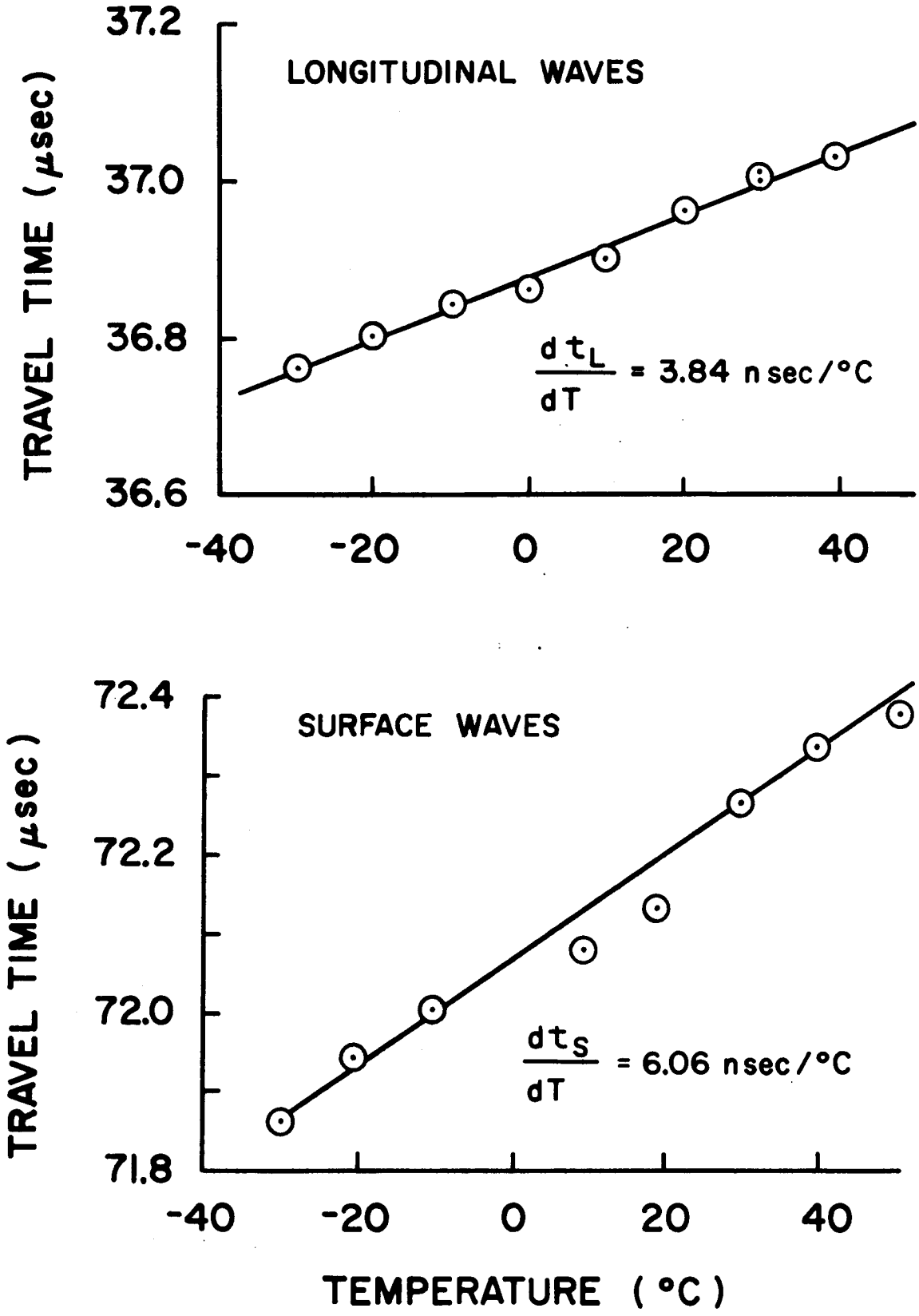

Figure 3-15 Temperature Induced Changes in Travel Time Measurements for Probe II.

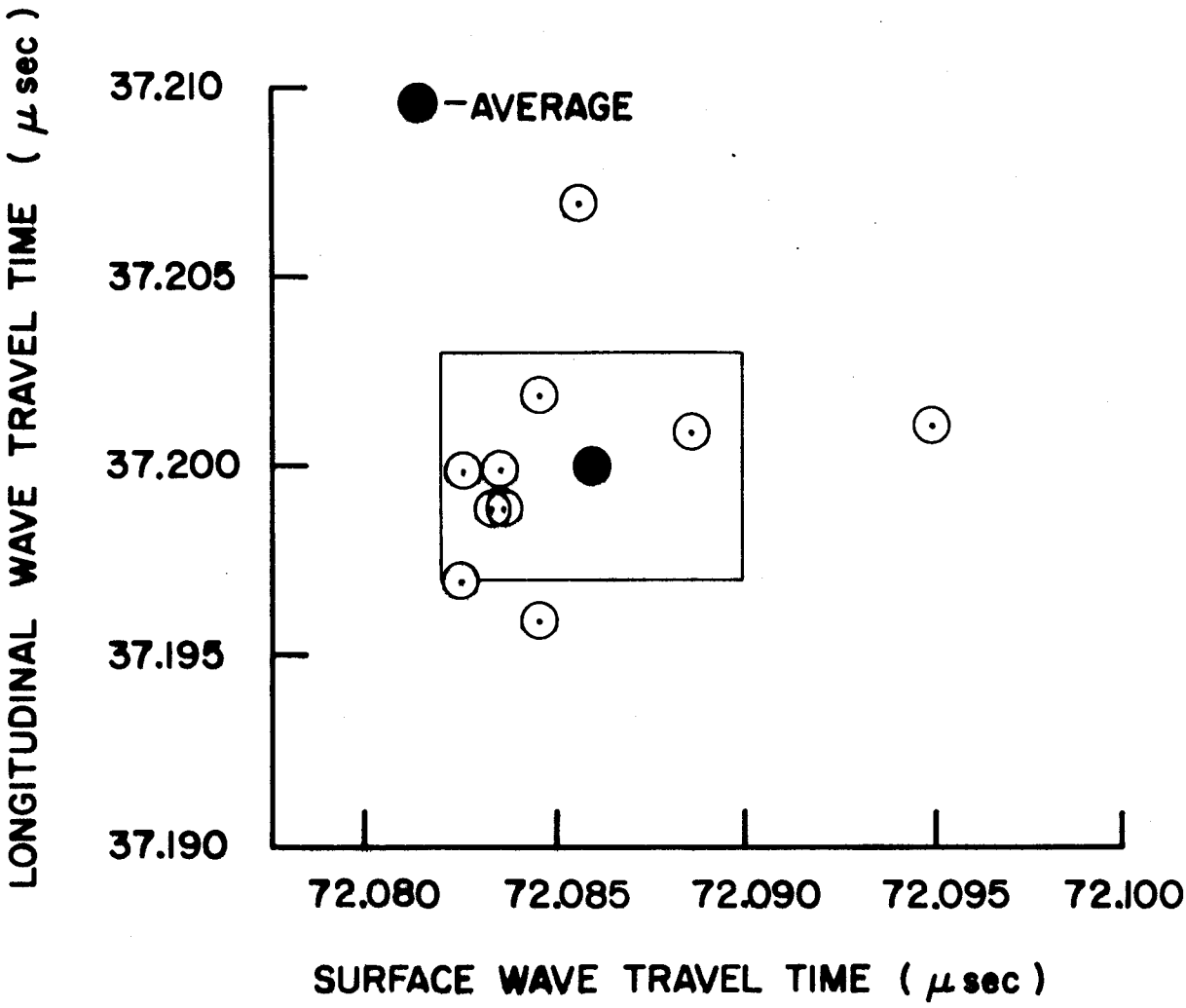

Figure 3-16 Repeated Travel Time Measurements on Rail Specimen 4 Using Probe II.

$\pm$ 3 nsec and $\pm$ 4 nsec for the longitudinal and surface wave travel-times, respectively.

The second step in evaluating probe repeatability was to to make repeated measurements on a typical rail surface. Data typical of these measurements are shown in figure 3-17 from which the expected variations can be seen to be $\pm$ 3 nsec for both measurements. It should be noted that, for the data shown in figures 3-16 and 3-17, temperature variations are minimal since these sequences of measurements can be conducted within a time span of about 60 minutes. Temperature of the respective surfaces were monitored and showed maximum changes of $0.2^{o}C$.

The conclusion drawn from data shown in these figures is that a travel-time measurement made on surface typical of rail webs or better can be expected two times out of three to be within three nanoseconds of the average value obtained over many measurements. The degree of repeatability is considered very good for the purpose to which this probe is intended.

The third step, consisted of measuring travel-times for eight different rail web surfaces described briefly in Table 3.2. A sequence of three measurements on each surface was repeated on three successive days. Repeatability in these measurements was not as good as that obtained in figures 3-16 and 3-17, but was $\pm$ 6 nsec or less. Figure 3-18 shows averages of the longitudinal and surface wave travel-times for the eight different rail web surfaces. As can be seen the longitudinal wave travel-times differ by no more than 225 nsec, while the surface wave travel-times are spread across a 2500 nsec range. Also shown in the figure is the theoretical relationship between the longitudinal and surface wave

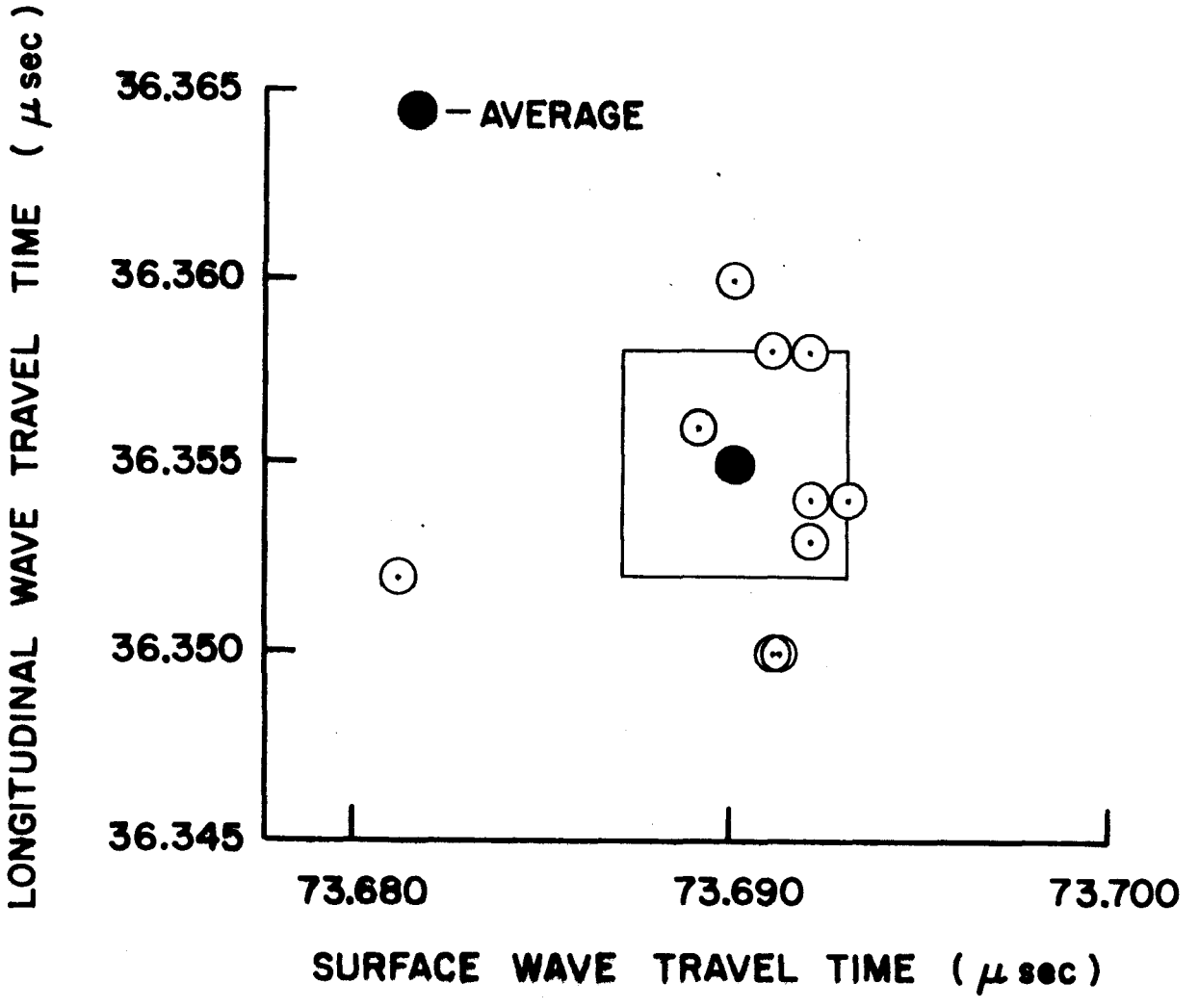

Figure 3-17 Repeated Travel Time Measurements on The Web of Rail 9 Using Probe II.

Rail No.	Description of Web Surfaces
1	Both front and back surfaces rough but free from large pits and embossing.
2	Front side has raised lettering and not usable. Back surface free of pits and embossing.
6	Front surface free of large pits and embossing. Back surface has raised lettering but is marginally usable.
7	Front has recessed lettering which falls in the wave path. Back surface has raised lettering and is not usable.
8	Front and back surfaces rough but not severely pitted and usable.
9	Front surface has recessed lettering which falls in wave path. Back surface has raised lettering and is not usable.
10	Front surface has raised lettering in wave path but is usable. Back surface is severly pitted but usable.
11	Both front and back surfaces have clear areas.

TABLE 3-2 Condition of Rail Sample Web Surfaces Used in Repeatability Study

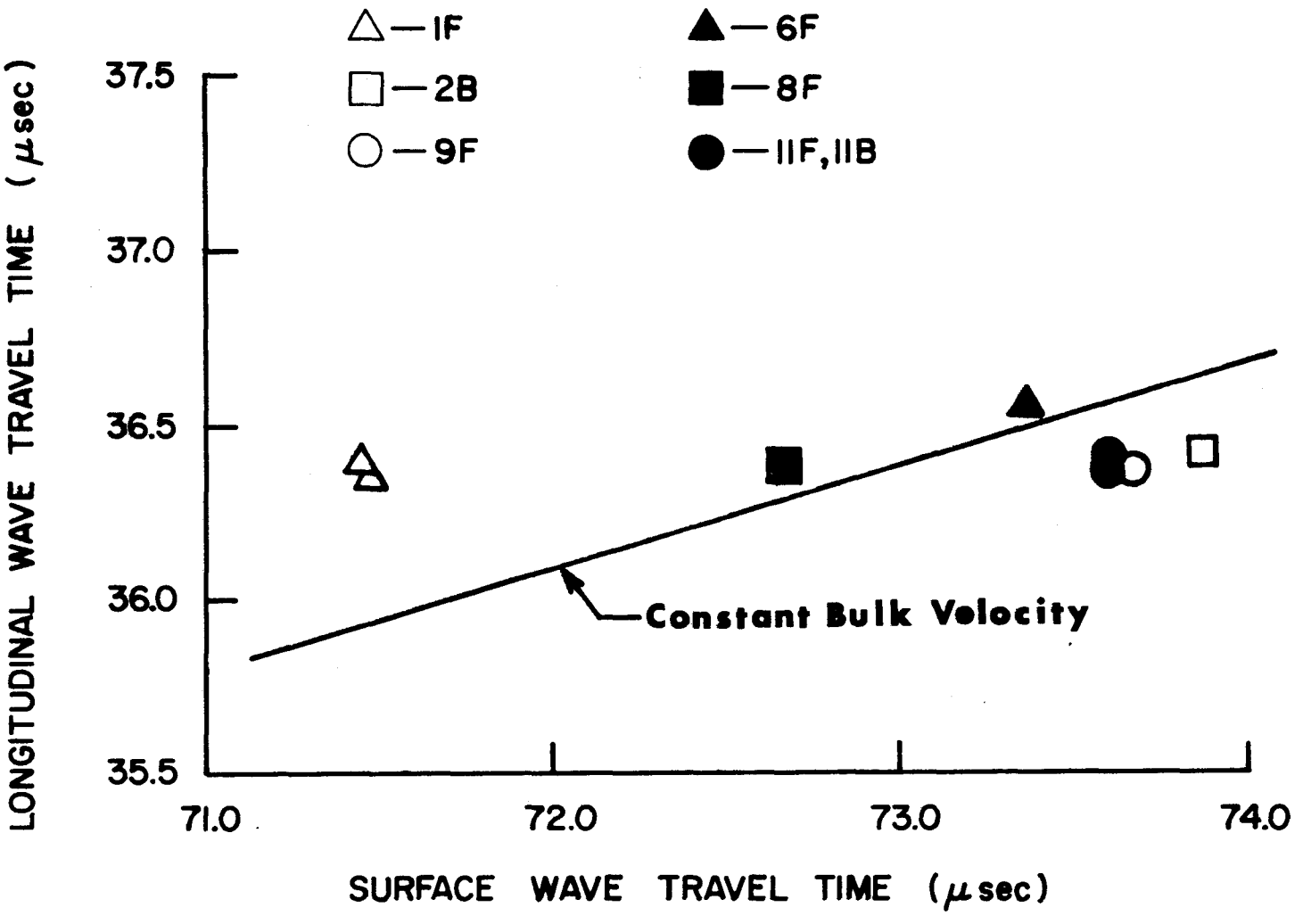

Figure 3-18 Travel Time Measurements for Eight Rail Web Surfaces Using Probe II.

travel-times for constant bulk velocity. As shown below one might reasonably expect the data to group parallel to this line if the differences in wave speeds are due to variations in elastic moduli. The fact that the data does not follow the line implies that the variations are the result of other factors.

In fact, the large variations in surface wave travel-time measurements were attributed to the sensitivity of the metal combs to guided wave modes arriving at the two receivers with different phases relative to the surface waves. The presence of these guided wave modes produced apparent variations in the composite signal travel-time which were very sensitive to the rail-web thickness. Since the effective rail web thickness varies with the exact vertical location of the probe on the web and from rail to rail, the travel-time of these composite waves did not really reflect the speed of surface waves.

The conclusions reached from the data collected with probe II were that the differential technique and metal combs reduced the undesirable thermal effects but the metal combs introduced an extraneous factor that made accurate measurement of surface wave speed impossible.

Probe III

The third version of the probe is shown in figure 3-19. The differential technique from probe II was retained but the metal combs were replaced by plastic wedges. As before two transmitters and two pairs of receivers were used to generate and detect longitudinal and surface waves. The probe is held in contact with the rail web by three C clamps placed on the upper surface of the transmitter and two receiver wedge pairs.

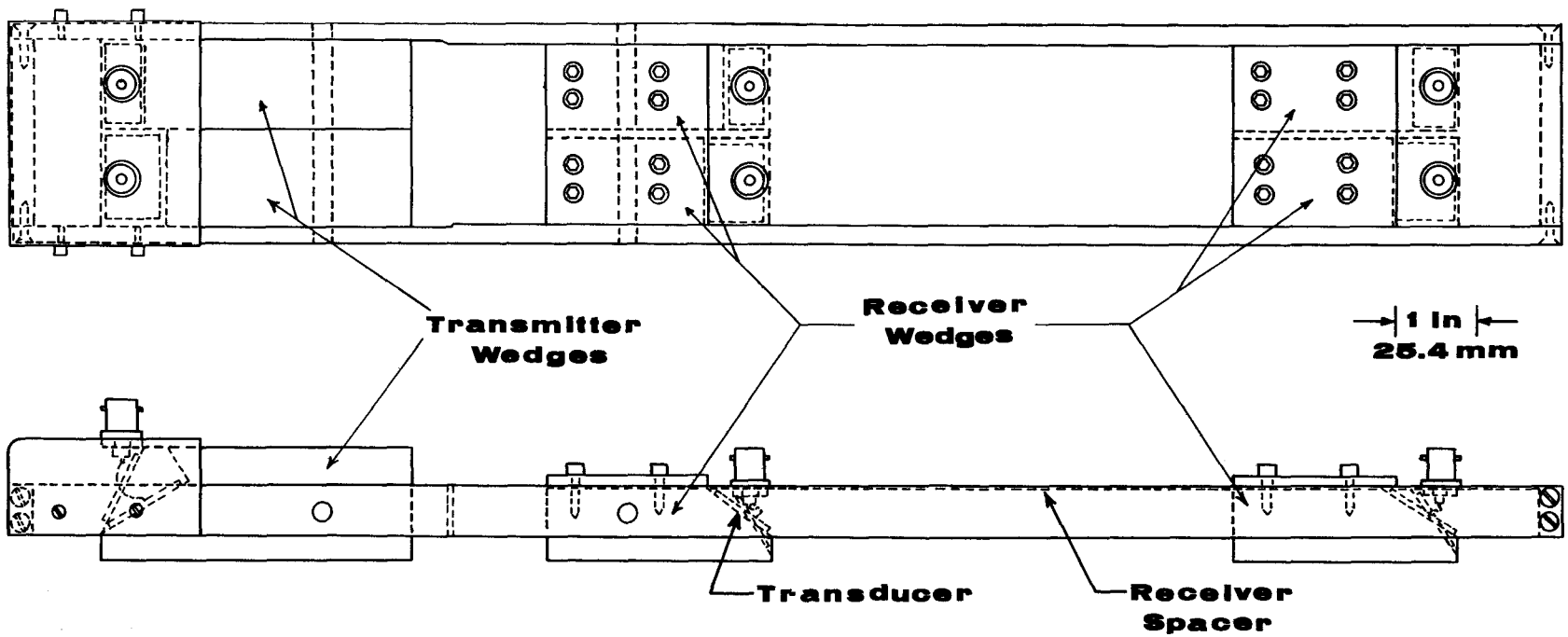

Figure 3-19 Two View Drawing of Probe III.

The repeatability of travel-time measurements was determined as before by repeated measurements on ten different rail web surfaces. The repeatability averaged $\pm$ 0.003 μ sec with the largest being $\pm$ 0.005 μ sec and several surfaces repeating at $\pm$ 0.001 μ sec . A plot of these travel-time measurements is shown in figure 3-20. The reduction in spread for the surface wave travel-time as compared to the data obtained with probe II in figure 3-18 is evident.

The results of wave speed measurements made with probe III on two new full length 119 lb AREA rails are shown in figure 3-21. Measurements were made at approximately 0.61m (2 ft) intervals on both sides of the web with the exception of those locations having embossed characters. Several sets of measurements at each location show the repeatability to be $\pm$ 0.003 μ sec . Although the measurements on one rail show better coherence than the measurements on the other, the spread in surface wave travel-time for both rails was more than expected.

A brief study of the effect of cleaning the rail surface showed no change in the measurements with a light wire brush cleaning but a more thorough removal of surface oxides with 200 grit emery paper produced about equal increases of approximately 30 nsec in both travel-times.

The spread in the surface wave travel-time is attributed to the sensitivity of surface wave speed to surface condition. The travel-time can be easily influenced by the quantity of excess couplant on the surface. For this reason the use of surface waves is not feasible for the present purpose.

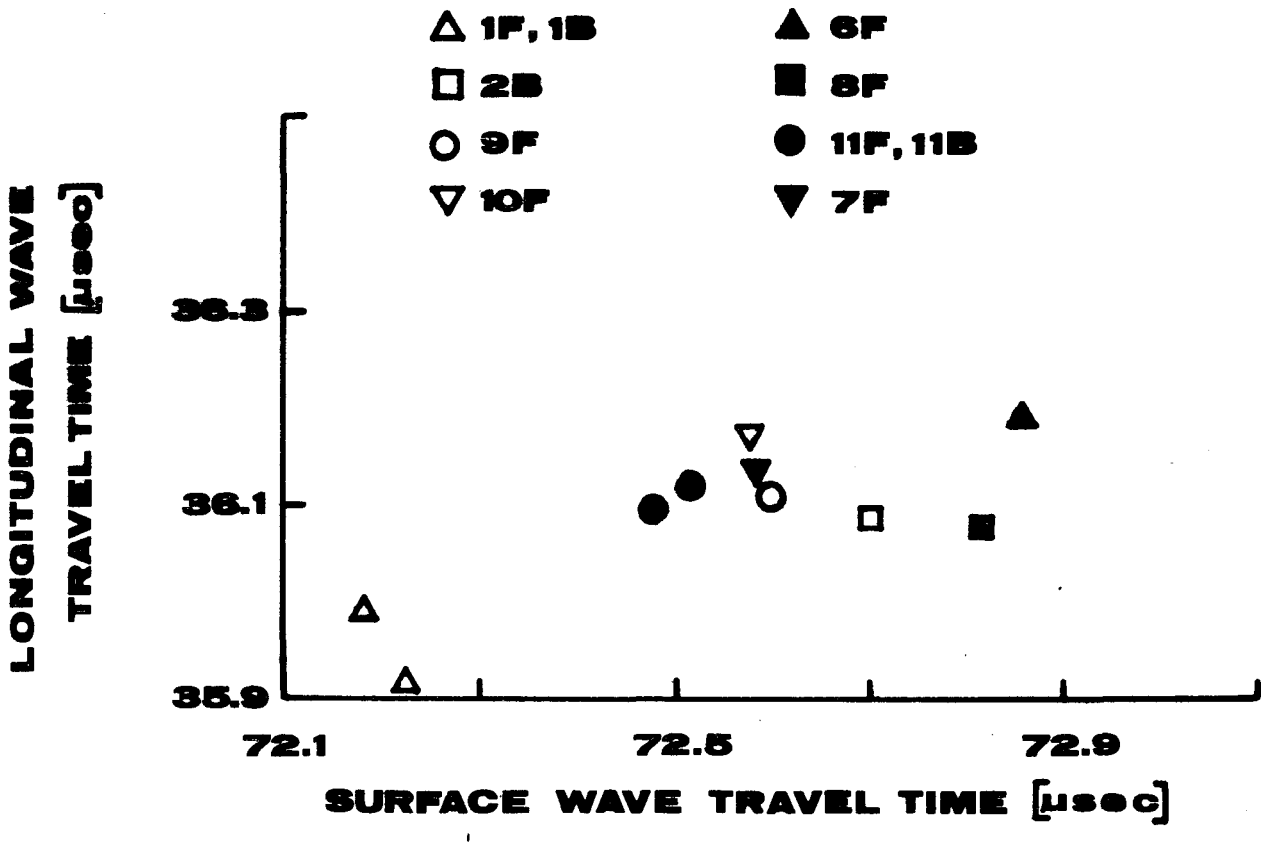

Figure 3-20 Travel-Time Measurements on Rail Web Surfaces with Probe III.

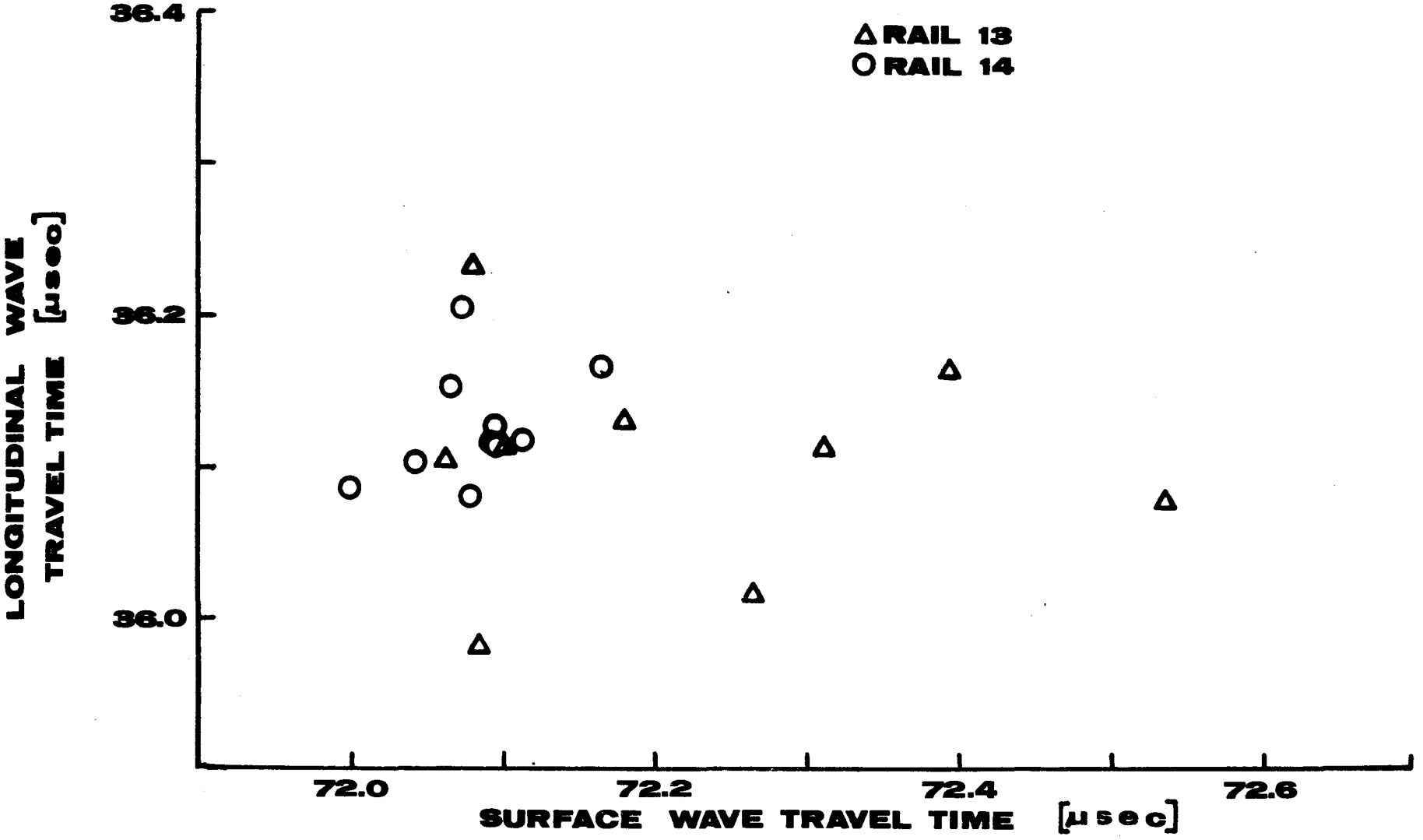

Figure 3-21 Travel-Time Measurements on Two Full Length Rails with Probe III.

Probe IV

The final modification made to the probe design was to replace the surface wave wedges with shear wave units. This was done with the expectation of obtaining better correlation between the shear wave and longitudinal wave travel-times than were obtained with Probe III. Measurements on several rail surfaces over several days showed the repeatability to be $\pm$ 0.003 μs.

The results of travel-time measurements on the two full length rails are shown in figure 3-22. Although the spread in shear wave travel-times is not as great as that in the surface wave travel-times, the correlation between the two measurements is not as good as was expected. The data for rail 13, with the exception of two points, do show reasonable agreement with the constant bulk velocity line. Two possibilities for the disagreement with the expected variations are first that other uncontrolled parameters are affecting the measurements or secondly the presence of residual stresses in the rail web is causing increases (or decreases) in the travel-times.

A plot of the longitudinal wave travel-time as a function of position on rail 14 is shown in figure 3-23. Only the data from those locations allowing travel-time measurements on both sides of the web are shown. If it is assumed the variations in longitudinal wave travel-time is due to stress, this data indicates a range of residual stress of 96 MN/m^2 (14 ksi), which is not unreasonable.

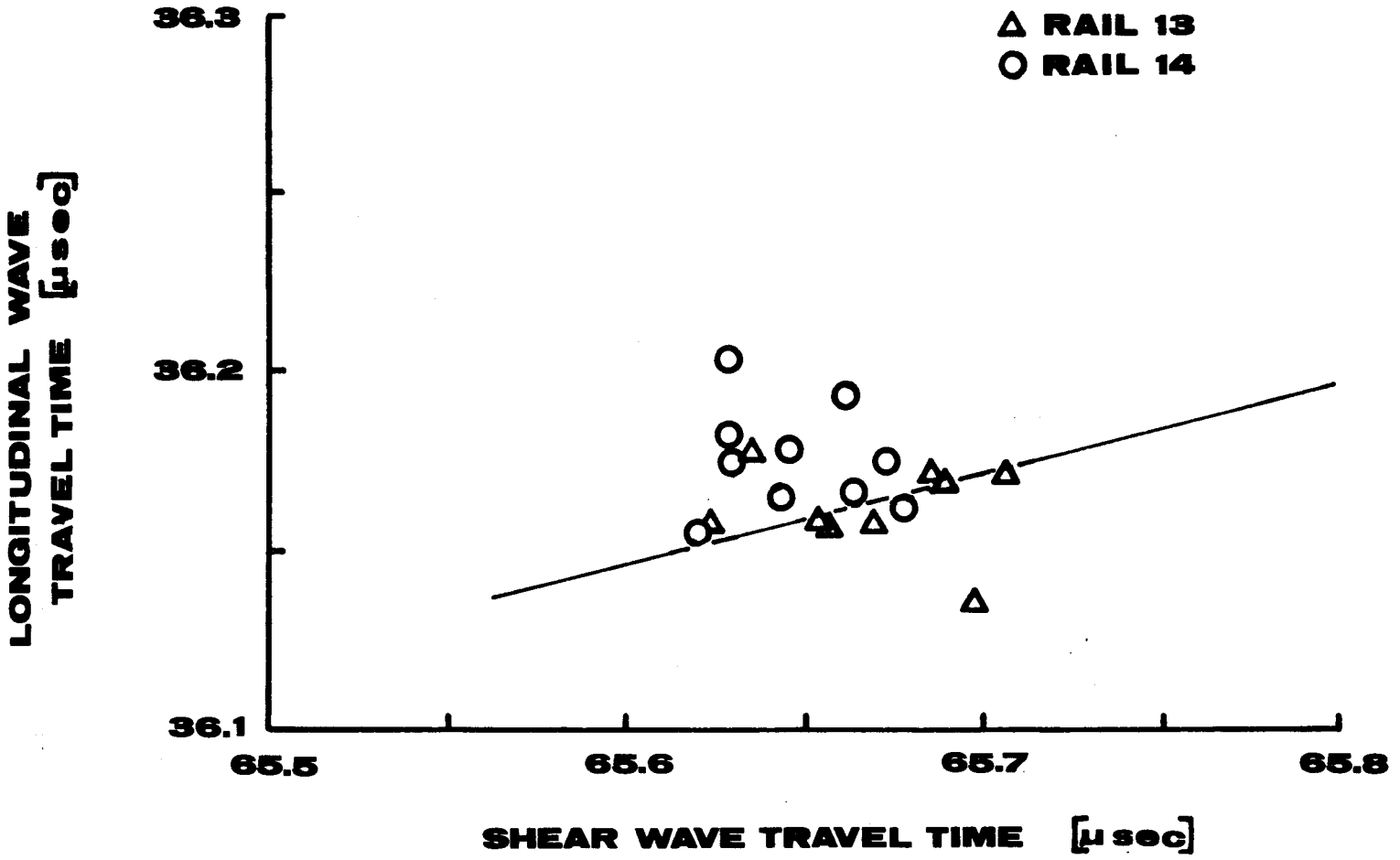

Figure 3-22 Travel-Time Measurements on Two New Full Length Rails with Probe IV.

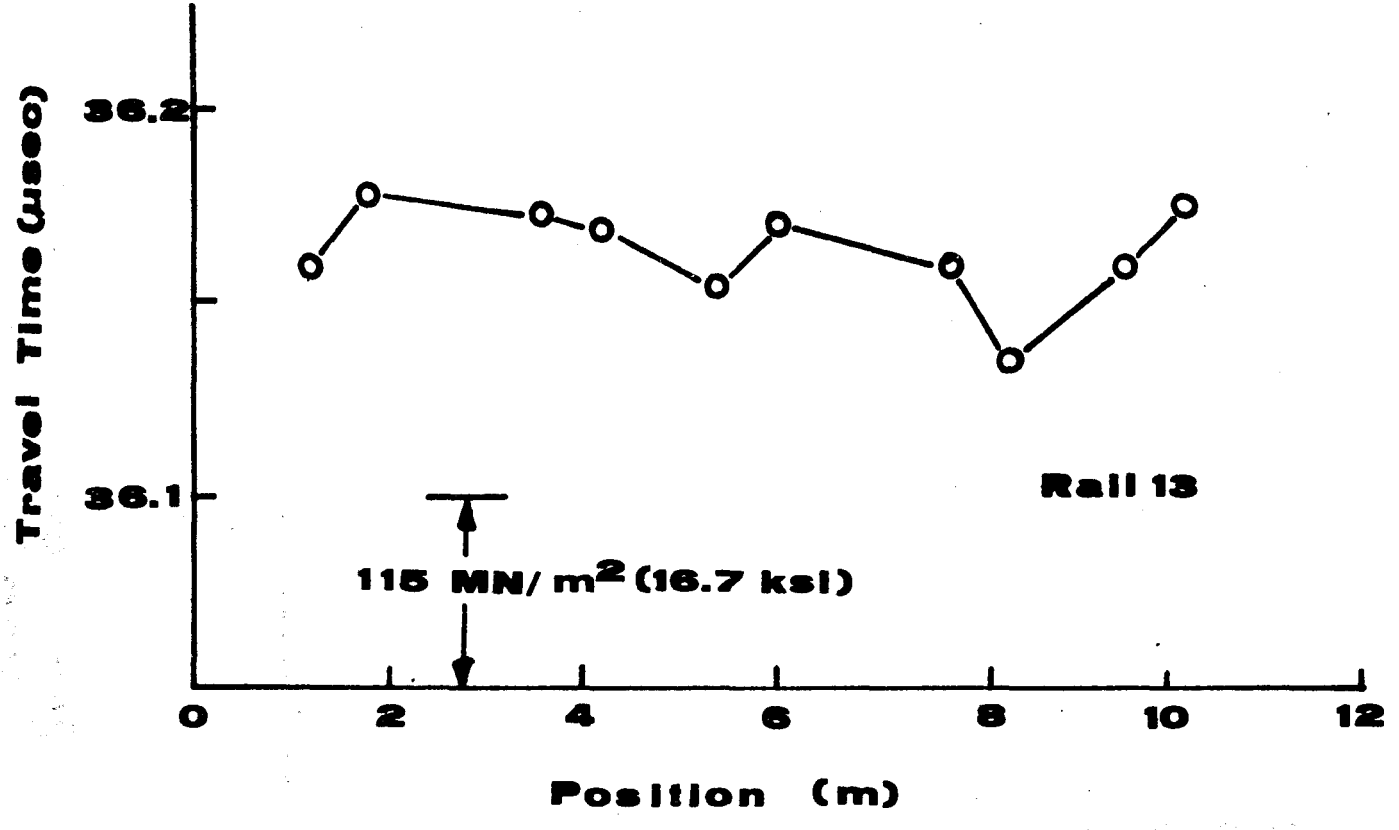

Figure 3-23 Longitudinal Wave Travel-Time Along the Length of a New 119 lb, 11.9 m (39 ft) Rail.

Changes in Wave Travel-Times Associated with Varying Elastic Properties

One of the problems associated with using the acoustoelastic technique for stress measurement lies in the fact that nominally identical materials exhibit slightly different wave speeds. For this reason measuring changes in stress is significantly simpler than measuring absolute values of stress. If however, the variations of wave speed due to elastic property changes can be measured, an absolute measure of stress becomes feasible. As was mentioned at the beginning of this section, this concern led to the incorporation of both longitudinal and surface (or shear) wave travel-time measurements in the probe design. Since the longitudinal wave is more sensitive to changes in stress, the surface (or shear) wave travel-time may be considered a reference measurement to be used for determining the value of the longitudinal wave travel-time in the absence of stress. We consider next an hypothesis of the effect of the variations in material properties on wave speeds in order to test their applicability to the present measurement.

If we assume the variation in elastic properties are caused by variations in the rolling porcess by which the rail is formed then, following Bradfield [25], it is reasonable to assume the bulk modulus of the rail is constant. We also assume the density is constant, thus requiring that the bulk velocity remain unchanged. Since the bulk velocity is related to the longitudinal and shear velocities by

$$V_B^2 = V_L^2 - \frac{4}{3} V_T^2 \qquad (3\text{-}5)$$

where V_B is the bulk velocity

V_L is the velocity of longitudinal waves

V_T is the velocity of transverse waves

If V_B is constant, then

$$\frac{dV_L}{dV_T} = \frac{4}{3} \frac{V_T}{V_L} \qquad (3\text{-}6)$$

Since

$$dV_L/V_L = - dt_L/t_L \quad \text{and}$$

$$dV_T/V_T = - dt_T/t_T$$

equation (3-6) can be written

$$\frac{dt_T}{dt_L} = \frac{3}{4} \left(\frac{t_T}{t_L} \right)^3 \qquad (3\text{-}7)$$

For the typical wave travel-times associated with probe IV of 36.2 μsec and 64.7 μsec, equation (3-7) yields

$$\frac{dt_T}{dt_L} = 4.28$$

Figure 3-24 shows the travel-time measurements before and after annealing a cold rolled bar of 4140 steel. The measurements were made with probe IV at six locations along 3.66 m (13 ft) length of a bar of cross section 25.4 x 102 mm (1 x 4 in). The travel-times were measured on opposite sides of the bar and averaged to eliminate curvature effects. The bar was heated to 815°C (1500°F) for an hour and oven cooled for 24 hours. The travel-time measurements after annealing show good coherence indicating that the

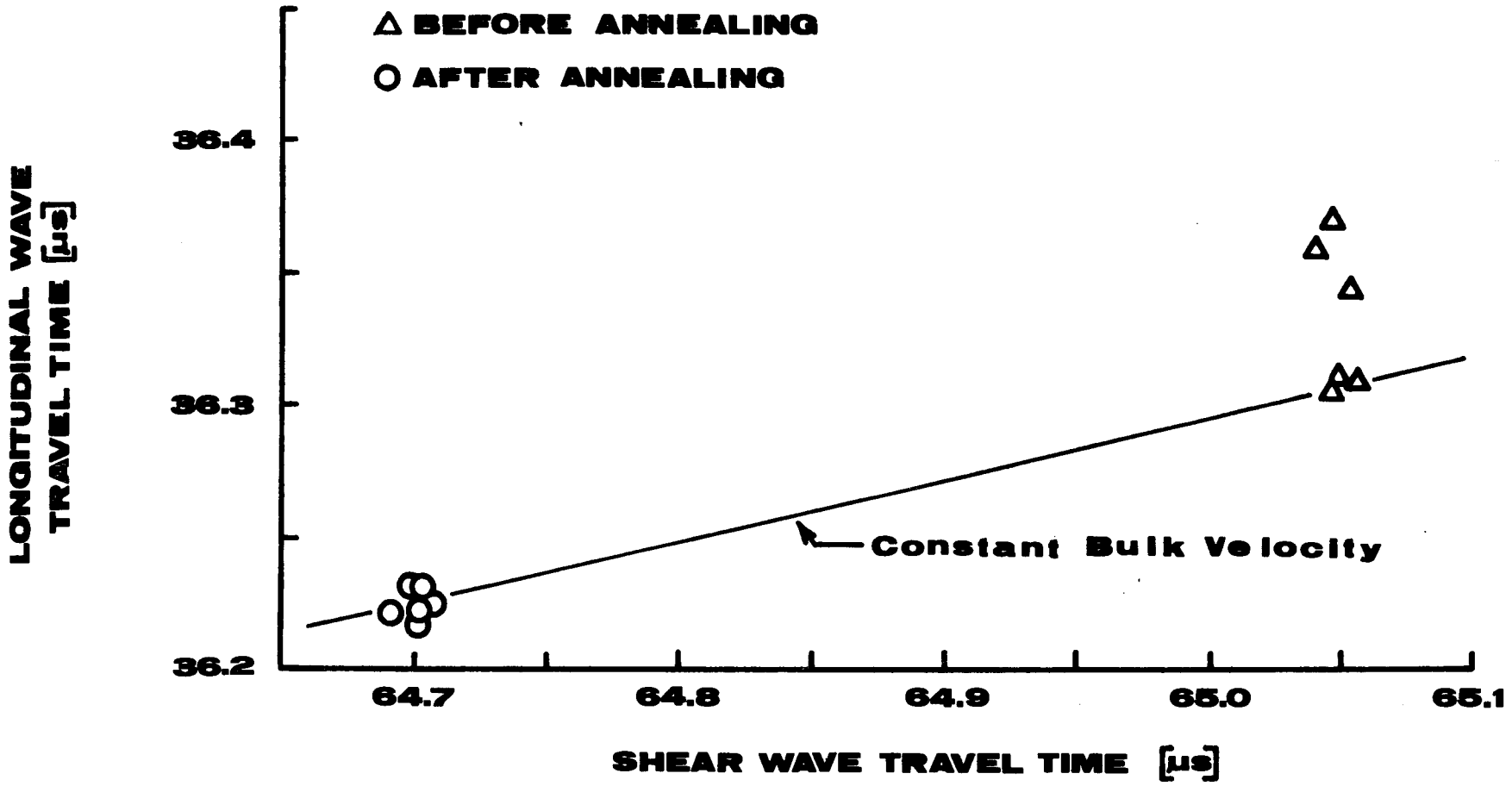

Figure 3-24 Travel-Time Measurements Before And After Annealing a 4140 Cold Rolled Steel Bar.

initial differences were probably due to residual stresses. Also shown in figure 3-23 is the expected change in travel-times for constant bulk velocity. The apparent agreement enforces the theory that the plastic deformation to which the material has been subjected produces no change in the bulk velocity in the absence of residual stresses.

Summary

The data presented in this section show that the probe design IV, which utilizes a differential time measuring technique and plastic wedges for the generation and reception of waves is capable of measuring longitudinal and shear wave travel-times along the axis rail with a repeatability of $\pm$ 0.03 nsec for typical rail web surfaces. This accuracy in longitudinal wave travel-time measurements is equivalent to $\pm$ 6.9 MN/m^2 (1 ksi) longitudinal stress change.

Variations in measured longitudinal wave travel-times for new rail having no applied longitudinal stress indicate apparent longitudinal stress variations of approximately 100 MN/m^2 (14.5 ksi) which are likely due to residual stresses in the rail primarily and secondarily due to material property variations. The presence of these variations makes absolute measurement of longitudinal stress questionable without further evidence of the correlation between the variations and residual stresses.

However the measurement of longitudinal stress to an accuracy of $\pm$ 6.9 MN/m^2 (1 ksi) changes at any particular location on a rail is feasible with this probe design provided measurements of the longitudinal wave travel-time can be made on opposite sides of the web and averaged to eliminate curvature effects.

FIELD EVALUATION OF THE ULTRASONIC PROBE

Two field tests were conducted in order to evaluate the sensitivity of the ultrasonic measurements to actual rail stress variations. The first test was conducted on the main line of the Atchison, Topeka and Santa Fe Railway at Norman, Oklahoma. The second test occurred at the Department of Transportation's Transportation Test Center, Pueblo, Colorado where strain gauge and ultrasonic data were recorded for one complete 24 hour period.

Field Tests at Norman

The preliminary tests on the Santa Fe Railway were used to assess the operational procedures for conducting field measurements. No strain gauge data were recorded and tests were made at only two times, early morning and early evening. A single station was used for this test. It was located near mile 400, precisely 226 m (741 ft) from a switch on the north end and 243 m (798 ft) from a joint on the south end.

This track is North-South oriented and has regular main-line freight and passinger service. The rail is 119 lb control-cooled, manufactured by Inland in 1956 and originally installed in that year. It was reworked in January of 1976. Wood ties, spaced at at 0.49 m (19 1/2 inches), are used and the rail is box anchored on both sides of every other tie. The ballast is Pueblo slag. Compared to the Pueblo track test section, the Santa Fe track has considerably greater flexibility.

Weather conditions were favorable for this test with a cool night and a warm day. Skys were clear and there was negligible wind.

Field Tests at Pueblo

The field tests at Pueblo were conducted from approximately 3:00 p.m., 10 December 1976, to 4:00 p.m. next afternoon. Weather through this period was generally favorable to conducting the tests. Skys were clear and the ambient temperature reached a low of -12°C (11°F) at 5:00 a.m., 11 December 1976. The high ambient reading was 8.3°C (47°F) and was reached at 4:00 p.m., 11 December 1976. Rail temperatures peaked near to 15.5°C (60°F) at noon. There was very little wind.

Four stations were instrumented for strain and temperature data. These locations were 91.4 m (100 yards) apart toward the middle of a 609.m (2000 feet) tangent section of the access track to the test section used for operating the linear induction motor (LIM) rail vehicle as indicated in Fig. 4-1. No station was closer than 0.61m (2 feet) from a weld (station 35). Station 29 was 4.5 (15 feet) from the nearest weld, station 32 was 3.6 m (12 feet) from the nearest weld, and the station 26 was 1.2 m (4 feet) from the weld.

The track is oriented East-Northeast and is constructed of 119 lb rail with 23-inch tie spacings. This is a conventional track section except that bolted rail clamps are used and particular care was taken to insure good alignment. The result is a track more rigid than usual. Although the track was constructed almost seven years ago, it has not seen heavy usage and therefore might not have completely equalized stress levels along its length. As can be seen from figure 4-2 sand impacting in the ballast has resulted in an even more rigid track structure.

The rail was control-cooled and manufactured by Colorado Fuel and Iron Company in 1970. The rail designation at each location was as follows:

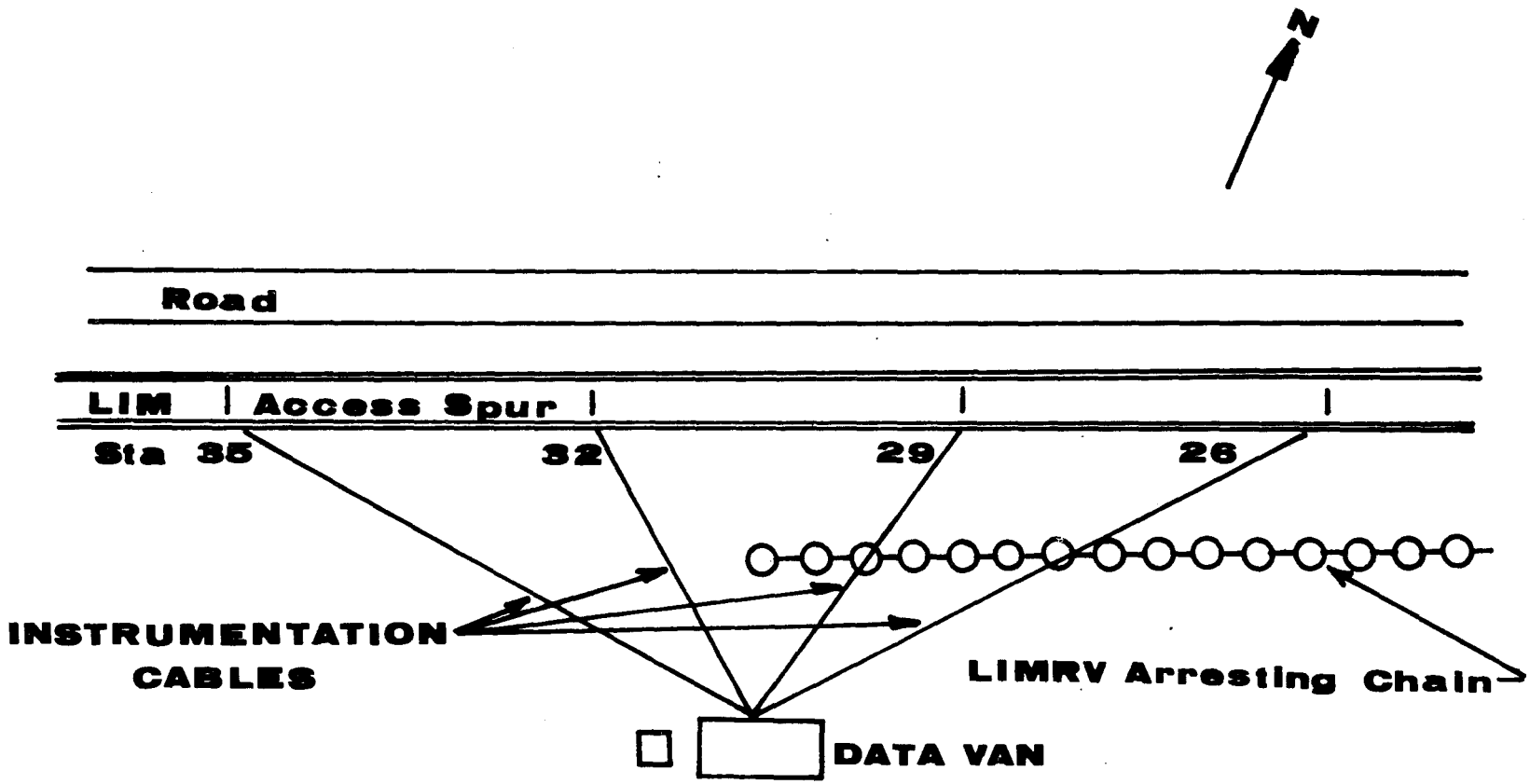

Figure 4-1 Schematic Diagram of the Test Zone at Pueblo.

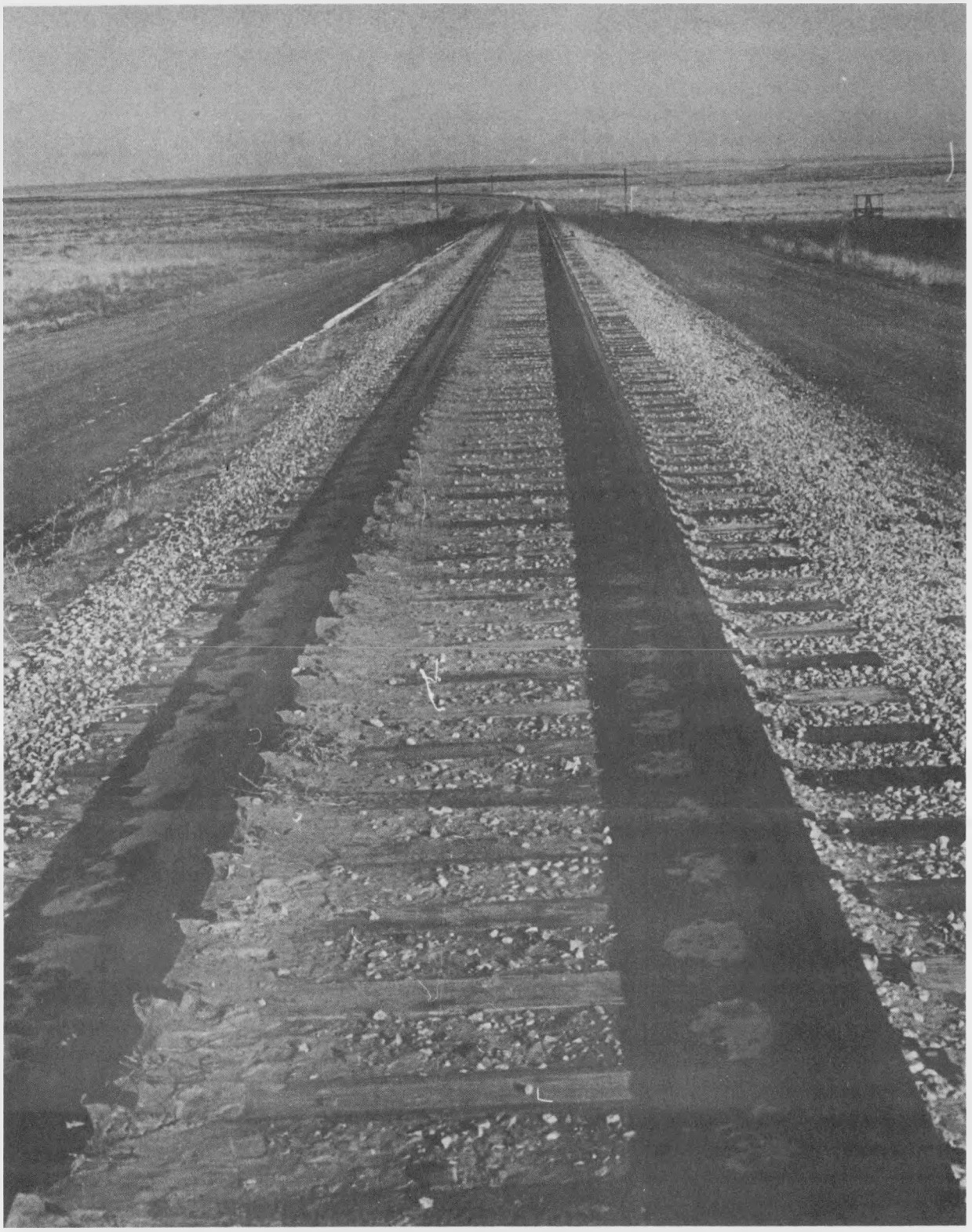

Figure 4-2 LIM Access Spur Looking West.

Station 26-C rail; Station 29-F rail; Station 32-B; and Station 35-B rail. These designations give the placement of the rail in the string as originally manufactured at the rolling mill.

Each station was instrumented to read longitudinal strain at the neutral axis on each side of the rail, vertical strain at the same location and lateral strain at the top of the rail. Rail temperature was also recorded. A typical strain gage installation is shown in figure 4-3. Each of the four test stations was instrumented with five 350 ohm bonded strain gages and two thermocouples. Temperature compensation for each strain gage was provided by applying compensating bridge strain gages to three-foot lengths of unstressed rail. This compensating rail was placed parallel to the test rail at each of the four test points. Data from all four test stations was multiplexed and recorded on a 14 track FM tape recorder. IRIG-4 time code was recorded. Real time data was available through a Brush recorder.

The ultrasonic probe was alternately placed on each side of the rail at each station and a full set of time-differential data were recorded for both the shear wave and the longitudinal wave. The ultrasonic instrumentation was housed in a van located on the road adjacent to the track. Two 15.2 m (40-foot) coaxial cables were used to transmit the electronic signals to and from the ultrasonic probe. One was connected to the sending transducer and the other would be alternately connected to each of the receiving transducers for the particular wave.

The probe was held in place by the C-clamps as shown in figure 4-4. No special surface preparation was required other than wire brushing of the web area. Low viscosity motor oil was used as the ultrasonic couplant. Precautions were taken to be sure that both the rail and the probe surface

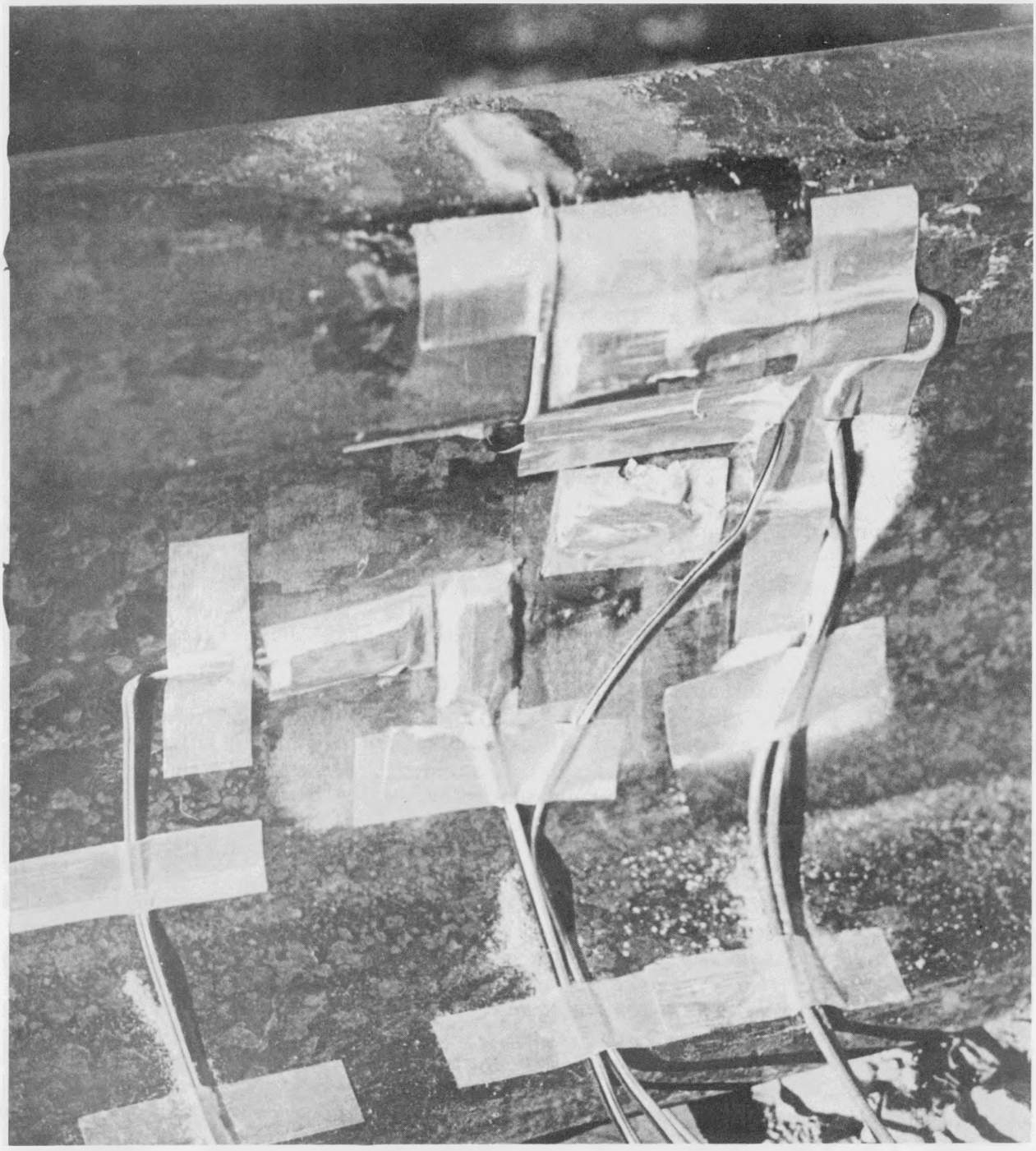

Figure 4-3 Typical Strain Gage Installation.

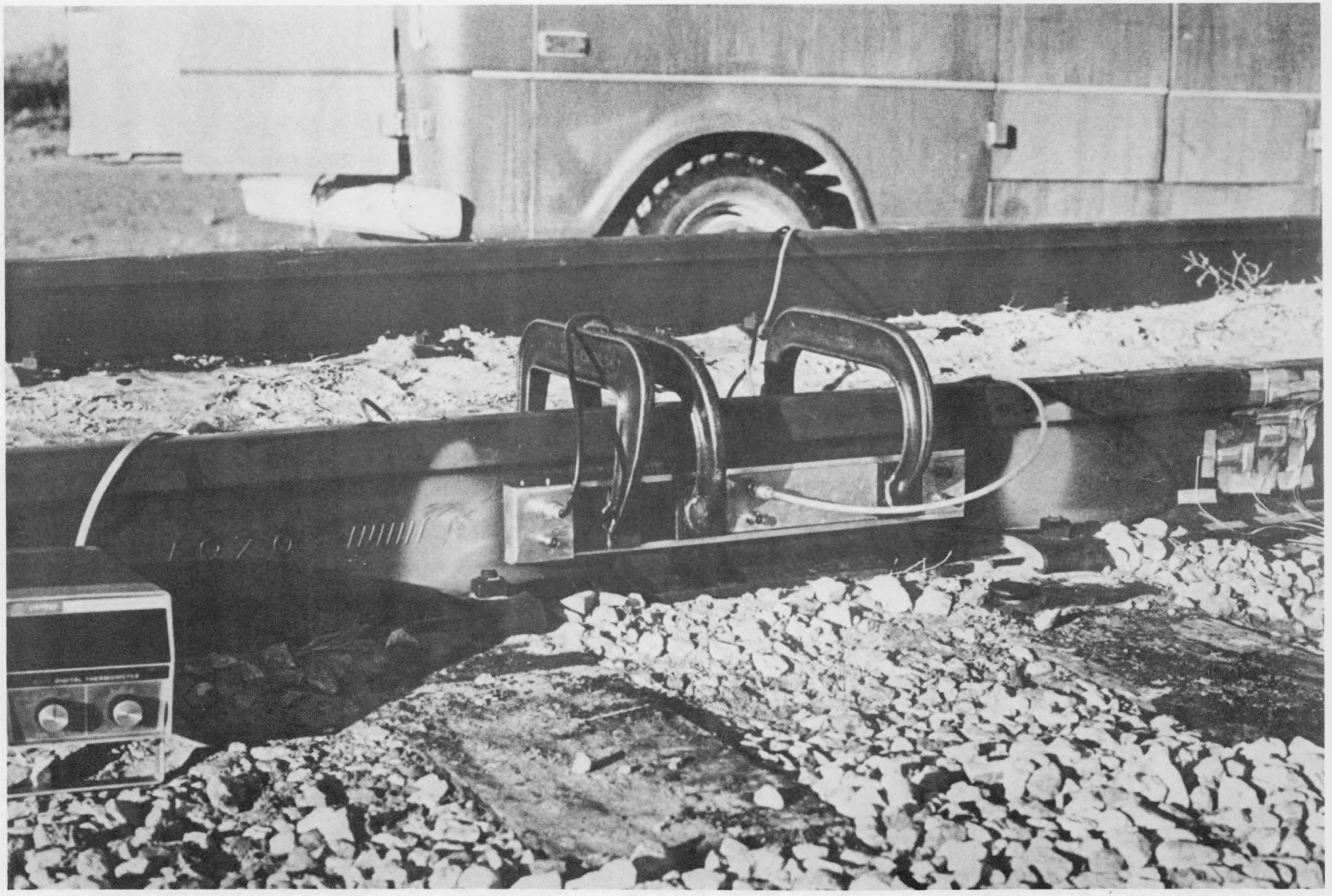

Figure 4-4 Ultrasonic Probe Clamped to Rail Web.

were free from grit and other loose particles since this presence would yield erratic readings.

A 1 m (3 ft) length of 110 lb/yd AREA rail located near the stressed rail was used in both field tests as a measuring reference. Travel-time measurements on the reference rail were used to assess temperature effects and to detect abnormalities in the probe.

Field Test Results

Results of Norman Field Test - The travel-time measurements made on the reference rail and at mile post 400 are shown in figure 4-5 and 4-6. The variations in travel-time for the reference rail are presumed due to temperature induced changes in wave speeds only. The longitudinal wave travel-time shows an increase of 0.0033 μ sec for a 1^{o}C change in temperature which is somewhat higher than the increases encountered in laboratory tests. The shear wave trave-time showed no significant change with temperature as contrasted to laboratory tests which showed a significant increase with temperature. The differences experienced between the laboratory and field temperature-induced changes in travel-time measurements are believed due to unequal temperatures of the probe and rail standard in the field test.

The data in figure 4-6 are shown as measured and as corrected for temperature according to the variations measured on the standard rail. The corrected longitudinal wave travel-time is computed according to

$$(t_L)_c = (t_L)_u - 0.0033\ (T-25) \qquad (4\text{-}1)$$

where

$(t_L)_c$ is the corrected travel-time in μ sec

$(t_L)_u$ is the measured travel-time in μ sec

T is the measured temperature in ^{o}C

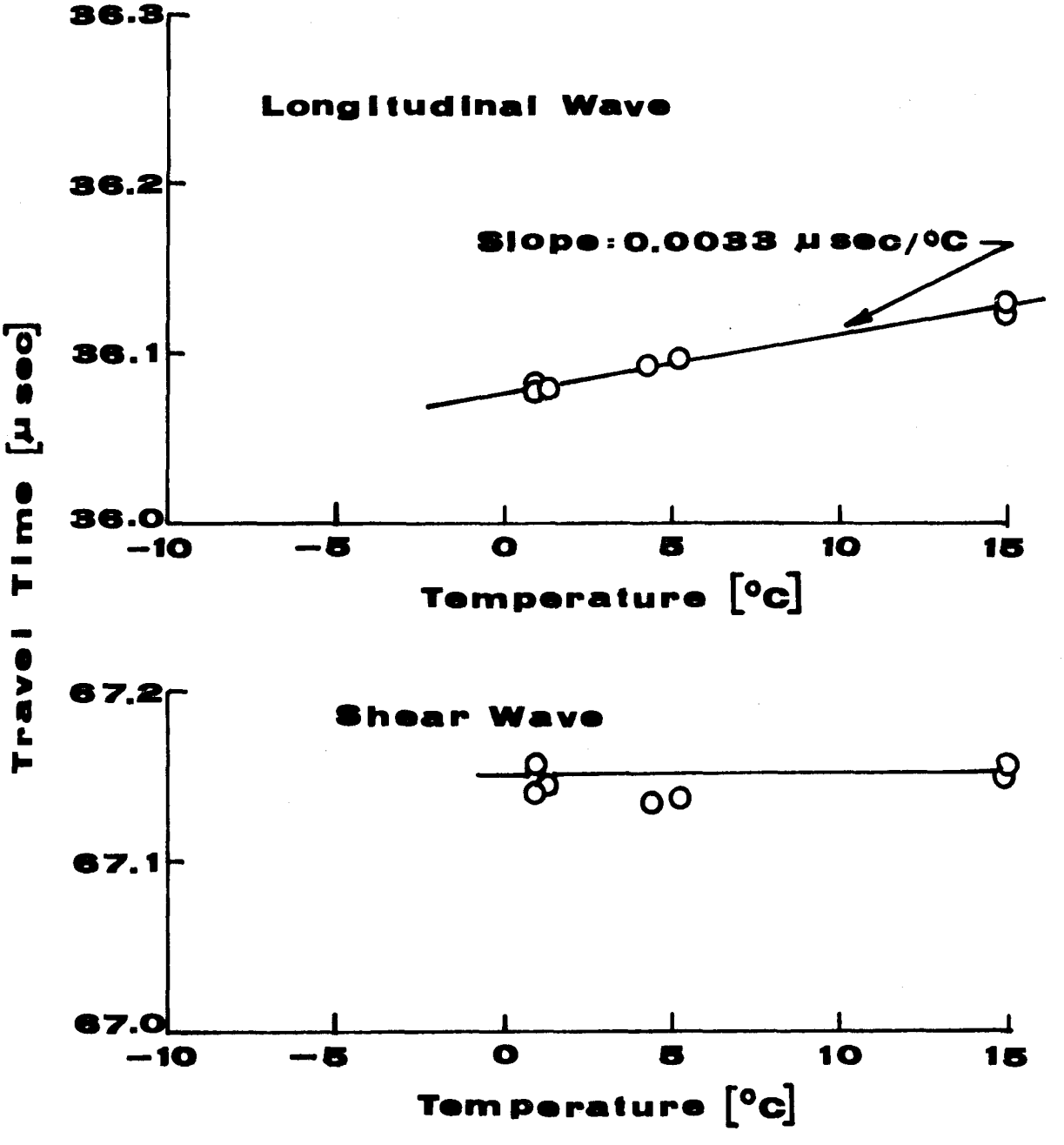

Figure 4-5 Travel Time Measurements on Reference Rail-Field Test at Norman

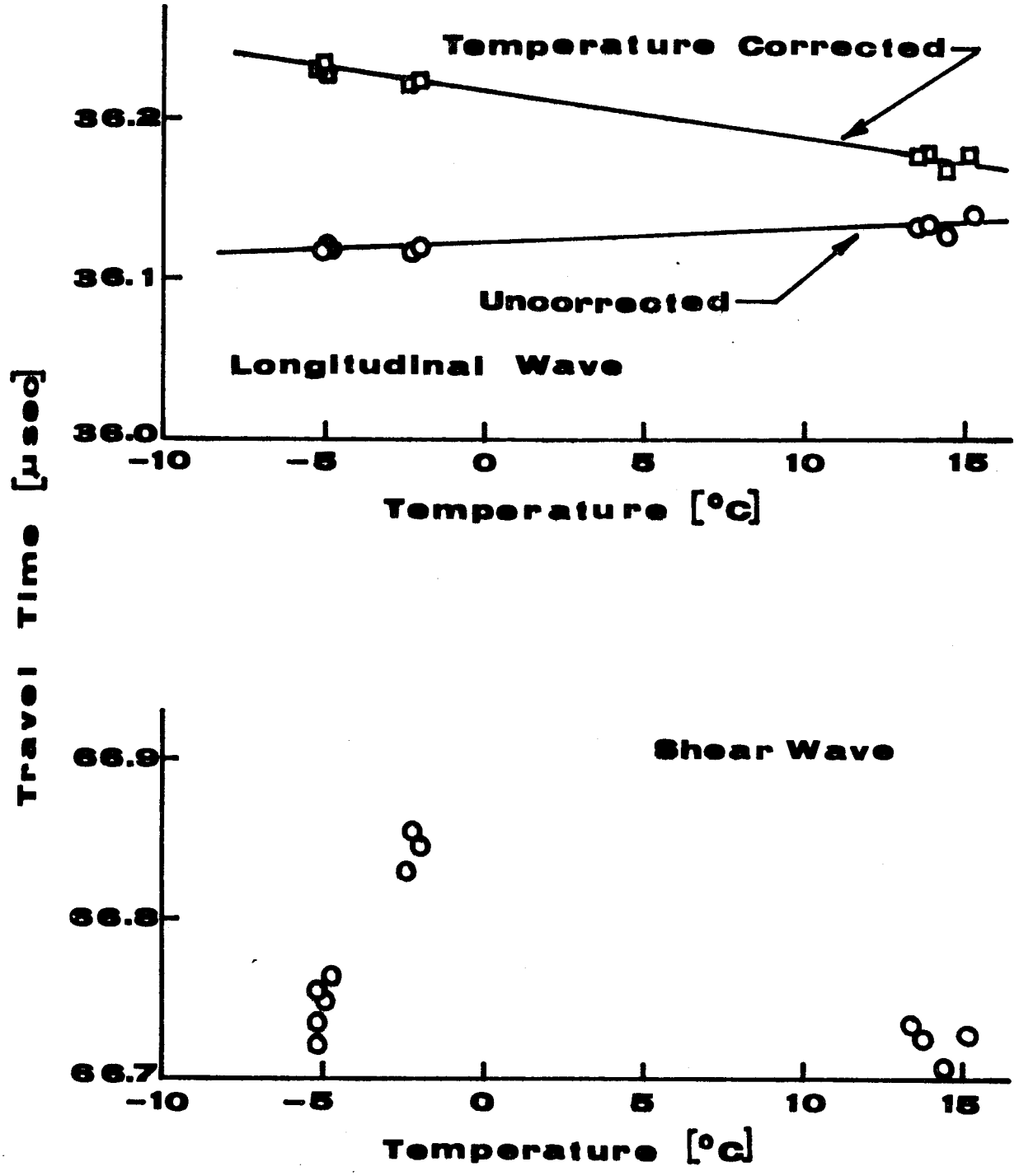

Figure 4-6 Travel Time Measurements at Mile Post 400-Norman Field Test

The corrected travel-time measurements show a change with rail-temperature which is about four times as great as the expected change due to thermal stress. For a temperature change of 20°C the change in stress is 32.1 MN/m^2 (4.66 ksi) which should yield a longitudinal wave travel time change of 14 nsec. The measured change is 60 nsec. The difference is attributed to changes in curvature which also affect the travel-times. Because measurements were made on one side of the web only, the curvature effects could not be separated from the stress effects. The shear wave travel-time shows an unexpected increase at -2.5°C compared to the data at -5°C and 15°C. At this time the cause of this increase has not been isolated. Three possible contributing factors are: (1) interference of the shear wave with a guided wave mode in the rail web, (2) data acquisition error, and (3) curvature effect.

In spite of the unexpectedly high changes in longitudinal wave travel-time and the unexplained changes in the shear wave travel-time, the results did demonstrate two useful points. First, the travel-time measurements could be made in the field with a reasonable precision and, secondly, the longitudinal wave travel-time measurements showed the correct trend. Further this preliminary test was very useful in debugging the operation of the unit in the field and contributed to the smoothness of the Pueblo field test.

Results of the Pueblo Field Test - The strain histories recorded at the four rail stations are shown in figures 4-7 and 4-8. The strains plotted are not absolute strains but are relative to the strain present in the rail when the bridges are initially balanced. Because of operational

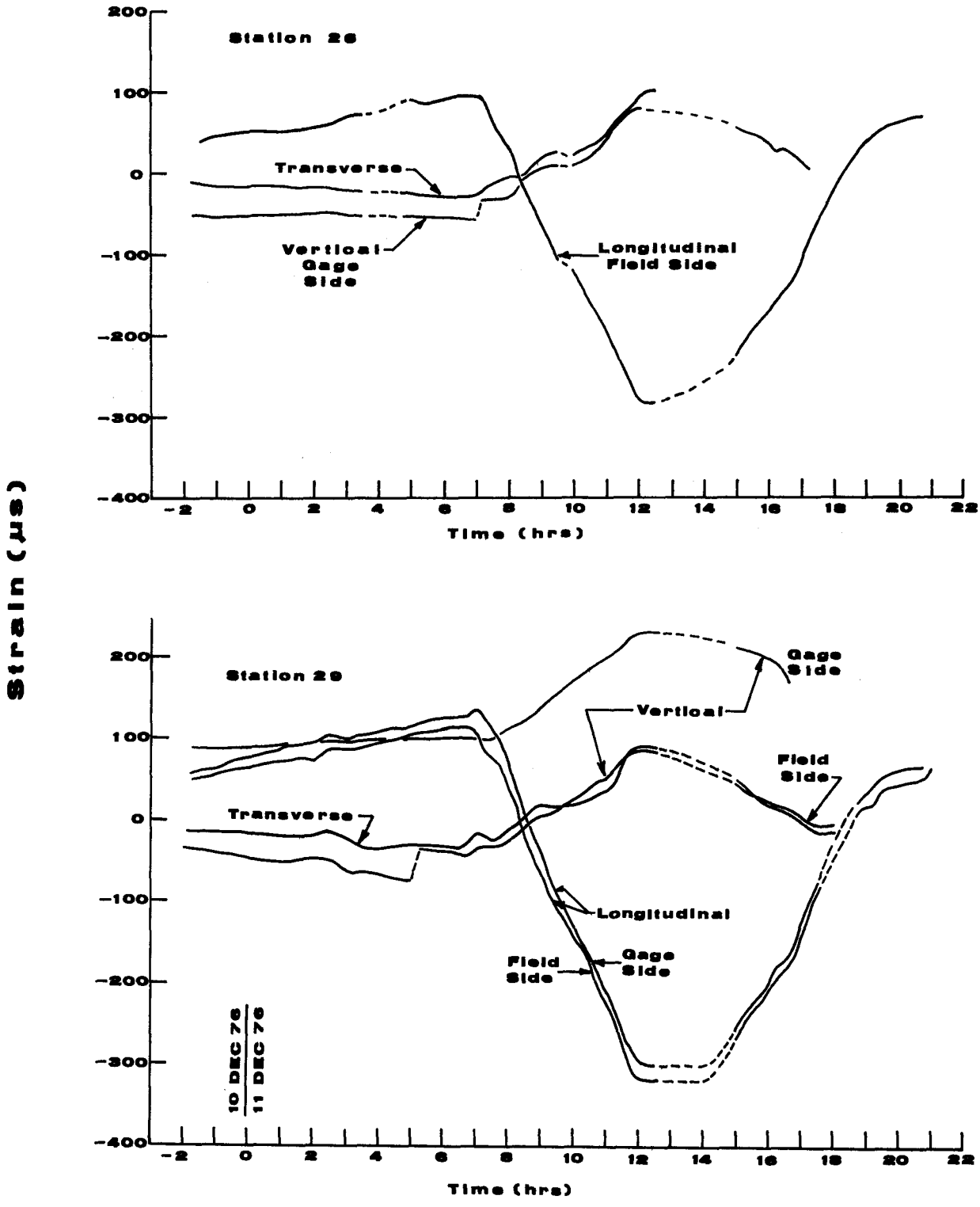

Figure 4-7 Strain Histories at Stations 26 and 29-Pueblo Field Test.

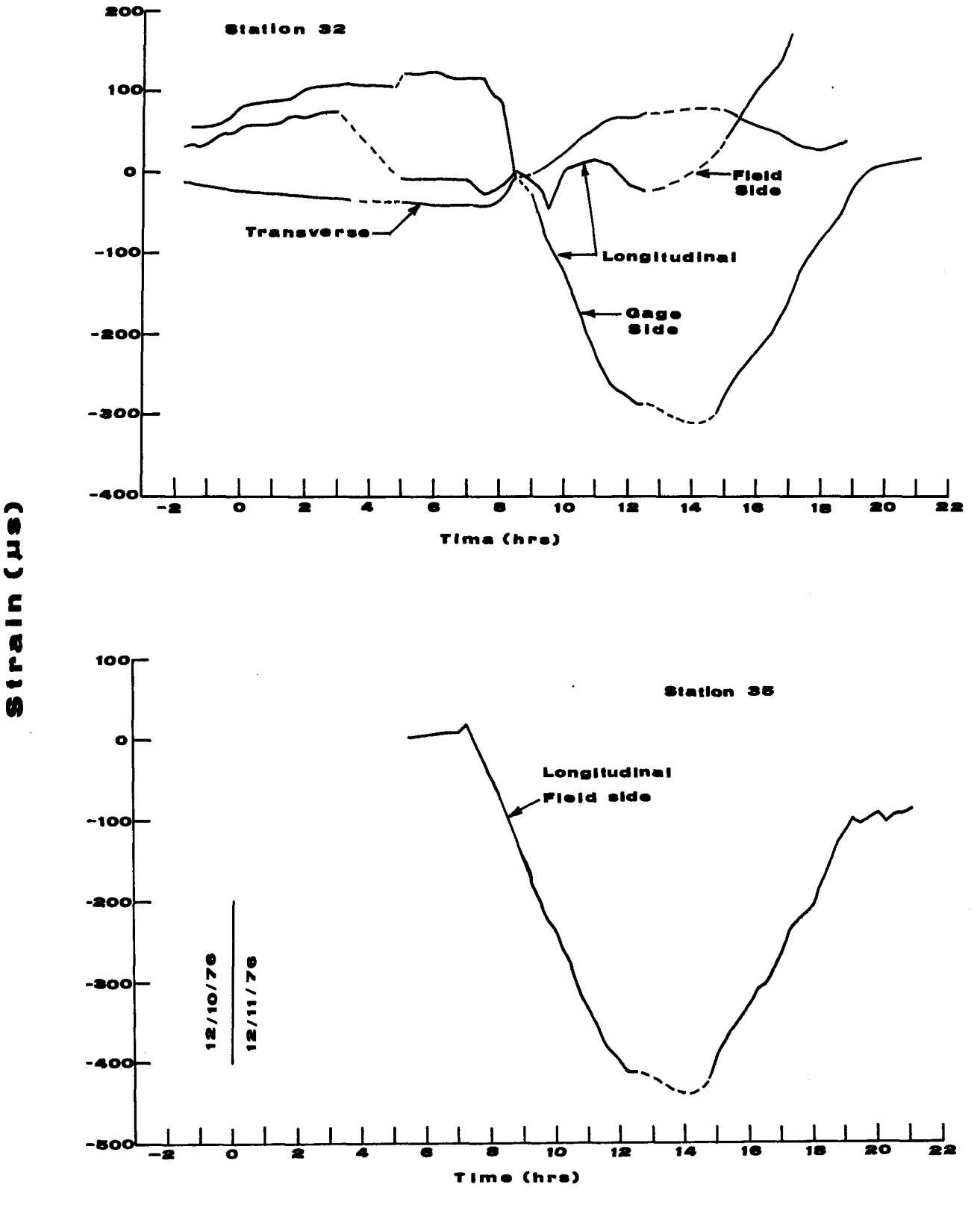

Figure 4-8 Strain Histories at Stations 32 and 35-Pueblo Field Test.

difficulties all of the bridges were not balanced at the same time, hence, the data shown only represents changes in strain from an unknown reference. The strains are plotted as functions of time beginning at about 2200 hours on 10 December 1976 (shown as -2 hrs) and continuing to about 2100 hours on 11 December 1976. The dotted lines shown in figures 4-7 and 4-8 are interpolations during periods when the data recorded was obviously in error or when the data was not recorded. The discontinuities which are seen in several of the strain histories, e.g. at station 26, the vertical strain on the gage side of the rail at 7 hours, are due to bridge rebalancing necessitated by operational problems and should be disregarded.

The strain histories are reasonably consistent with expectations. The maximum longitudinal tensile strain occurs at all four stations at approximately 700 hours which was shortly after sunrise. The histories show rapid changes from 700 to 1200 hours due to solar heating, and a rapid increase in tensile strain due to cooling from 1500 hours to 1800-1900 hours. Most of the vertical transverse strain histories show trends consistent with the longitudinal strains.

The stress changes computed from the measured longitudinal strains at the four stations are shown as a function of rail temperature in figure 4-9. Although the scatter is higher than is normally expected with strain gage measurements, the trend of the data agrees with the expected change of 2.24 $MN/m^2/^oC$ (325 $psi/^oC$). The data at station 35 shows a shift of 16.6 MN/m^2 (2.4 ksi) because those strain gages were not operational for the full span of the test and, hence, were zeroed at a different strain level than the remainder of the gages. The scatter in figure 4-9 can be attributed to three causes. First, unequal temperatures between the unstressed lengths

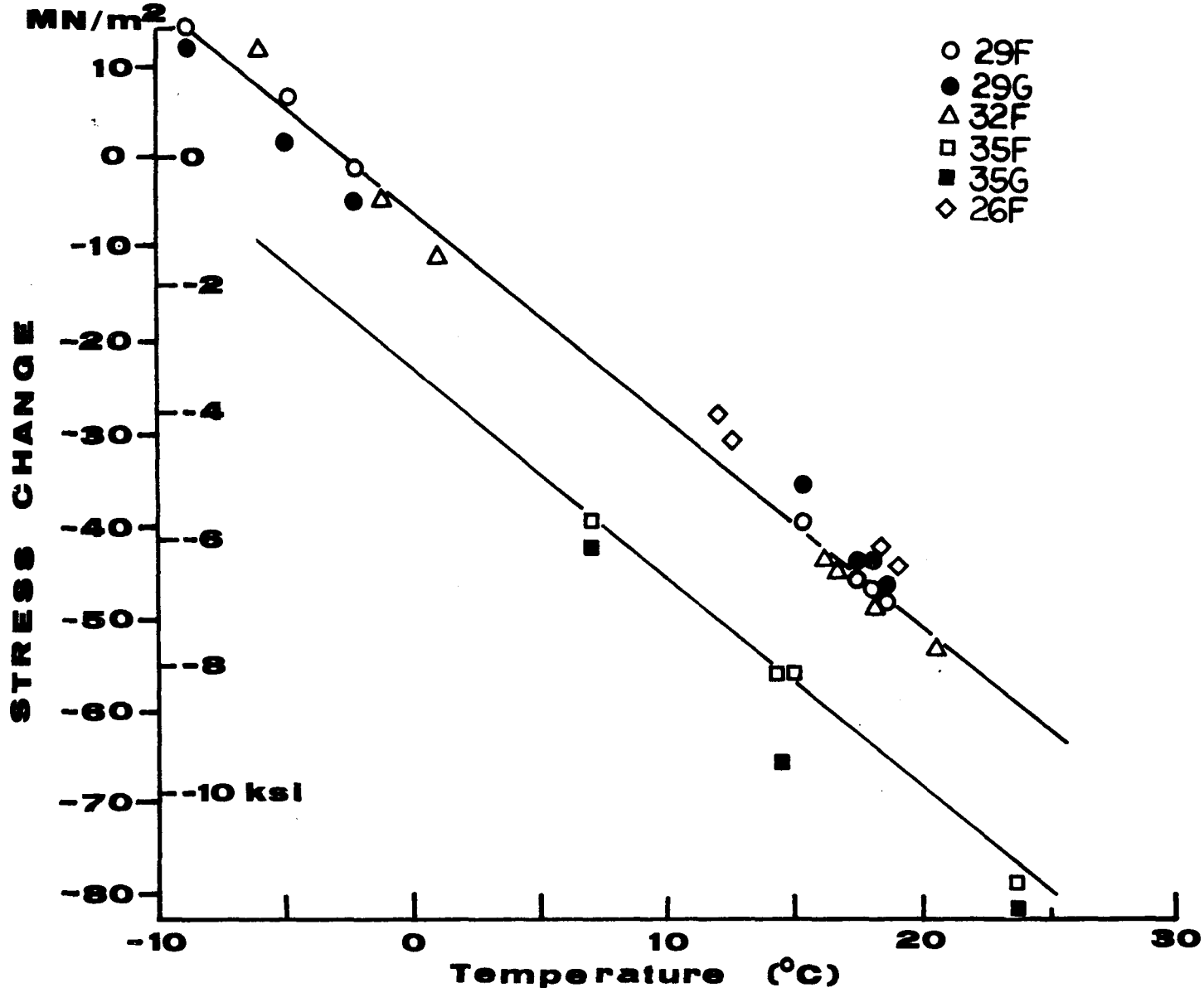

Figure 4-9 Stress Changes Measured with Strain Gages During The Pueblo Field Test.

in which the bridge completion gages were located and the rail will cause an apparent strain. Secondly, flexure induced in the rail due to unequal heating of one side of the rail will cause apparent discrepancies. Thirdly, inaccuracies in temperature measurement may be responsible for some of the scatter because rail head temperatures were used in figure 4-9.

The results of the travel-time measurements on the reference rail are shown in figure 4-10. The longitudinal wave measurements show the expected change with temperature. The shear wave measurements, however, show considerable scatter, the cause of which is not evident. The slope of the longitudinal wave travel-time data agrees very well with the slope measured in the Norman field test, figure 4-5. The average slope of the shear wave data is greater than that measured in the Norman field test but is approximately the same as measured in the laboratory.

The travel-time measurements at the four stations on the rail are shown in figures 4-11 and 4-12. The data shown is the average of measurement made on the field and gage sides of the rail web and has been temperature corrected according to equation 4-1 and

$$(t_T)_c = (t_T)_u - 0.0069\ (T-25) \qquad (4\text{-}2)$$

where

$(t_T)_c$ = corrected shear wave travel-time in μ sec

$(t_T)_u$ = uncorrected shear wave travel-time in μ sec

T = rail temperature in ^{o}C

Additionally the stress data for station 35 have been incremented by 16.6 MN/m^2 (2.4 ksi) to account for the different zero stress level associated with this station as noted above.

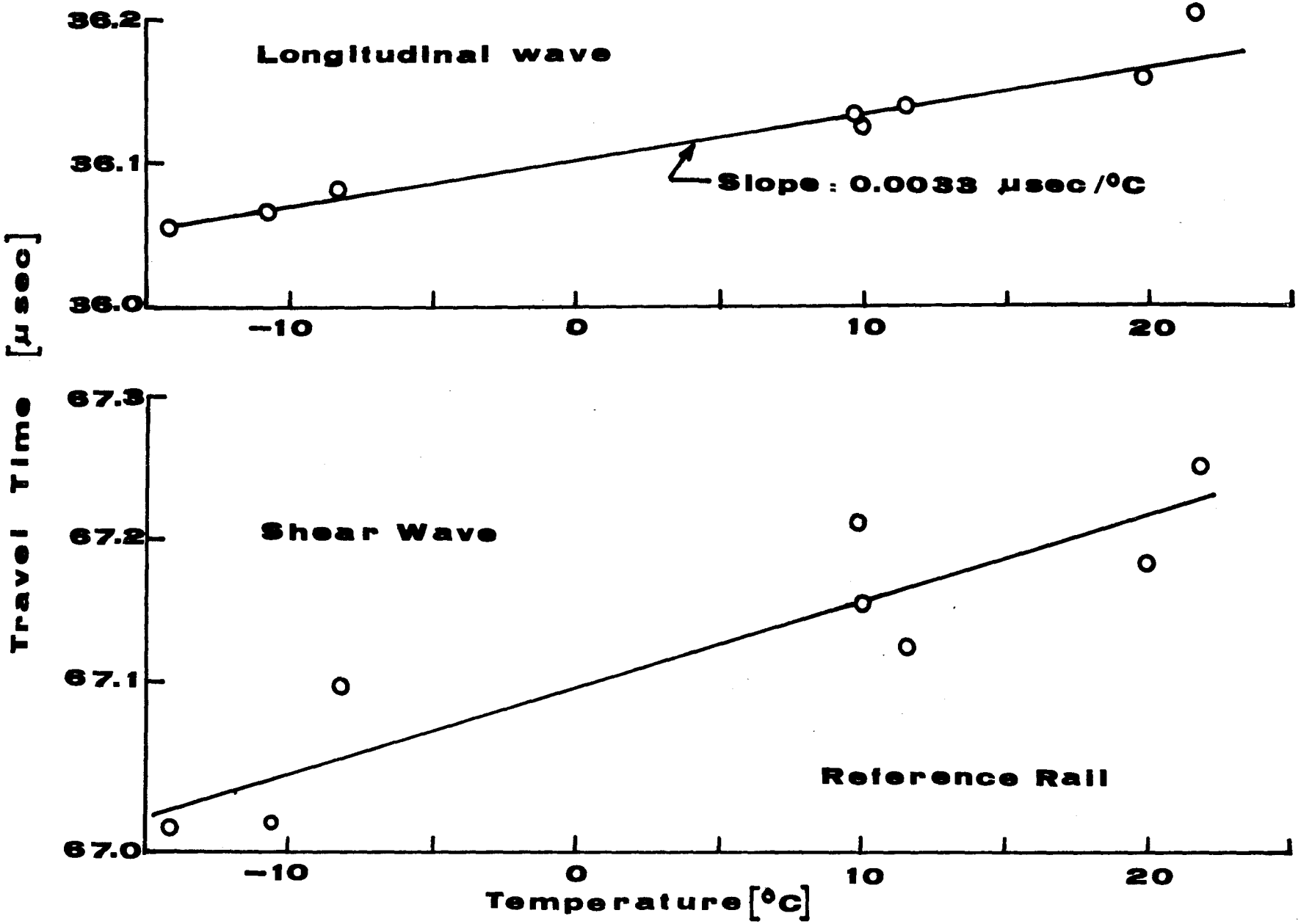

Figure 4-10 Travel-Time Measurements on Reference Rail During Pueblo Field Test.

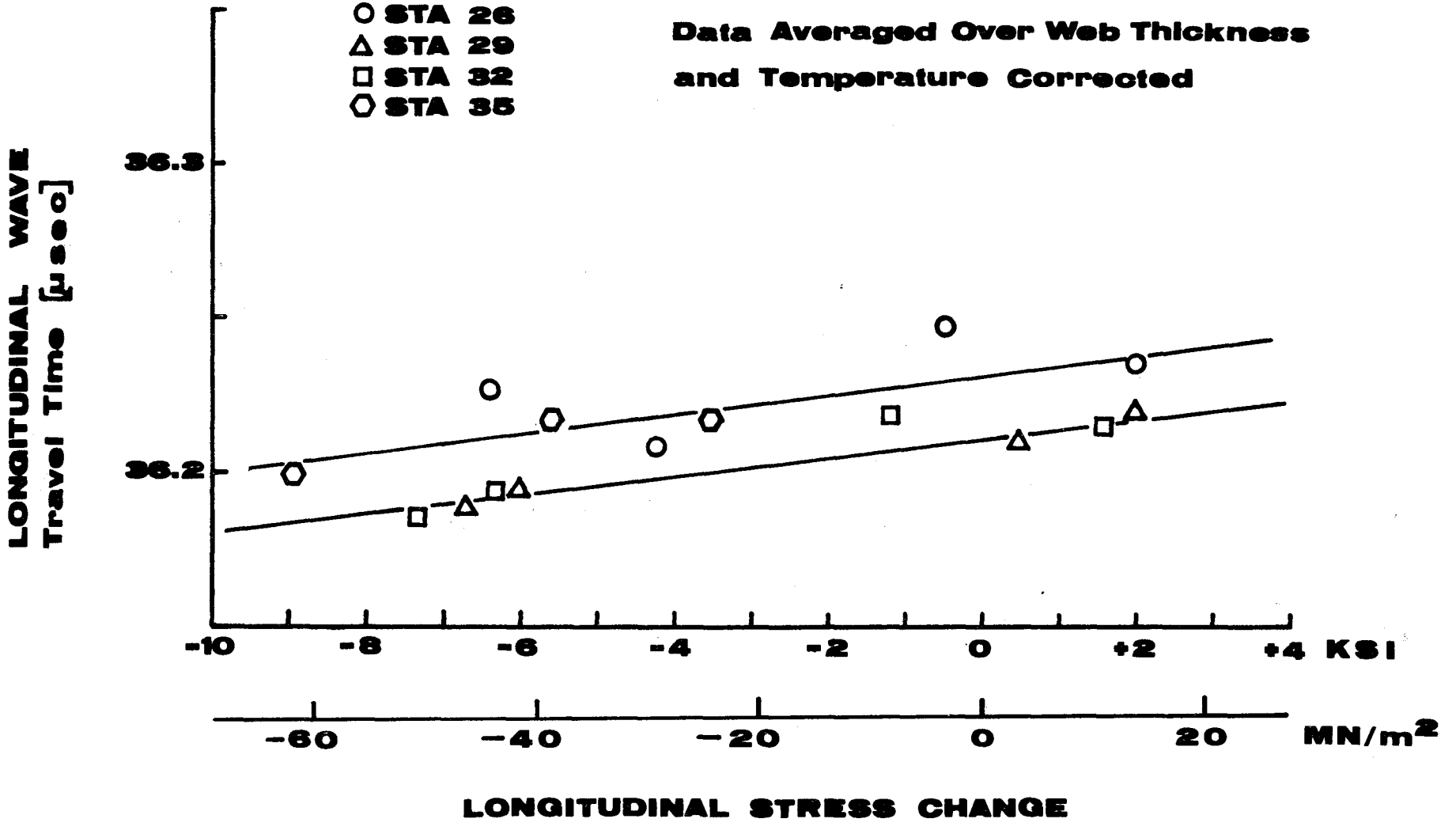

Figure 4-11 Longitudinal Wave Travel-Time Measurements on Four Rail Stations at Pueblo.

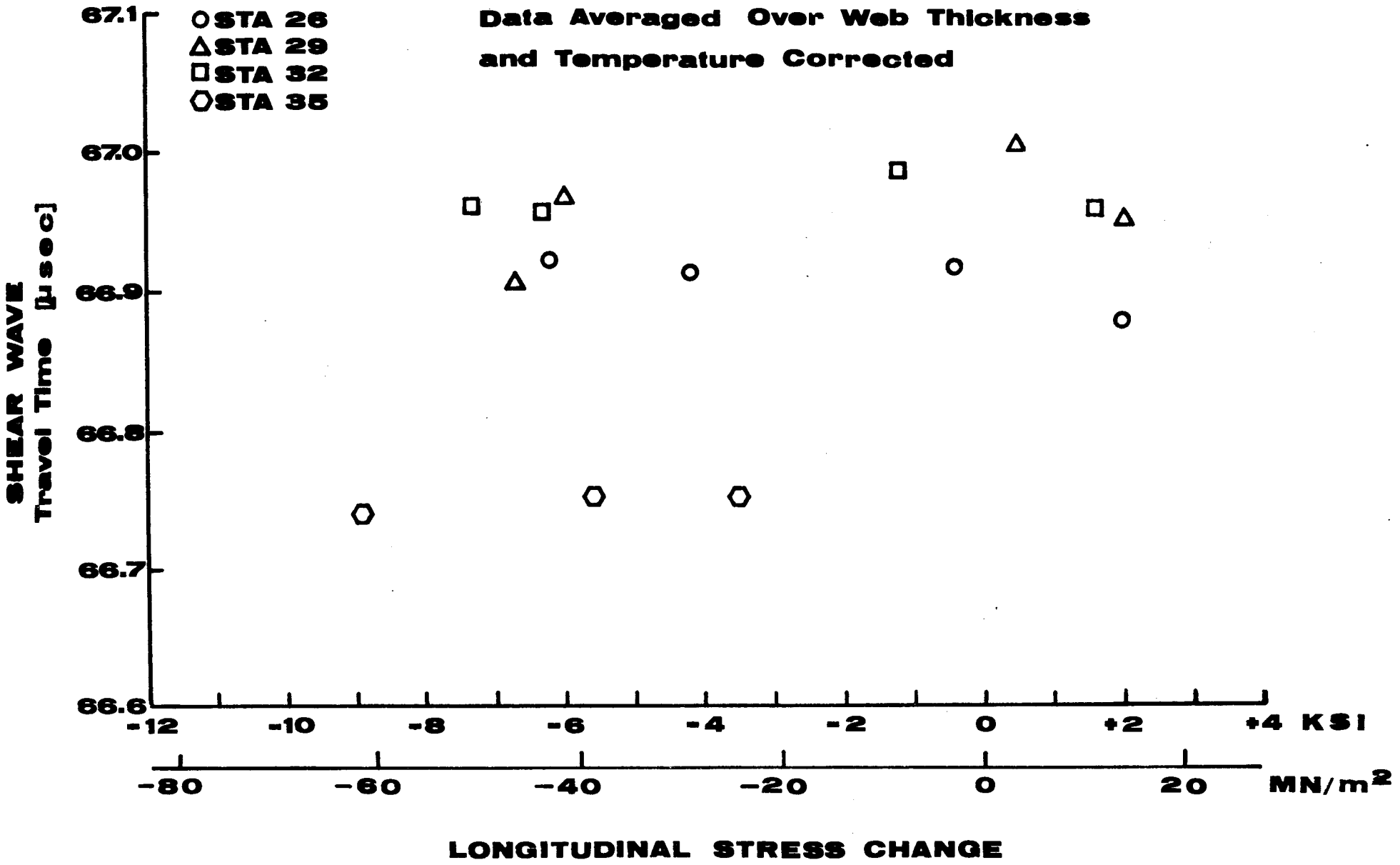

Figure 4-12 Shear Wave Travel-Time Measurements on Four Rail Stations at Pueblo.

The straight lines shown in figure 4-11 are the expected relationships between longitudinal wave travel-time and stress change. They have a common slope of 0.44 nsec/MN/m^2 (3 nsec/ksi). The experimental data at station 26 show considerable inconsistency. However, the data for stations 29, 32 and 35 with one exception agree with the expected values to within approximately $\pm$ 6.9 MN/m^2 ($\pm$ 1ksi) which is same measurement accuracy experienced in the laboratory evaluation.

The shear wave travel-times shown in figure 4-12 for station 26, 32 and 35 are relatively independent of stress level but the data for station 32 show larger variations than were expected. Further the shear wave data for stations 26, 29 and 32 show reasonable agreement but that for station 35 are considerably lower. This indicates that the elastic properties at station 35 are significantly different than those at the other locations.

It is speculated that the inconsistencies in the data shown in figures 4-10, 4-11 and 4-12 are in part due to the presence of small particles which tend to adhere to the rail web surfaces. Although reasonable care was used to clean the web surfaces before attaching the probe, the extremely high resolution required for the measurement coupled with the relatively slow wave speed in the coupling oil (1250 m/sec) make the measurement extremely sensitive to changes in path length between the probe and the web surfaces.

Stress Relieving Tests at Station 32 - After all of the ultrasonic and strain gage data had been compiled for the 24 hour period of the test, a decision was made to cut the rail at station 32 in order to establish the true stress levels throughout the 24 hour test. Full strain gage data

were recorded for the stress relieving test but no ultrasonic measurements were made.

The tests were conducted in five stages at a time in the afternoon when rail temperature was reasonably uniform at approximately 26.1°C (79°F). Readings from all five strain gages at each stage are shown in figure 4-13.

The first stage was the recording of data with the rail fully constrained. Next, the rail clips were removed from seven ties on the side of the planned cut containing the strain gage. Data were recorded after this event. Then, the tie plates were removed from the same seven ties and the strain gage data were recorded. Following that, the rail was saw cut and the strain gage data taken. Finally, the loose rail was hit with a hammer along its length in order to be sure that it was lying free on the ties.

The strain data shown in figure 4-13 behave as expected. The longitudinal strains on either side of the rail are not severely affected until after the saw cut. It is interesting to note that greater longitudinal strain is shown for the gage side of the rail than for the field side indicating that the rail was not entirely straight.

The vertical gages on the opposite sides of the rail are of opposite sign until the rail clips are removed. After that, they are both compressive, countering the tensile longitudinal stresses. This behavior can most likely be related to the rail being slightly bent. The transverse gage on the top of the rail head remains compressive as would be expected.

With this data, the true rail stresses can be estimated for a

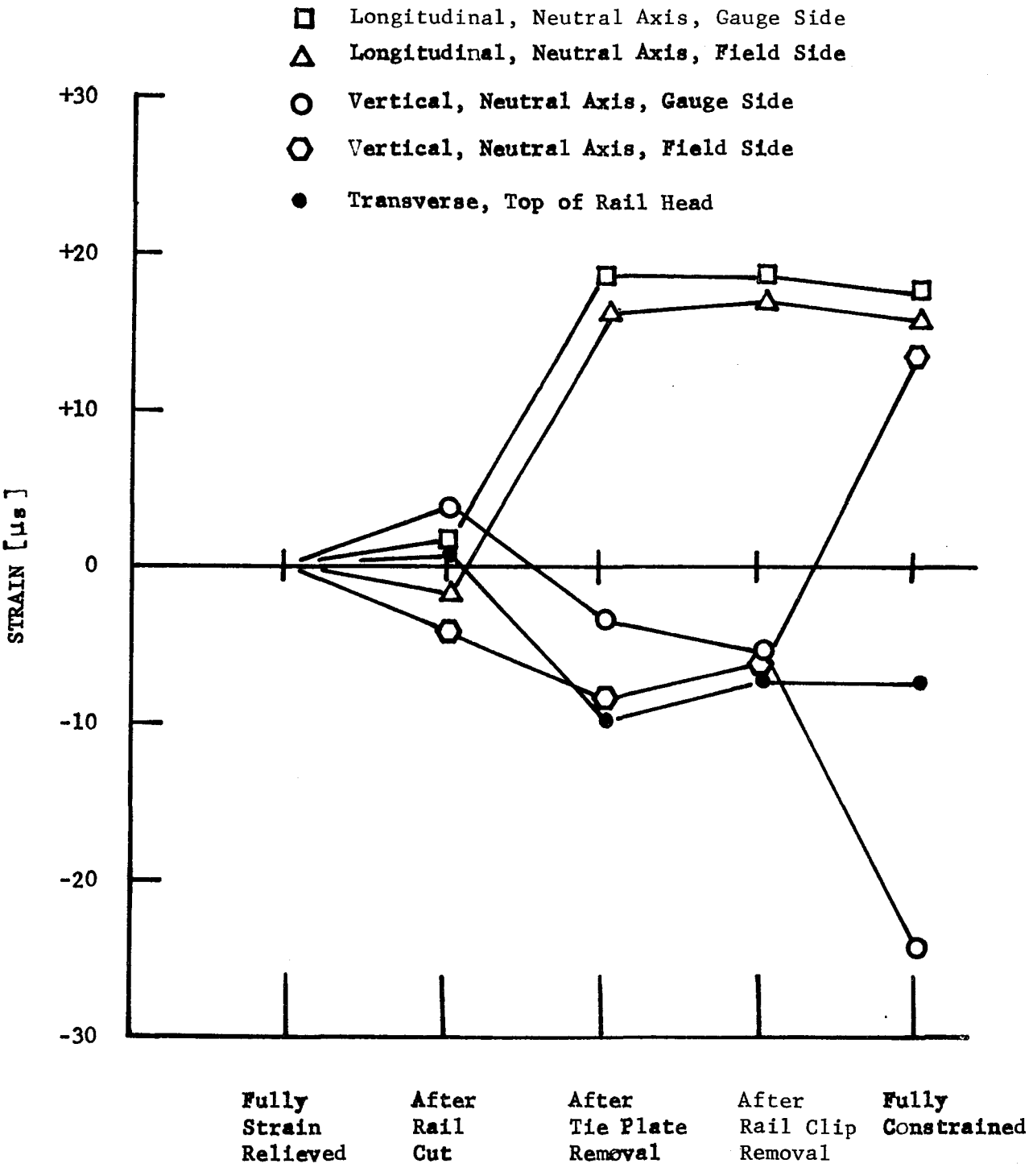

Figure 4-13 Strain Measurements During Stress Relief Test at Station 32.

given temperature range as shown in figure 4-14. The mean stress free temperature is approximately 24.5°C (76.1°F). For the temperature encountered during the ultrasonic tests, the true longitudinal rail stresses ranged from approximately 6.9 MN/m^2 (1 ksi) to 74.5 MN/m^2 (10.8 ksi) in tension.

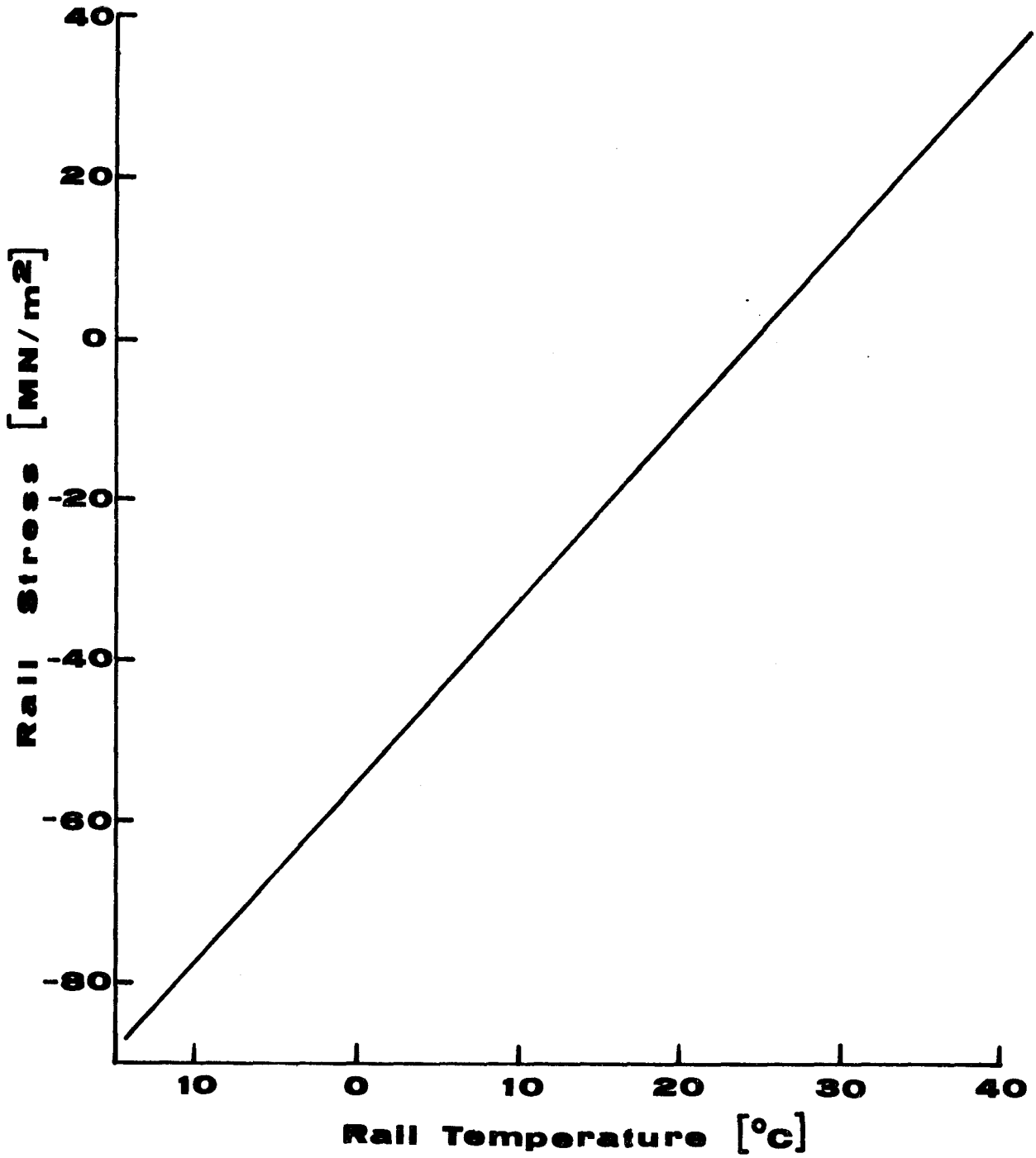

Figure 4-14 True Rail Stress at Station 32.

CONCLUSION

An ultrasonic probe has been designed which is capable of measuring longitudinal stress changes in rail. The measurement is based on the acoustoelastic effect which was shown to be greatest for longitudinal waves propagating parallel to the applied stress. The probe design incorporates conventional ultrasonic wave generators and receivers which use plastic-steel interfaces to generate and detect longitudinal and shear waves propagating parallel to the axis of the rail. Although temperature induced changes in wave speeds affect the probe, a differential travel-time measurement technique plus a stress-free reference measurement provide a means to cancel these undesirable effects. Laboratory evaluation of the probe showed that best precision obtainable with this probe design is approximately $\pm$ 0.003 μ sec which corresponds to $\pm$ 6.9 MN/m^2 ($\pm$ 1 ksi) stress change. Field evaluation of the probe showed that the travel-time measurements when corrected for temperature effects did correctly reflect the expected changes as a function of rail stress change. The field test also showed that the probe was capable of measuring stress changes at a particular rail locations with an accuracy of $\pm$ 6.9 MN/m^2 ($\pm$ 1 ksi).

At the present time, measurement of absolute stress using the acoustoelastic principle is not considered feasible. Although efforts to relate shear wave travel-time to longitudinal wave travel-times for zero applied stress showed that the effects of material properties variations could be partially eliminated, larger variations in longitudinal wave travel-times apparently due to residual stresses and difficulties encountered with shear wave measurements in the field lead to the conclusion that absolute stress measurement is not feasible at this time.

Additional research on the topic of ultrasonic measurement of rail stresses should be concentrated in two areas. First, a larger data base of travel-times (or wave speeds) from various locations, using the basic probe design presented here should be assembled. This could yield considerable information on wave velocity variations from rail to rail, and could assist in learning more about the true stress patterns in rail. An evaluation of this data would be necessary in order to determine the actual usefulness of the method for the measurement of absolute rail stresses.

The second area which needs additional investigation is the relationship between material properties, wave speeds and prior deformation history. The development of a relationship between these factors could help resolve the question of the origin of the variations in longitudinal wave travel-travel times.

APPENDIX A

Rail Stress Measurement in the Union of Soviet Socialist Republics (USSR) and the United Kingdom (UK)

Introduction

A delegation from the United States visited railway technical facilities in the USSR at the end of August 1975. Mr. Bray was a member of that delegation. It appears that there is no effort in the Soviet Union to monitor longitudinal rail stresses other than by traditional strain gage techniques. A complete report [26] of the findings of the U.S. delegation has been prepared by Mr. F. L. Becker, another member of the delegation.

Upon returning to the United States from the visit to the Soviet Union, Mr. Bray spent one day (9/1/75) at the Rail Technical Center of British Rail at Derby. The rail force measuring system was discussed with Mr. Denis Holt and his staff.

The complete rail force measuring system developed by British Rail consists of a transducer permanently mounted through a hole at the neutral axis of the rail, and a separate read-out instrument. One instrument can serve for reading several transducers, depending on the distance between the transducers. Each transducer can be individually monitored or an electrical harness could connect a group of transducers to a single monitoring station. The individual readout system is currently being used by British Rail.

Experience to date shows the minimum sensitivity of the system to be on the order of 44.5×10^3 N (10,000 lb) change in force. Sensitivity near to 17.8×10^3 N (4,000 lb) force changes have been often encountered.

For a typical 11 sq in rail, this resolution is equivalent to detecting stress changes of 6.27 x $10^6 N/m^2$ (910 lb/in^2) and 2.49 x $10^6 N/m^2$ (362 lb/in^2) respectively. More detailed information is contained in bulletin BRT-475 [27]. A summary of this plus personal observations are in the following comments.

Transducer - The transducer consists of two parallel wires permanently fixed across the horizontal diameter of an annulus measuring approximately 29 mm in outside diameter, as shown in figure A-1. The annulus width (W) is near to that of the rail web thus placing the wires just inside the web when the transducer is in place.

Operation - The operating principle is to simply excite the wire with an electrical impulse and then to automatically measure the decay rate (i.e. relative amplitude) as the wire vibrates over one hundred cycles. The wire tension affects the decay rate and thus the force is measured. An initial calibration is required. Later readings must be compared to the original in order for the correct stress to be determined.

Temperature effects upon the rail stress have been found to be important. The best time for reading is during the night or early morning hours since the temperature is generally uniform across the rail at those times. Hard sun shining on one side of the rail will create inconsistent results because of unequal temperature distribution. Both wires must be read and the results should be in reasonably close agreement.

Application and Results - At this time, there are approximately 80 transducers installed in track with 50 or more planned. Two of the reading instruments have been assembled.

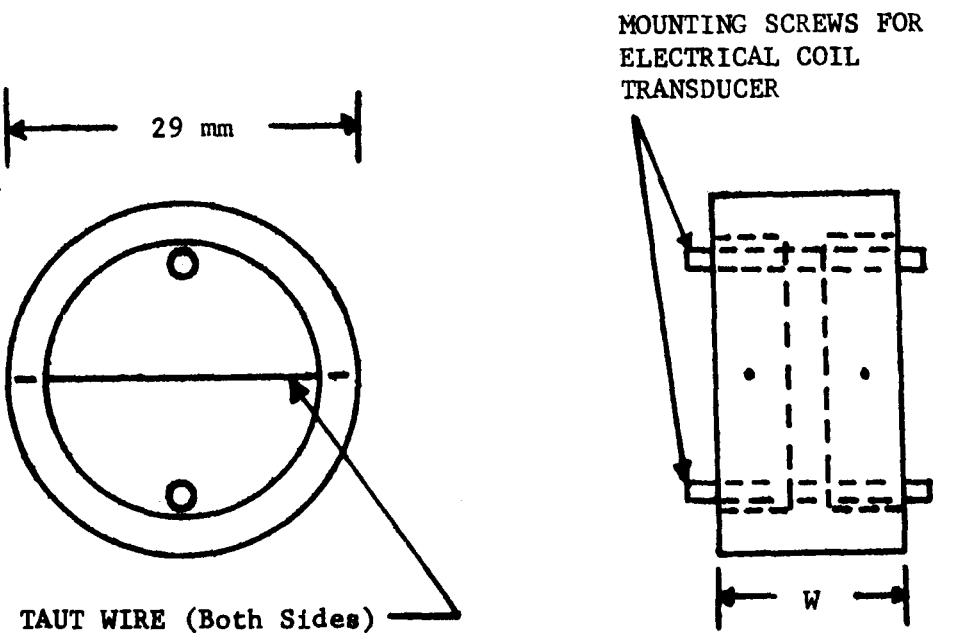

Figure A-1 Annulus for Rail Force Measuring Transducer. (British Rail)

On several instances, force indications read from the transducer have been compared to results obtained by sectioning the rail. In virtually all cases, very good comparisons have been obtained.

Results from several installations in long welded rail have shown the expected settling behavior in newly laid rail where, with traffic, the stresses in the center portion may tend to relax from the original tensile condition creating a more uniform distribution over the entire rail length. After settling, stress changes over several months period showed regular fluctuations over a mean stress level.

Evaluation and Comparison to Proposed Ultrasonic Measurement Technique - The rail force measuring system of British Rail has the distinct advantages of 1) availability; 2) accurate and proven results and 3) relatively low cost (probes negligible costs, instruments approximately $1200 each). The disadvantage of requiring a machining operation in the rail is certainly a major one.

Other Discussion Topics at British Rail - The Railway Technical Center performed tests on the acoustoelastic measurement of rail stresses over two years ago. They experienced difficulties caused by material variations and the program was not pursued. It is suspected that the success of the rail force transducer program diminished interest in the ultrasonic approach.

APPENDIX B

RESIDUAL STRESS MEASUREMENT IN USED RAIL

The presence of residual stress in a rail will be manifested by a change in wave speed. The use of the acoustoelasticity to measure longitudinal stresses may be affected by the presence of residual stresses. In order to learn more of this interaction, an independent study was undertaken to measure the residual stress distribution in typical samples of used rail. The measurements are compared to ultrasonic wave velocities to assess the effect of residual stresses on the acoustoelastic technique for measuring longitudinal stress.

Method

After surveying the literature on the techniques available for residual stress measurement, it became apparent that a material removal technique would be necessary. Further since interest centered primarily on the vertical distribution, the removal of successive layers parallel to the base of the rail would yield sufficient information to be useful.

The method chosen for removing the layers of rail is milling. A preliminary study on a fully annealed block of steel of dimensions 229 x 76 x 32 mm (9 x 3 x 1.25 in) showed that a cut of 0.15 mm (0.006 in) or less with a continuous coolant flow did not introduce residual stresses due to the milling process. Sensitivity requirements dictated that the stresses be average over thicknesses of 1.27 mm (0.050 in), hence, these layers were removed by ten passes of the mill, each pass removing 0.127 mm (0.005 in).

As the layers are removed, the relaxed residual stress causes deformation in the remaining rail. The most suitable method for measuring that deformation is electrical resistance strain gages. Two different strain gage configurations have been employed. Initially single gages were mounted longitudinally at the four locations shown in figure B-1. While reasonable data was obtained with external bridge completion, the long waiting period needed to achieve thermal equilibrium made use of a four active arm bridge more attractive. For the second residual stress measurement, two-gage rosettes (0^{o}-90^{o}) of gage length 1.6 mm (0.062 in) were mounted in pairs as indicated in figure B-1. With two longitudinal and two transverse gages at each location sensitivity was increased by 2.6 and zero stability and temperature compensation were virtually perfect.

Data Analysis

In order to calculate the initial state of stress in the rail, the following assumptions are employed:

(1) the strains caused by removing material are elastic,

(2) the stress distribution is uniaxial and uniform along the length of the rail and linear through the width of the rail,

(3) flexure of the rail obeys the Bernoulli-Euler beam theory, and

(4) the removal of material does not introduce new residual stresses.

Removing layer ℓ is equivalent to imposing a longitudinal force and bending moments as shown in figure B-2. The force and bending

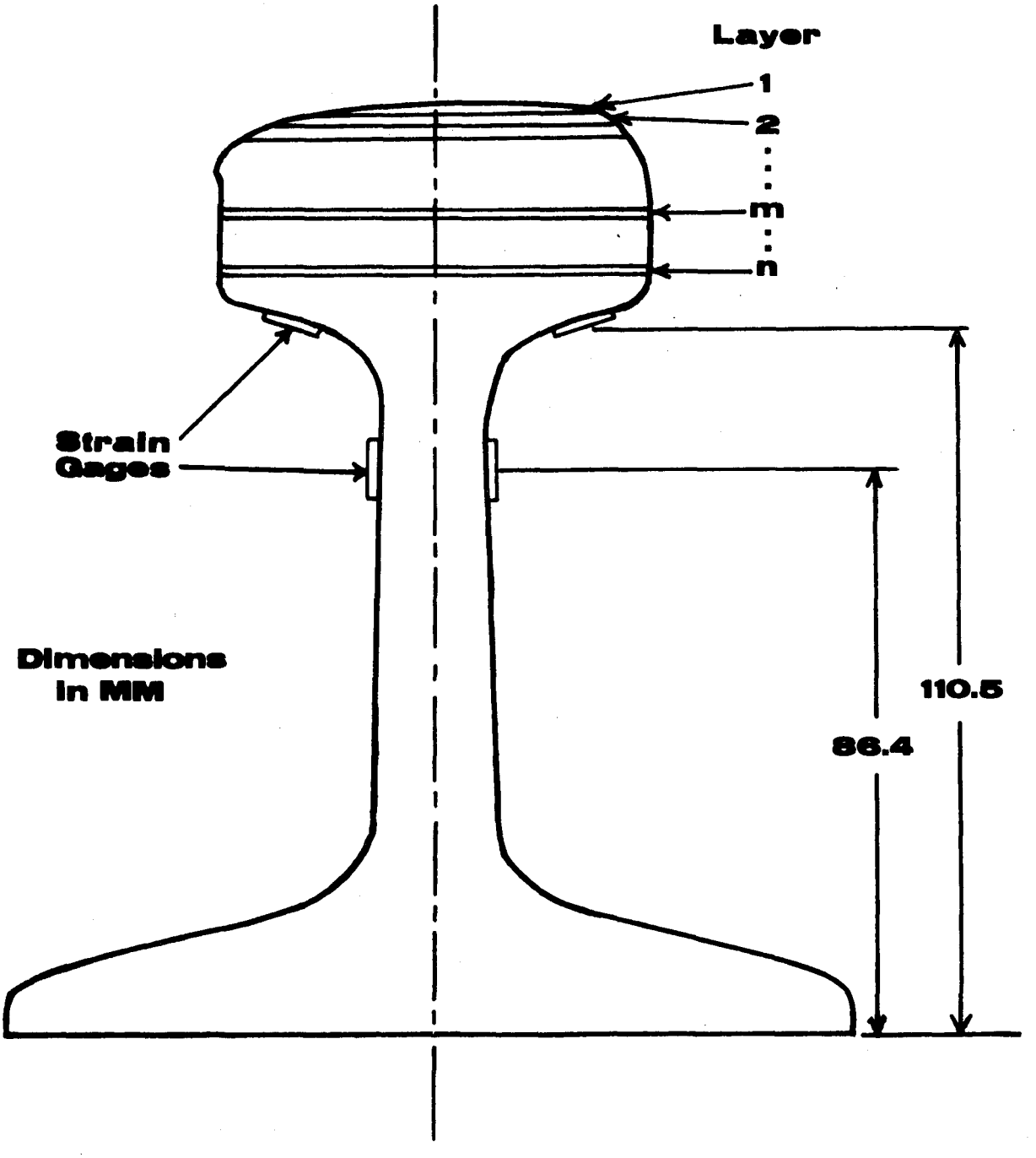

Figure B-1 Strain Gage Locations for Residual Stress Measurement in Rail.

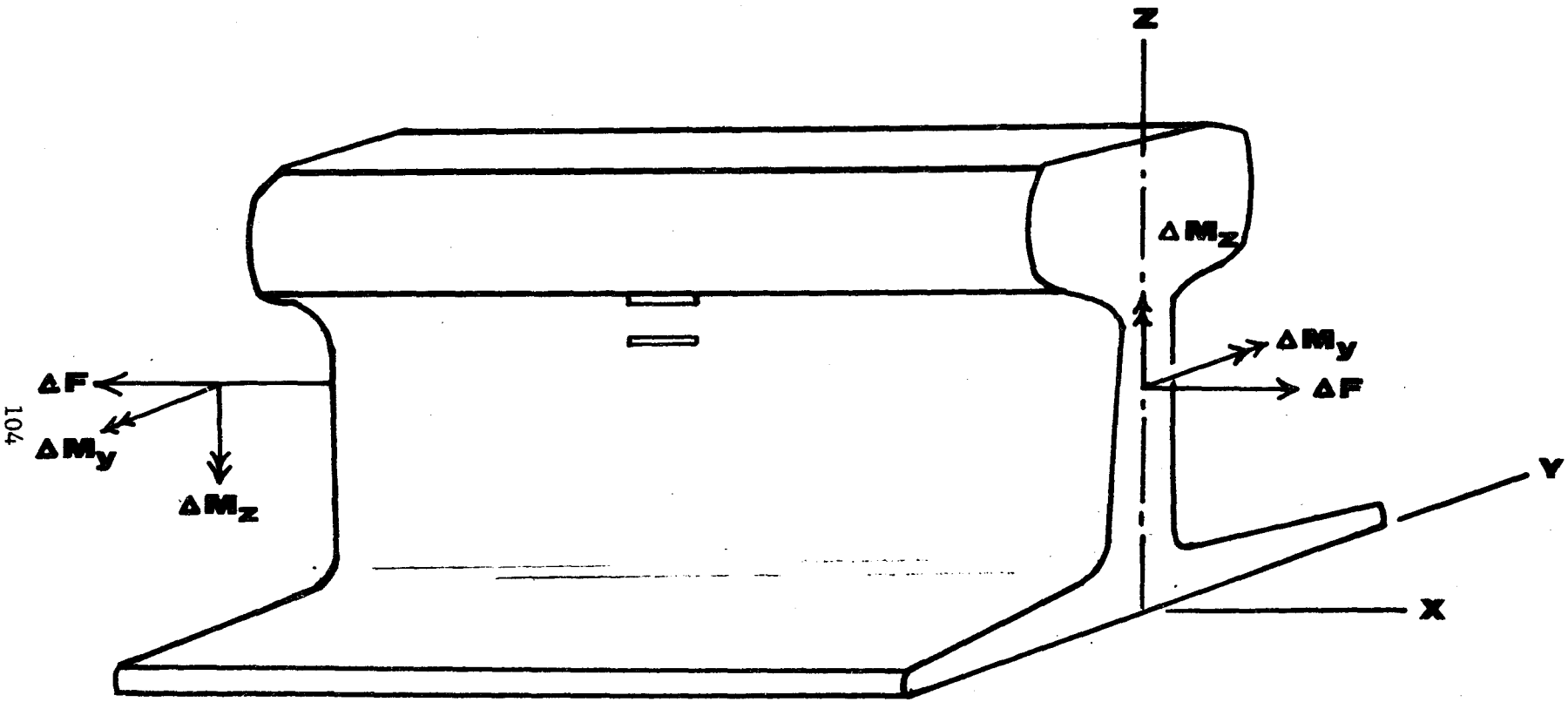

Figure B-2 Nomenclature for Data Analysis.

moments are given by

$$(\Delta F_x)_\ell = (\bar{S}_x)_\ell b_\ell t_\ell \tag{B-1}$$

$$(\Delta M_y)_\ell = (\bar{S}_x)_\ell b_\ell (z_\ell - z_{c\ell})\ t_\ell \tag{B-2}$$

$$(\Delta M_z)_\ell = (\bar{S}_{x,y})_\ell (b_\ell^3/12)\ t_\ell$$

where

$(\bar{S}_x)_\ell$ = average stress in layer ℓ

$(\bar{S}_{x,y})_\ell$ = gradient of the stress in layer ℓ

b_ℓ = width of layer ℓ

z_ℓ = z coordinate of the centroid of layer ℓ

$z_{c\ell}$ = z coordinate of the centroid of the rail cross-section after layer ℓ is removed.

t_ℓ = thickness of layer ℓ

The force and bending moments cause a strain at any point (y*, z*) given by

$$\Delta\epsilon_\ell(y^*, z^*) = \frac{(\Delta F_x)_\ell}{EA_\ell} + \frac{(\Delta M_y)_\ell (z^* - z_{c\ell})}{EI_{yc\ell}} + \frac{(\Delta M_z)_\ell y^*}{EI_{zc\ell}} \tag{B-4}$$

where $\Delta\epsilon_\ell(y^*, z^*)$ = change in longitudinal strain at point (y*, z*) due to the removal of layer ℓ

A_ℓ = area of remaining cross section of rail after removal of layer ℓ

$I_{yc\ell}, I_{zc\ell}$ = second moment of area about centroidal axes parallel to y,z of rail cross-section after layer ℓ is removed.

Substituting equations (B-1, B-2, B-3) into equation (B-4) yields

$$\Delta\epsilon_{\ell}(y^*,z^*) = \frac{(\bar{S}_x)_{\ell} b_{\ell} t_{\ell}}{EA_{\ell}} + \frac{(\bar{S}_x)_{\ell} b_{\ell} (z_{\ell} - z_{c\ell})(z^* - z_{c\ell})\, t_{\ell}}{EI_{yc\ell}}$$

$$+ \frac{(\bar{S}_{x,y})_{\ell} b_{\ell} y^* t_{\ell}}{12\ EI_{zc\ell}} \qquad \text{(B-5)}$$

If $(\bar{S}_x)$ and $(\bar{S}_{x,y})$ are to be determined from the strains, two strains must be measured. Assume the two strain gages, a and b, are placed such that

$$z^*_a = z^*_b = z^* \quad , \quad y^*_a = -y^*_b = y^*$$

The sum and difference of the strains at points a and b are

$$\Delta\epsilon_{\ell a} + \Delta\epsilon_{\ell b} = \frac{2(\bar{S}_x)_{\ell} b_{\ell} t_{\ell}}{E} \left\{ \frac{1}{A_{\ell}} + \frac{(z_{\ell} - z_{c\ell})(z^* - z_{c\ell})}{I_{yc\ell}} \right\} \qquad \text{(B-6)}$$

$$\Delta\epsilon_{\ell a} - \Delta\epsilon_{\ell b} = \frac{(\bar{S}_{x,y})_{\ell} b_{\ell}^3 y^* t_{\ell}}{6\ EI_{x.c\ell}} \qquad \text{(B-7)}$$

Thus $(\bar{S}_x)$, $(\bar{S}_{x,y})$ in layer ℓ can be related to the strains at a and b by

$$(\bar{S}_x)_{\ell} = \left(\frac{\Delta\epsilon_{\ell a} + \Delta\epsilon_{\ell b}}{2} \right) \frac{E}{b_{\ell} t_{\ell}} \frac{1}{\frac{1}{A_{\ell}} + \frac{(z_{\ell} - z_{c\ell})(z^* - z_{c\ell})}{I_{yc\ell}}} \qquad \text{(B-8)}$$

$$(\bar{S}_{x,y})_{\ell} = \left(\frac{\Delta\epsilon_{\ell a} + \Delta\epsilon_{\ell b}}{2} \right) \frac{12\ EI_{zc\ell}}{b_{\ell}^3 y^* t_{\ell}} \qquad \text{(B-9)}$$

When layer ℓ is removed, the stress is changed in every layer below ℓ . Using the equivalent force and bending moments given by

equations (B-1 thru B-3), the changes in average stress and stress gradient in any layer m due to the removal of any layer $\ell < m$ can be expressed as

$$\Delta(\bar{S}_x)_{m\ell} = \frac{(\bar{S}_x)_\ell b_\ell t_\ell}{A_\ell} + \frac{(\bar{S}_x)_\ell b_\ell y_\ell (z_\ell - z_{c\ell})(z_m - z_{c\ell})}{I_{yc\ell}} \qquad \text{(B-10)}$$

$$\Delta(\bar{S}_{x,y})_{m\ell} = \frac{(\bar{S}_{x,y})_\ell b_\ell^3 t_\ell}{12\, I_{zc\ell}} \qquad \text{(B-11)}$$

where $\Delta(\bar{S}_x)_{m\ell}$ = change in average stress in layer m due to removal of layer ℓ

$(\bar{S}_{x,y})_{m\ell}$ = change in stress gradient in layer m due to removal of layer ℓ

z_m = z coordinate of the centroid of layer m.

The average stress and the stress gradient in any layer m may be determined by the following expressions.

$$(\bar{\sigma}_x)_m = (\bar{S}_x)_m - \sum_{\ell=1}^{m-1} \Delta(\bar{S}_x)_{m\ell} \qquad \text{(B-12)}$$

$$(\bar{\sigma}_{x,y})_m = (\bar{S}_{x,y})_m - \sum_{\ell=1}^{m-1} \Delta(\bar{S}_{x,y})_{m\ell} \qquad \text{(B-13)}$$

Results

The longitudinal stress averaged over the rail width as a function of depth measured from the rail head is shown in figure B-3 for two adjacent

samples of the same rail. The samples were taken from a length of 92 lb/yd rail manufactured in 1921. It had seen moderate usage on the Missouri-Pacific line near Leonard, Oklahoma until a derailment in 1972.

The strain data for rail 1 was taken with four longitudinal gages mounted as shown in figure B-1. In figure B-3, the stresses calculated using the upper set of gages are labeled A and those calculated using the lower set B. For rail 1 bridge completion was external to the rail. The zero drift due to the specimen changing temperature during the milling process necessitated a long waiting period after milling for temperatures to equalize. Nevertheless the agreement between the stresses calculated from the strain data from the two locations A and B, indicate that the temperature influence was minimized by this procedure.

The strain on rail 2 was measured using a four active arm bridge at each location. This provides temperature compensation, eliminates contact resistance problems and, under the assumption of uniaxial stresses, increases the measurement sensitivity by a factor of 2.6. The average stress across the rail head calculated using this data and equations B-10, B-12 is also shown in figure B-3. The lack of agreement between the stresses calculated with the two sets of gages A and B is attributed to the presence of a biaxial stress field in the rail head. Since the transverse gages mounted under the head will be affected by stresses acting transverse to the rail axis, the strains measured by those gages would be different than the strains measured by the gages on the web at location B. However, the stresses calculated with the gages on the web of rail 2 agree reasonably well with the stresses of rail 1.

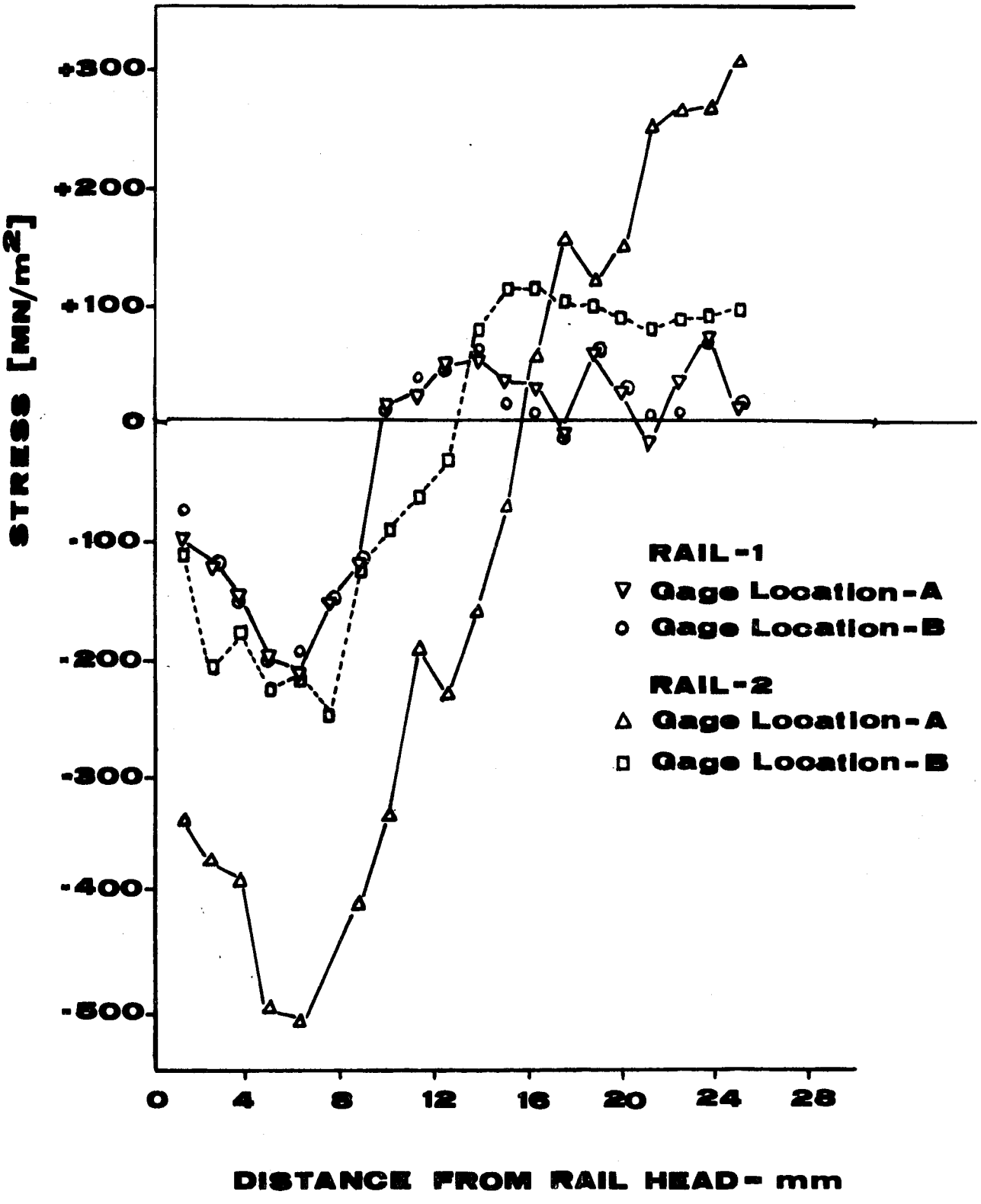

Figure B-3 Average Longitudinal Stress As A Function of Depth for a 92 lb/yd Used Rail.

Summary

A technique for the destructive measurement of the average longitudinal stress as a function of depth in short samples of railroad rail has been shown to be feasible. The quantitative agreement between two sets of measurements made with longitudinally oriented strain gages at two different locations on the same rail demonstrate the accuracy of the technique. Disagreement of measurements made with four arm bridges located under the rail head suggest the presence of a biaxial stresses in the rail head. Stress measurements on a 92 lb/yd rail having seen moderate usage show a maximum compressive residual stress of 200-250 MN/m^2 (29-36 ksi) at a depth of 6-8 mm (0.25-0.31 in).

REFERENCES

1. Egle, D.M. and Bray, D.E., "Nondestructive Measurement of Longitudinal Rail Stresses," Interim report, DOT project DOT-OS-40091, June 1975.

2. Coombs, D.H., ed., British Railway Track, London, Permanent Way Institution, 1971.

3. Hay, W.W., Railroad Engineering, New York, John Wiley, 1953.

4. Kerr, A.D., "A Model Study for Vertical Track Buckling," Report No. DOT-FRA-OHSGT, October 1971.

5. Kerr, A.D., "On the Stability of the Railroad Track in the Vertical Plane," DOT Report Contract No. DOT-FR-20064, November 1972.

6. National Transportation Safety Board, Railroad Accident Report, Penn Central Company, Train Second 115 (Silver Star) Derailment at Glenn Dale, Maryland, June 28, 1969, Report No. NTSB-RAR-70-1, June, 1970.

7. McGee, G.M., "Research and Development of Continuous-Welded Rail," Welding Journal, v 39, n 9, September 1960, pp. 881-889.

8. "Field Hanbook on Continuous Welded Rail," Committee 31, Report on Assignment 8, American Railway Engineering Association-Bulletin, v 74, no 646, January - February 1974, pp. 614-625.

9. Letter from Mr. E.T.Franzen, Missouri Pacific Railroad, to Mr. D.H. Stone, Association of American Railroads, June 25, 1975.

10. Pasley, R.L., "Barkhausen Effect -- An Indication of Stress," Materials Evaluation, v 28, no 7, July 1970, pp. 157-161.

11. Klug, H.P., and Alexander, L.E., X-Ray Diffraction Procedures, New York, Wiley, 1954.

12. American Railway Engineering Association, "Report on Pennsylvania Railroad M. of W. Test No. 591, Determination of Plastic Flow in Rail Head," Appendix 8-b, Report of Committee 4 - Rail, Report on Assignment 8, Chicago: Proceedings of the Fifty-Seventh Annual Meeting of the Railway Engineering Association, v 59, 1959, pp. 962-975.

13. Egle, D.M. and Bray, D.E., "Measurement of Acoustoelastic and Third-Order Elastic Constants for Rail Steel," Jour. Acoustical Society of America, v 60, no. 3, September 1976, pp. 741-744.

14. King, R.R., Birdwell, J.A., Bray, D.E., Clotfelter, W.N. and Risch, E.R., "Improved Methods for Nondestructively Measuring Residual Stresses in Railway Wheels," Proceedings of the Ninth Symposium on Nondestructive Evaluation, San Antonio, April 1973, pp. 91-105.

15. Noronha, P.J., Chapman, J.R. and Wert, J.J., "Residual Stress Measurement and Analysis Using Ultrasonic Techniques," Journal of Testing and Evaluation, v 1, no 3, May 1973, pp. 209-214.

16. Noronha, P.J. and Wert, J.J., "An Ultrasonic Technique for the Measurement of Residual Stresses," Jour. Testing and Evaluation, v 3, no 2, March 1975, pp. 147-152.

17. Becker, F.L., "Ultrasonic Determination of Residual Stress," Battelle-Pacific Northwest Laboratories, Richland, Washington, January 1973.

18. Hsu, N.N., "Acoustical Birefringence and The Use of Ultrasonic Waves for Experimental Stress Analysis," Experimental Mechanics, v 14, no 5, May 1974, pp. 169-176.

19. Clotfelter, M.W. and Risch, E.R., "Ultrasonic Measurement of Stress in Railroad Wheels and in Long Lengths of Welded Rail, " NASA Technical Memorandum, NASA TM X-64863, July 1974.

20. Hughes, D.S. and Kelly, J.L., "Second-Order Elastic Deformation of Solids," Physical Review, V 92, no 4, December 1953, pp. 1145-1149.

21. Murnaghan, D., Finite Deformations of an Elastic Solid, John Wiley & Sons, Inc., New York, 1951.

22. Schreiber, E., Anderson, O.L. and Soga, H., Elastic Constants and Their Measurement, New York, McGraw-Hill Book Company, 1973.

23. Gardfalo, F., Malenock, P.R., Smith, G. V., "The Influence of Temperature on the Elastic Constants of Some Commercial Steels," Symposium on Determination of Elastic Constants, ASTM STP 129, pp. 10-30, 1952.

24. _____, "Thermophysical Properties of Solid Materials. Volume II-Alloys, WADC Technical Report 58-476, November 1960 (AD 253710).

25. Bradfield, G., "Strength, Elasticity and Ultrasonics," Ultrasonics, v 10, no 4, pp. 166-172, 1972.

26. Becker, F. Larry, Trip Report US-USSR Rail Inspection Information Exchange, August 24-September 1, 1975, Department of Transportation, Transportation Systems Center, Cambridge, Massachusetts, DOT-TSC-979, BNW 2311102378, December 1975, Battelle-Pacific Northwest Laboratories.

27. _____, British Rail's Force Transducer; Bulletin BRT-475, Gage Techniques, LTD., Trowbridge, Wiltshire.